THE MOBILITY AND DIFFUSION OF POTASSIUM IONS IN GASES

A THESIS

Presented to

The Faculty of the Division of Graduate

Studies and Research

by

David Randolph James

In Partial Fulfillment

of the Requirements for the Degree

Doctor of Philosophy

in the School of Physics

Georgia Institute of Technology

April, 1975

THE MOBILITY AND DIFFUSION OF POTASSIUM

IONS IN GASES

Approved:

Earl W. McDaniel, Chairman

I. R. Gatland

T. L. Weatherly

Date approved by Chairman: 7 May 1975

ACKNOWLEDGMENTS

It is a pleasure to acknowledge the assistance of at least some of the many people who have been associated with the author during the course of this research. The author wishes to express sincere gratitude to his thesis advisor, Professor E. W. McDaniel, whose guidance, teaching, encouragement, and leadership have been invaluable. Appreciation is extended to Professor I. R. Gatland for his many contributions to this research, and in particular for his mathematical analysis which has been so important in this work. The author also wishes to thank Professor T. L. Weatherly, who served on his reading committee, for providing many helpful suggestions regarding the writing of this thesis.

The author is indebted to his predecessors in this laboratory, Drs. D. L. Albritton, T. M. Miller, J. T. Moseley, R. M. Snuggs, and J. H. Schummers. The association with Dr. George Thomson, who worked closely with the author in the early part of this research, has been most rewarding. A special thanks must go to Dr. Ed Graham IV who not only assisted the author in obtaining some of the data, but also shared many of the problems and successes encountered over the course of this research. The author would like to acknowledge the aid of Dr. W. C. Keever, Dr. Harry Ellis, and Mr. Russell Akridge for helping take much of the data for this experiment. Many lively discussions with them and Dr. Bob Pai have been most helpful.

The author is also indebted to Professor E. A. Mason of Brown

University, and Drs. J. H. Whealton and L. A. Viehland for use of their theoretical results before publication. Their collaboration in this research has been most beneficial. Thanks must also be extended to Rick Morrison for making some helpful calculations on beam data.

Finally, the author must acknowledge the financial support of this work by the Office of Naval Research and the U. S. Air Force Office of Scientific Research.

TABLE OF CONTENTS

		Page
ACKNOWLEDGMENTS		ii
LIST OF TABLES		vi
LIST OF ILLUSTRATIONS		vii
SUMMARY		ix
Chapter		
I.	INTRODUCTION	1
	Review of Past Research	4
	Motivation for Present Research	9
II.	EXPERIMENTAL APPARATUS AND MATHEMATICAL ANALYSIS	11
	Mathematical Analysis	16
III.	THEORETICAL CONSIDERATIONS	21
	Review of Past Theory	21
	The Viehland-Mason Transport Theory	32
IV.	MOBILITIES	44
	Ion Production and Boundary Effects	45
	Experimental Data	48
	Error Analysis	59
	Omega Integrals	64
V.	LONGITUDINAL DIFFUSION COEFFICIENTS	70
	Longitudinal Diffusion Coefficient Data	71
	Diffusion Error Analysis	83
VI.	CONCLUSIONS	91

TABLE OF CONTENTS (Concluded)

Appendices Page

I. TABULATION OF MOBILITIES AND LONGITUDINAL DIFFUSION COEFFICIENTS. 94

II. USEFUL FORMULAS 112

BIBLIOGRAPHY 116

VITA 119

LIST OF TABLES

Table		Page
1.	Zero-field Reduced Mobilities of K^+ Ions in Various Gases as a Function of the Effective Temperature	41
2.	Zero-field Reduced Mobilities of K^+ Ions in Various Gases Expressed in $cm^2/V\text{-sec}$	60
3.	Uncertainties in the Measurement of Mobilities.	64
4.	Energies Associated with K_0 Peak and ND_L Breakaway	83
5.	Comparison of Measured Low-field ND_L with Einstein Value.	86
6.	Error Estimates in the Measurement of ND_L	88
7.	Transport Data for K^+ Ions in Helium.	95
8.	Transport Data for K^+ Ions in Neon.	97
9.	Transport Data for K^+ Ions in Argon	99
10.	Transport Data for K^+ Ions in Hydrogen Gas.	101
11.	Transport Data for K^+ Ions in Nitrogen.	103
12.	Transport Data for K^+ Ions in Oxygen Gas.	105
13.	Transport Data for K^+ Ions in Carbon Monoxide	106
14.	Transport Data for K^+ Ions in Nitric Oxide.	107
15.	Transport Data for K^+ Ions in Carbon Dioxide.	109

LIST OF ILLUSTRATIONS

Figure		Page
1.	Sectioned View of the Drift Tube, the Outer Vacuum Enclosure and the Analysis Region.	12
2.	Cut-away View of the Drift Chamber and Mass Analysis and Detection Apparatus.	14
3.	Sample Arrival Time Spectrum with Theoretical Fit for D_L.	20
4.	Reduced Mobilities for K^+ Ions in Argon as a Function of E/N at 300°K.	51
5.	Reduced Mobilities for K^+ Ions in He and H_2 as Functions of E/N at 300°K.	53
6.	Reduced Mobilities for K^+ Ions in Ne and O_2 as Functions of E/N at 300°K.	56
7.	Reduced Mobilities for K^+ Ions in NO and CO_2 as Functions of E/N at 300°K.	58
8.	Omega Integrals for K^+ in He, Ne, and Ar as Functions of Effective Temperature.	66
9.	Omega Integrals for K^+ in H_2, NO, and O_2 as Functions of Effective Temperature.	68
10.	Omega Integrals for K^+ in N_2, CO, and CO_2 as Functions of Effective Temperature.	69
11.	Longitudinal Diffusion Coefficients for K^+ in Ar, N_2, and CO Compared to Original and Modified Wannier Predictions.	72
12.	Longitudinal Diffusion Coefficients for K^+ in H_2, He, and Ne Compared to Wannier Predictions.	75
13.	Longitudinal Diffusion Coefficients for K^+ in O_2, NO, and CO_2 Compared to Wannier Predictions	77
14.	Longitudinal Diffusion Coefficients for K^+ in Ar, N_2, and CO Showing Modified Wannier Prediction with Whealton-Mason First Order Correction	79

LIST OF ILLUSTRATIONS (Concluded)

Figure Page

15. Longitudinal Diffusion Coefficients for K^+ in H_2, He, and Ne Compared to Modified Wannier Prediction with Whealton-Mason First Order Correction. 80

16. Longitudinal Diffusion Coefficients for K^+ in O_2, NO, and CO_2 Compared to Modified Wannier Expression with Whealton-Mason First Order Correction. 81

SUMMARY

The drift velocities, mobilities, and longitudinal diffusion coefficients of K^+ ions in various gases were measured as a function of the energy parameter E/N, where E is the magnitude of the electric field strength and N is the number density of the gas molecules. The ion-gas combinations investigated were K^+ in He, Ne, Ar, H_2, O_2, NO, and CO_2. The apparatus used in this experiment was a drift tube mass spectrometer of ultra-high vacuum construction. Ion swarms were repetitively gated into the drift region which contained the neutral gas that was held at a predetermined pressure. Concentric guard rings provided a static, uniform, electric field directed along the axis of the drift tube. The ion cloud quickly assumed a steady-state drift velocity in the field direction, and the ion population diffused both transversely and longitudinally to the axis. After the ions traversed a known distance, they were mass selected, individually detected, and sorted according to total drift time. A histogram of ion arrival times was built up and analysis of the spectrum yielded the drift velocity and hence the mobility. Comparison of the shape of the spectrum to the results of a mathematical model determined the longitudinal diffusion coefficients.

The measured zero-field reduced mobilities in $cm^2/V\text{-}sec$ for K^+ in each gas were: He (21.6 ± 0.4), Ne (7.43 ± 0.15), Ar (2.66 ± 0.05), H_2 (13.1 ± 0.3), O_2 (2.72 ± 0.05), NO (2.28 ± 0.05), and CO_2 (1.45 ± 0.03). Omega, or collision, integrals were calculated from the mobility data

using the theory of Viehland and Mason, and the results compared favorably with omega integrals obtained from beam experiments. A comparison was made between the measured longitudinal diffusion coefficients and theoretical predictions.

CHAPTER I

INTRODUCTION

Shortly after Roentgen discovered X rays in 1895, J. J. Thomson, Ernest Rutherford, and J. S. Townsend began to investigate the strange phenomenon of conductivity in gases. Their work marked the beginning of the field of gaseous electronics and transport phenomena of ions in gases. Although these early investigators were handicapped by a lack of advanced electronic and vacuum technology, they managed to obtain some useful measurements of the drift velocities of gaseous ions and they gained considerable qualitative knowledge about the subject. However, it was not until the 1930's when Tyndall made a series of drift velocity measurements that we had any very reliable data on transport properties. Since its beginning, the history of the field has seen experiment and theory proceed at different rates with one leading the other for a while and then vice versa. At present we believe that experiment has advanced to the point where the data are now accurate enough over a wide range of experimental parameters to be used for much improved calculations of interaction potentials. The availability of highly reliable data coupled with recent advances in the theory should bring about a much better understanding of the physical processes involved in transport phenomena.

One of the most fundamental concepts in the study of transport properties of ions in gases is that of a drift velocity, denoted $\vec{v}_d$.

Consider a neutral atomic or molecular gas of number density N at thermal equilibrium, i.e., obeying the Maxwell velocity distribution law. Now, introduce a static electric field which is uniform throughout the volume of gas. A localized cloud or swarm of non-interacting ions placed in the gas will then move in the field direction, with each individual ion on the average losing some of its energy upon collision with a gas particle and gaining energy from the field between encounters. A balance between the gain and loss of energy on the atomic level leads to a macroscopic steady state in which the center of mass of the ion cloud assumes a constant drift velocity $\vec{v}_d$ in the field direction. One can picture an ion as having this drift velocity superimposed upon the random motion produced by many collisions.

When the electric field intensity $\vec{E}$ approaches zero, the ionic velocity distribution tends to Maxwellian, and the drift velocity becomes proportional to $\vec{E}$, that is

$$\vec{v}_d = K\vec{E} \ . \tag{1-1}$$

The constant of proportionality is termed the zero-field mobility, and is usually expressed in units of $cm^2/V\text{-sec}$. Since K varies inversely with N, it is convenient when comparing data to use a reduced mobility K_0 given by

$$K_0 = K \frac{P}{760} \frac{273.16}{T} \ , \tag{1-2}$$

where P is the pressure of the gas in Torr and T is the temperature in

degrees Kelvin at which the measurement was made. The zero-field reduced mobility will be denoted by $K_0(0)$. As E is increased above the zero-field regime, the ratio v_d/E no longer remains a constant but becomes a function of the parameter E/N expressed in units of the Townsend (Td), where 1 Td is 10^{-17} V-cm^2. Is is still conventional to call the ratio v_d/E the mobility and measure it over a wide range of E/N. A useful relation between these parameters is

$$v_d = 0.02687\ K_0\ E/N\ , \tag{1-3}$$

with E/N in Td, v_d in units of 10^4 cm/sec, and K_0 in cm^2/V-sec. It can be seen from the theory that the quantity E/N determines the transport coefficients and in particular the average energy gained from the field between collisions.

When the ion cloud is localized, there is necessarily a gradient in the ionic number density n. Therefore, diffusion of the ion swarm will occur. For isotropic space and small gradients in the number density (i.e., E = 0), Fick's Law,

$$\vec{j} = - D\vec{\nabla}n\ , \tag{1-4}$$

relates the ionic current density $\vec{j}$ to the spatial gradient via a scalar diffusion coefficient D. Under such conditions a relation exists between D and K called the Einstein or Nernst-Townsend equation,

$$K = \frac{eD}{kT}\ . \tag{1-5}$$

Here e is the charge on an electron and k is Boltzmann's constant. As we move out of the zero-field region of E/N, D becomes a tensor of the form

$$\overline{\overline{D}} = \begin{bmatrix} D_T & 0 & 0 \\ 0 & D_T & 0 \\ 0 & 0 & D_L \end{bmatrix} \qquad (1\text{-}6)$$

if $\vec{E}$ is directed along the z axis. D_T and D_L are numbers called the transverse and longitudinal diffusion coefficients, respectively. Eq. (1-5) is no longer valid outside the zero-field range. As might be expected, D_L is usually greater than D_T due to the influence of the electric field. Both coefficients are inversely proportional to the gas number density, and to eliminate this explicit dependence experimental data are reported as the product ND_L and ND_T.

Review of Past Research

Charge carriers drifting through a neutral gas may undergo several processes through which their identity changes. The ion may transfer its charge to an impurity or the neutral molecule in the gas or participate in an ion-molecule reaction which produces an entirely new type of ion. A neutral gas molecule may also attach itself to the ion to form a cluster which may alternately break up and reform. The necessity for positive identification of the ionic species is apparent. The work on mobilities and diffusion coefficients prior to the early 1960's was done without the benefit of direct mass analysis of the observed ion, and hence much of

these data are unreliable. With the advent of the drift tube mass spectrometer of McDaniel[1,2] the problem of proper ion determination was largely eliminated.

There are situations, however, in which fairly dependable mobilities have been measured in drift tubes lacking mass spectrometers. Usually these experiments have been done with the alkali ions which are produced thermionically from certain mineral substances like Kingman feldspar and others. These ion sources emit predominantly one type of ion with traces of the other alkalis, so that the experimenter can be reasonably sure of the identity of his ions. Although the alkali ions have only a small tendency to undergo ion-molecule reactions due to their closed shell structure, at high pressures and low E/N clusters of K^+ ions in CO_2, NO, CO, N_2, O_2, and Ar have been observed in drift tube mass spectrometers.[3] Thus, even with alkali ions, there is still the danger of mistaking the identity of the ion.

In the late 1930's Tyndall[4] made a series of mobility measurements on alkali ions in various gases without benefit of direct mass analysis, and he obtained reliable zero-field reduced mobilities in most cases. These values in cm^2/V-sec for K^+ ions in gases of interest in this experiment are given in parentheses after the gas: He(21.5), Ne(7.50), Ar(2.63), H_2(12.7), and N_2(2.53). The variation with E/N was not reported.

The next dependable data were those of Crompton and Elford in 1959[5] on the mobility of K^+ in N_2 and Ne at 294°K. They used the electrical shutter method of the type developed by Bradbury and Nielsen.[6] A mass spectrometer was not employed. The zero-field reduced mobilities obtained for N_2 and Ne were 2.54 and 7.42 cm^2/V-sec, respectively. The

Ne measurements involved pressures of 3.3, 4.6, and 12.5 Torr with the range of E/N extending from about 4 to 30 Td.

Elford[7] in 1967 measured the mobility of K^+ in H_2 at 293°K as a function of E/N in the interval from 0.6 to 91 Td. The zero-field reduced mobility obtained was 12.75 cm^2/V-sec. The apparatus was a Bradbury-Nielsen type drift tube without provision for direct mass analysis; however, Elford made independent checks of similar ion sources with a quadrupole mass spectrometer and found predominantly K^+ ions with a 1% trace of Na^+. He also saw no indication of clustering in this work. Again Elford in 1971[8] made some interesting measurements for K^+ ions in He, Ne, Ar, H_2, and N_2 in which, contrary to current theoretical predictions, an explicit pressure dependence of the reduced mobility was observed. Gatland[9] explained the anomaly in terms of diffusion effects and reversible reactions involving clustered ions. However in a later paper Elford and Milloy[10] reexamined the effect and attributed it to the formation of ion-atom or ion-molecule complexes in orbiting resonant states. In the case of N_2, formation of clusters was found to be responsible for the pressure effect. The measurements reported in this paper were made on K^+ ions in He, Ar, H_2, and N_2, and the zero-field reduced mobilities were found to be 21.3 ± 0.2, 2.64 ± 0.02, 12.8 ± 0.1, and 2.50 ± 0.02 cm^2/V-sec, respectively. The pressure range was 1.4 to 190 Torr, and E/N varied between 1 and 28 Td.

Fleming, Tunnicliffe, and Rees,[11] using a Bradbury-Nielsen drift tube, in 1969 reported the mobility of K^+ in H_2 for E/N between 3 and 200 Td. The gas pressures ranged from 0.63 to 13.3 Torr and the temperatures from 290 to 300°K. Direct mass analysis of the ions was not made, but

an independent check of the source in a mass spectrometer under conditions similar to those in the drift tube showed the ions to be K^+. The zero-field reduced mobility was found to be 12.70 ± 0.1 cm^2/V-sec, which is in good agreement with previous work. Fleming, et al., also measured the transverse diffusion coefficient for $1.5 \leq E/N \leq 350$ Td.

Starting with Albritton[2] and Miller[12] in 1968, the group at the Georgia Institute of Technology has made an extensive study of the transport properties of slow ions in gases. The apparatus employed in these measurements has been a drift tube mass spectrometer providing direct mass analysis of the observed ions. Albritton[2] obtained the mobilities for K^+ in H_2 for E/N between 1.59 and 143 Td. The zero-field reduced mobility obtained was 12.9 cm^2/V-sec. Miller[12] remeasured K^+ in H_2 over a much larger range of E/N (1.41 to 422 Td) for pressures in the range 0.035 to 0.950 Torr and obtained a zero-field K_0 of 12.8 ± 0.6 cm^2/V-sec.

Moseley[13] in 1969 measured the mobility of K^+ in N_2 over a large range of E/N and confirmed the results of earlier experimenters not using mass analysis techniques. In this work Moseley also reported the first measurements of longitudinal diffusion coefficients for K^+ ions in a gas. Snuggs[14] (1971) obtained the mobilities and longitudinal diffusion coefficients for K^+ in O_2. His mobility for the zero-field case was 2.68 ± 0.07 cm^2/V-sec. The energy parameter E/N varied from less than 2 Td to slightly more than 300 Td for the mobilities and for ND_L the range was 3.4 to 308 Td. In work also done on the Georgia Tech drift tube, Volz[15] made similar measurements of K^+ in NO in 1971 over a substantial variation of E/N; however, his low-field longitudinal diffusion

coefficients exhibited considerable scatter, and the agreement with the Einstein value was not good.

In 1973 Skullerud[16] investigated the motion of K^+ ions in Ar using a modified Tyndall-Powell type double shutter drift tube[4] with drift distance variable from 0 to 5 cm. No mass analysis was employed, but pressures between 0.14 and 1.0 Torr were used so that clustering was likely to be unimportant. The mobilities and longitudinal diffusion coefficients were measured over a large range of E/N, 22.9 to 793 Td. They are the only data in the high field region for comparison with the Ar measurements done at Georgia Tech to be presented in Chapter IV. Skullerud quotes an accuracy of ± 10% on the values of ND_L.

Again at Georgia Tech, Thomson, et al.,[3] studied potassium ions in N_2 and CO, both over ranges of E/N from about 4 to 640 Td. The longitudinal diffusion coefficients obtained were compared with the Wannier[17] predictions, and agreement at low and intermediate E/N was seen to be quite good. However, for high electric fields the experimental points fell significantly below the theory for both N_2 and CO. At the higher ionic energies, ion-molecule interactions which are not taken into account by the theory become significant and probably lead to the discrepancy. To gain further knowledge about the validity of the Wannier theory, James, et al.,[18] (1973) measured K_0 and D_L for K^+ in Ar from 1 to 610 Td. Again low and intermediate field values of ND_L agreed well with the Wannier theory, but at high fields a similar depression of the diffusion coefficient was observed. Agreement with the data of Skullerud confirmed the observation. Keller, Beyer, and Colonna-Romano[19] (1973) found the zero-field reduced mobility for K^+ in Ar to be 2.73 ± 0.06 cm^2/V-sec measured

at 310°K.

Using the Bradbury-Nielsen technique Creaser[20] in 1974 obtained the mobilities of K^+ in He, Ne, and Ar at room temperature. His zero-field reduced mobilities were 21.5(He), 7.41(Ne), and 2.67(Ar) cm^2/V-sec. The pressure was varied from 0.543 to 3.1 Torr and E/N from 9 up to 107 Td in the case of Ar. Spot checks on the identity of the observed ions were made with a quadrupole mass filter incorporated into the apparatus. Also in this paper Creaser derived the ion-atom interaction potentials using his mobility data and the Kihara[21] theory as presented by Mason and Schamp.[22]

In an important paper appearing in 1953 Wannier[17] made considerable advances in the theory of transport phenomena of gaseous ions moving in strong electric fields. In this work the energy gained by the ion from the field was not assumed small in comparison to the thermal energy. Ion-ion interactions could be neglected due to the assumption of small ion densities, and collisions between ions and gas molecules were taken to be elastic. A more detailed discussion of the theory appears in Chapter III.

Viehland and Mason[23] have recently developed a rigorous kinetic theory for the mobility of gaseous ions which applies at arbitrary field strengths. A brief survey of their work will be given in Chapter III.

Motivation for Present Research

One of the primary motivations for studying the transport properties of ions in gases has been to provide information from which interaction potentials can be derived. The variation of mobility with temperature

is one means to achieve this goal, but the experimental difficulties involved have limited progress in that direction. A more fruitful approach has proved to be the measurement of the mobility and diffusion coefficients as functions of the parameter E/N. The latter experiments are less difficult to perform, and they also investigate a significantly larger range of ionic energies, typically 1/25 to 7 eV. These measurements provide a useful complement to the beam scattering experiments, which are limited to rather high energies because of space charge effects and stray fields. It appears that with the recent advances in the theory by Viehland and Mason, interaction potentials may now be obtainable over a much wider range of separation distances.

A comprehensive set of mobility and diffusion measurements is also useful to check the regions of validity of the various theories. There is in addition the need for transport coefficients in the determination of ion-molecule reaction rates, ion-ion recombination coefficients, and the rates of dispersion of ions in a gas due to mutual repulsion. The mobilities of alkali ions in various gases is also important in connection with magnetohydrodynamic power generation.

The goals of this research are to measure to a high degree of accuracy the mobilities and longitudinal diffusion coefficients over the widest possible interval of E/N. Although the data by themselves are useful for the calculation of various atomic processes, the emphasis is placed on comparison with theoretical predictions available, in particular those of Wannier and those of Viehland and Mason.

CHAPTER II

EXPERIMENTAL APPARATUS AND MATHEMATICAL ANALYSIS

For the measurement of the mobilities and diffusion coefficients we employed a drift tube mass spectrometer described previously in detail in references 2, 12, 13, and 24. Only a brief description will be given here. Figure 1 is a sectioned view of the drift tube. The apparatus consists of the outer vacuum enclosure called the kettle, the drift tube proper contained within the kettle, and an analysis region housing the detection equipment. All major portions are made of stainless steel and are bakeable so that ultimate base pressures of 10^{-9} Torr are obtainable with 6" and 4" oil diffusion pumps.

Gas is admitted into the drift chamber through one of the ports near the top of the apparatus. The pressure is maintained at a constant selected value in the range from 0.025 to about 1 Torr by an MKS Baratron capacitance manometer which drives an automatic pressure controller and servo leak valve. A liquid N_2 refrigerated vapor bath located in the gas feedline traps out impurities. The circular, concentric guard rings within the drift tube proper produce a static, uniform electric field in the axial direction. All surfaces exposed to the ions are gold plated to prevent charge build up. An important feature of this apparatus is the movable ion source which can vary the drift length from 0 to nearly 44 cm. Seven source positions are accurately calibrated and the four corresponding to the longest drift distances are generally used in the routine

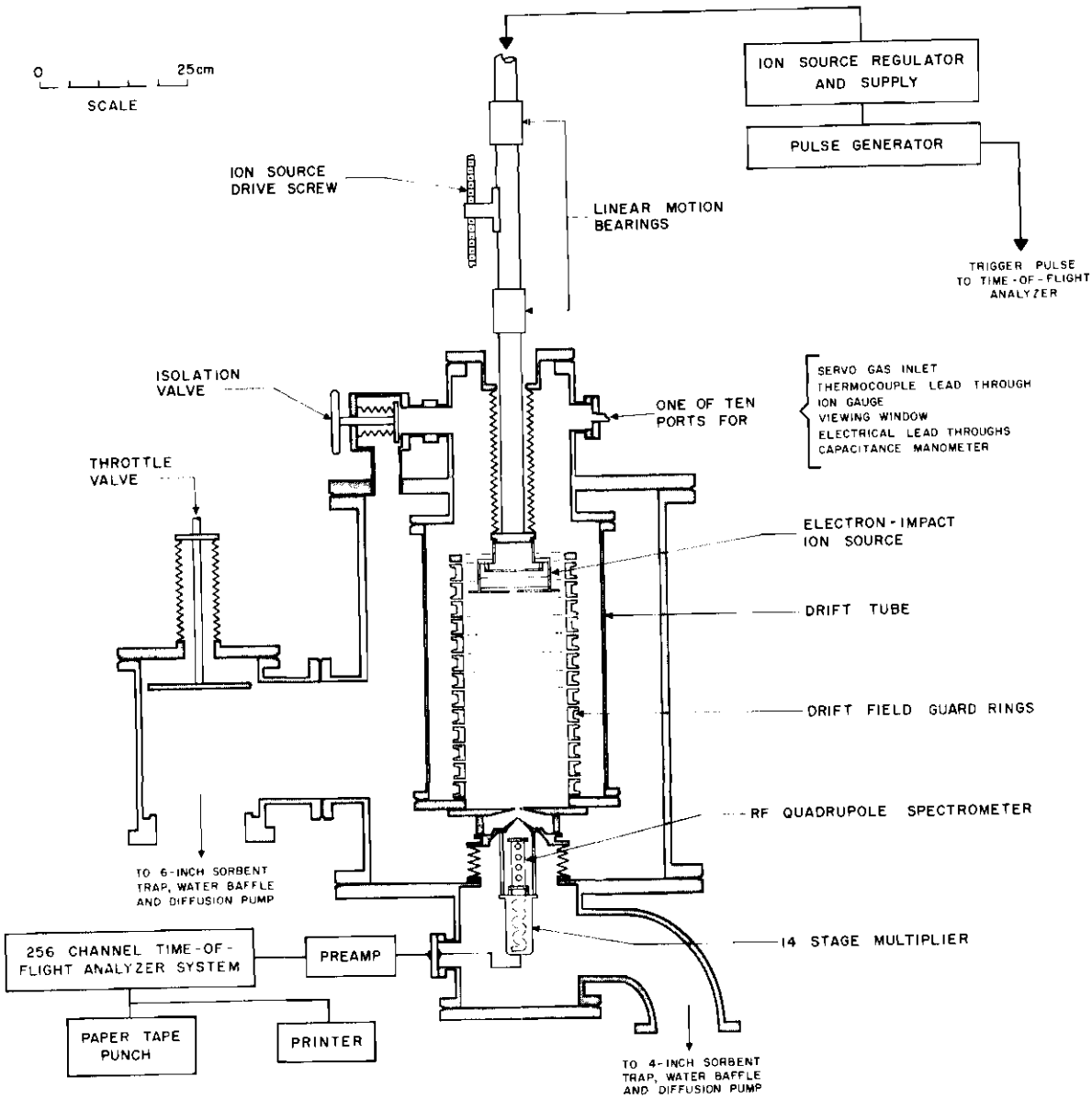

Figure 1. Sectioned View of the Drift Tube, the Outer Vacuum Enclosure and the Analysis Region

taking of data. The source of ions is a platinum mesh filament coated with potassium feldspar which when heated emits predominantly singly charged potassium ions in large quantities. Trace amounts of other alkali ions appear but in general are so small that they can not be studied. An electron impact ion source is also contained within the same movable structure, but was not used in this research. The magnets used with the electron source were removed.

The ions are pulsed out of the source and admitted into the drift region as a thin disc which begins to diffuse and drift down the axis of the tube. The ion cloud continues to drift until the swarm reaches the end plate which has in it a small pinhole (0.035 cm diameter) on the axis. A portion of the ions exit through the hole into the differentially pumped analysis region where they pass through a conical skimmer and then to the RF quadrupole spectrometer. The quadrupole passes only ions of the desired charge to mass ratio so that there can be no mistake as to the identity of the ions. A channel electron multiplier detects each ion which has traversed the mass filter. Figure 2 shows the drift tube and analysis regions in more detail. When an ion arrives at the detector, a pulse is sent to a 256 channel time of flight analyzer which records the total drift time of the ion. A large attenuation of the initial ion burst occurs because of transverse diffusion of the ion population and off axis rejection during mass analysis. The result is that at most one or two ions for every pulse gets detected, making it necessary to repetitively pulse the source to build up an arrival time spectrum. For a given gas pressure and electric field intensity E one obtains a near Gaussian distribution which may be analyzed to obtain the mobility and

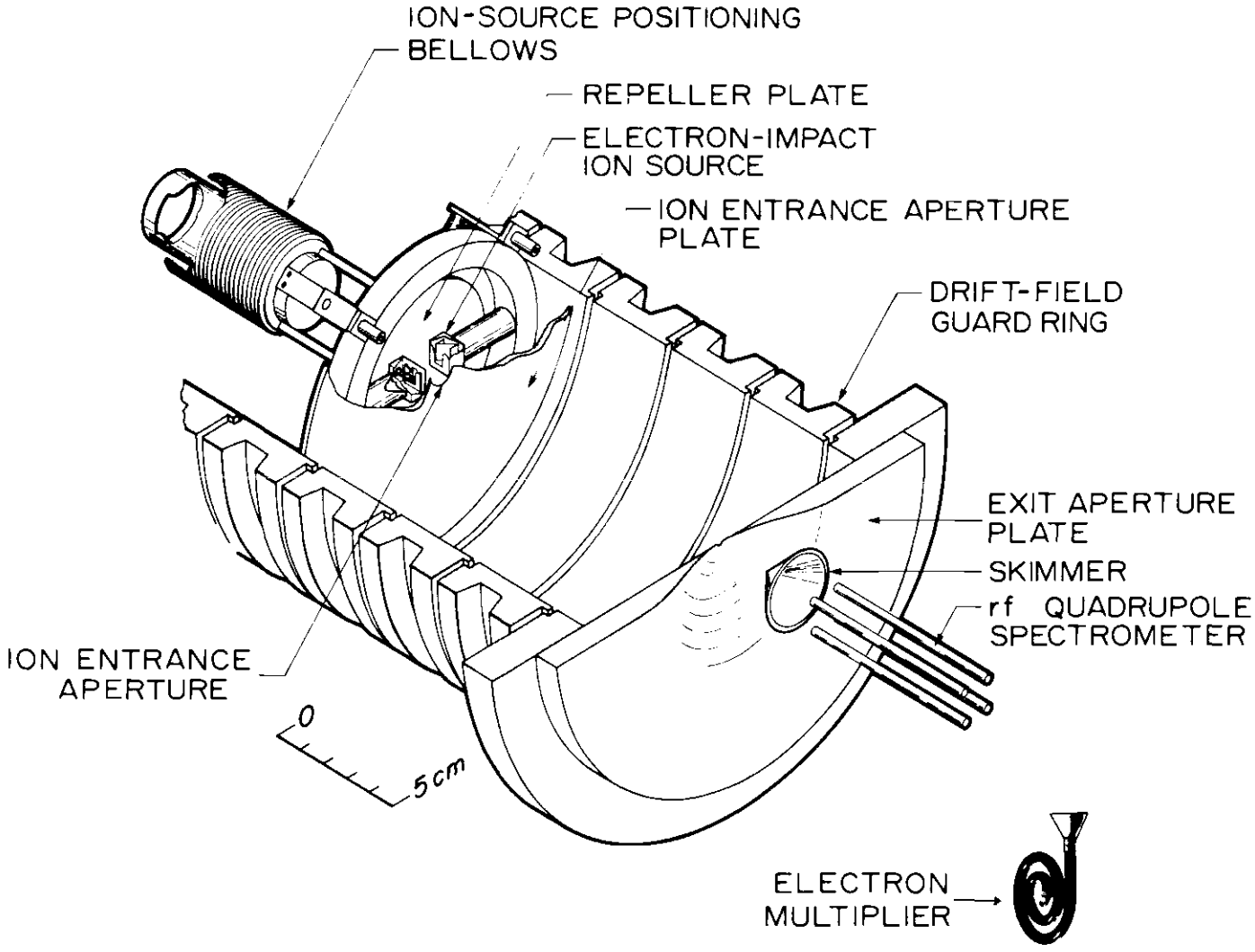

Figure 2. Cut-away View of the Drift Chamber and Mass Analysis and Detection Apparatus

longitudinal diffusion coefficient characteristic of that E/N. The number of counts in each channel of the time of flight analyzer are punched onto paper tape and fed into a central site computer via teletype. The transport properties are then calculated from the raw data by computer analysis by a method to be discussed in the next section.

Several features of this drift tube enhance the measurement of transport properties. First of all are the very large (0-44 cm) drift distances attainable. When the length is long, end effects such as the time required for mass analysis and detection (analysis time) act over a much smaller percentage of the total drift distance. Also if ions are injected into the drift region with a significant initial velocity, the time it takes for the ions to become thermalized (i.e., reach a steady state) is small compared to the total drift time for large distances. A long drift tube should therefore tend to reduce these types of errors. Wall effects are mostly eliminated by the use of large guard rings 17.5 cm in diameter. Another feature is the movable ion source mentioned before. By taking spectra at different drift lengths, end effects have a tendency to cancel out when corresponding drift times are subtracted. In the next section such a differencing technique for calculating mobilities will be explained. Of course each measurement at a source position provides an independent check on the others and gives information about statistical fluctuations. The quadrupole mass filter enables one to positively identify the ion being studied. In conjunction with mass analysis the effects of ion-molecule reactions on the transport properties can be determined by analysis of the arrival time spectrum. In particular, it is necessary

to know when the effects are negligible in order to verify that the charge carrier did not change its identity during its drift.

Mathematical Analysis

For each drift distance z_i we obtain an average arrival time $\bar{t}_i$ from the accumulated spectrum at a given E/N. An obvious estimate for the drift velocity would be $z_i / \bar{t}_i$, but not accounted for in this calculation are the effects of diffusion upon the arrival time histogram and the time the ions spend in the analysis region. The arrival time profile is not symmetrical about its peak due to the nature of the ion swarm sampling. If the ions were counted at the same instant in time, they would have a spatial Gaussian distribution, but instead they are detected individually as they arrive. Thus, while some ions have left the drift region, others remain inside and diffuse for longer times. The result is a skewed Gaussian effect in which the distribution exhibits an enhancement for ions arriving at later times. The net effect of longitudinal diffusion is to build up the arrival time spectrum at longer times, while transverse diffusion removes particles from the swarm and thus depletes the peak at later times. There is a slight depletion of the spectrum at longer times due to longitudinal diffusion, but the effect only occurs in a small region near the peak. Therefore $\bar{t}_i$, the average over this type of skewed distribution, is increased by the effects of longitudinal diffusion and decreased by that of transverse diffusion. In the Georgia Tech drift tube the ions must pass through an analysis region for proper mass selection and hence all drift times must be corrected for this corresponding transit time. The result is that the spectrum is shifted along the time axis by a constant amount.

The effects stated above can be reduced considerably by a differencing technique made possible by the movable ion source. By taking spectra at several different drift distances z_i and computing their average times we can calculate a drift velocity by the formula

$$v_d = \frac{z_i - z_j}{\bar{t}_i - \bar{t}_j} , \qquad (2\text{-}1)$$

where i and j refer to different source positions. Subtracting the $\bar{t}$'s eliminates the effect of constant analysis time as well as removing certain diffusion corrections to the drift velocity.[25] Another method for obtaining the drift velocity when data from several drift distances are available is that of a least squares fit to a straight line using the set of points $(z_i, \bar{t}_i)$. The drift velocity is calculated as the inverse slope of the resulting straight line and the analysis time is the intercept on the $\bar{t}$ axis. In every case the agreement between the two methods has been excellent.

Gatland[24,26,27] has developed a mathematical model for the motion of ions in a drift tube which is appropriate for the initial and boundary conditions of this experiment. His analysis accounts for various types of reaction schemes, including pure depletion reactions characterized by the frequency per ion α, "forward-backward" reversible processes as in the formation and breakup of clusters, and other more complicated mechanisms. However, in this experiment the pressures and electric fields were chosen so that reactions could be neglected. In this case the analysis takes on its simplest form. The diffusion equation to be solved is

$$\frac{\partial n(\vec{r},t)}{\partial t} = D_T \left[\frac{\partial^2 n}{\partial x^2} + \frac{\partial^2 n}{\partial y^2} \right] + D_L \frac{\partial^2 n}{\partial z^2} - v_d \frac{\partial n}{\partial z} - \alpha n + \beta(\vec{r},t) \ , \qquad (2\text{-}2)$$

where the source term is given by

$$\beta(\vec{r},t) = s\delta(t)\delta(z)\Theta(r_0 - r) \ .$$

The ionic number density is denoted by $n(\vec{r},t)$, and $\delta(z)$ and $\delta(t)$ are delta functions. The uniform surface density of ions is s, and r_0 is the radius of the entrance aperture of the source. $\Theta(r_0 - r) = 1$ if $r < r_0$ and 0 otherwise. The current density of ions $\vec{j}$ is given by the expression

$$\vec{j}(\vec{r},t) = \vec{v}_d \, n(\vec{r},t) - \overleftrightarrow{D} \cdot \vec{\nabla} n(\vec{r},t) \ , \qquad (2\text{-}3)$$

in which $\overleftrightarrow{D}$ is the diffusion tensor of equation (1-6). The flux $\emptyset(z,t)$ of ions in particles/sec along the axis is related to the current density through the relation

$$\emptyset(z,t) = Aj(z,t) \ , \qquad (2\text{-}4)$$

where A is the area of the exit aperture and j(z,t) is the z component of the axial current density. Hence substituting the solution $n(\vec{r},t)$ of the diffusion equation into (2-3) and using (2-4) Gatland gets for the flux of ions exiting the drift tube on axis at time t after their creation

$$\emptyset(z,t) = \frac{Ase^{-\alpha t}}{4[\pi D_L t]^{\frac{1}{2}}} \left(v_d + \frac{z}{t}\right)\left[1 - \exp\left(-\frac{r_0^2}{4D_T t}\right)\right] \exp\left[-\frac{(z - v_d t)^2}{4D_L t}\right] . \qquad (2\text{-}5)$$

This is the equation from the model which describes the arrival time spectrum. Here z is the drift distance from the source to the end plate. In the present case α is set to zero since we are assuming depletion reactions are negligible. For a fixed length z one can increment the time parameter and calculate a distribution of arrival times which is a function of D_L, D_T, v_d, A, and s. The theoretical and experimental distributions may then be compared to determine the longitudinal diffusion coefficient. The A and s dependence drops out when the peaks of the two curves are normalized to unity. Moseley[25] has shown that the shape of the mathematical curve is insensitive to large variations of D_T, although the magnitude of the flux is certainly not. Normalization of the curve to a peak height of one only changes the absolute magnitude and not the shape. Although D_T is not known a priori, a theoretical value from the Einstein equation or the Wannier theory (see Chapter III) may be used without loss of accuracy. The drift velocity is the measured value determined from the same set of arrival time spectra at the E/N under consideration. After a smoothing procedure is applied to the raw experimental data, D_L is varied systematically until a satisfactory fit between the model and the experiment is obtained. A computer program fitting routine has been written to determine a D_L in this manner for each source position taken at the given E/N. Figure 3 shows a sample arrival time spectrum and the matching theoretical curve. The value of D_L calculated by this method should be identical for each source position at the same E/N; however, there are slight statistical fluctuations between the coefficients usually less than about 5% making it necessary to average the values for a final result.

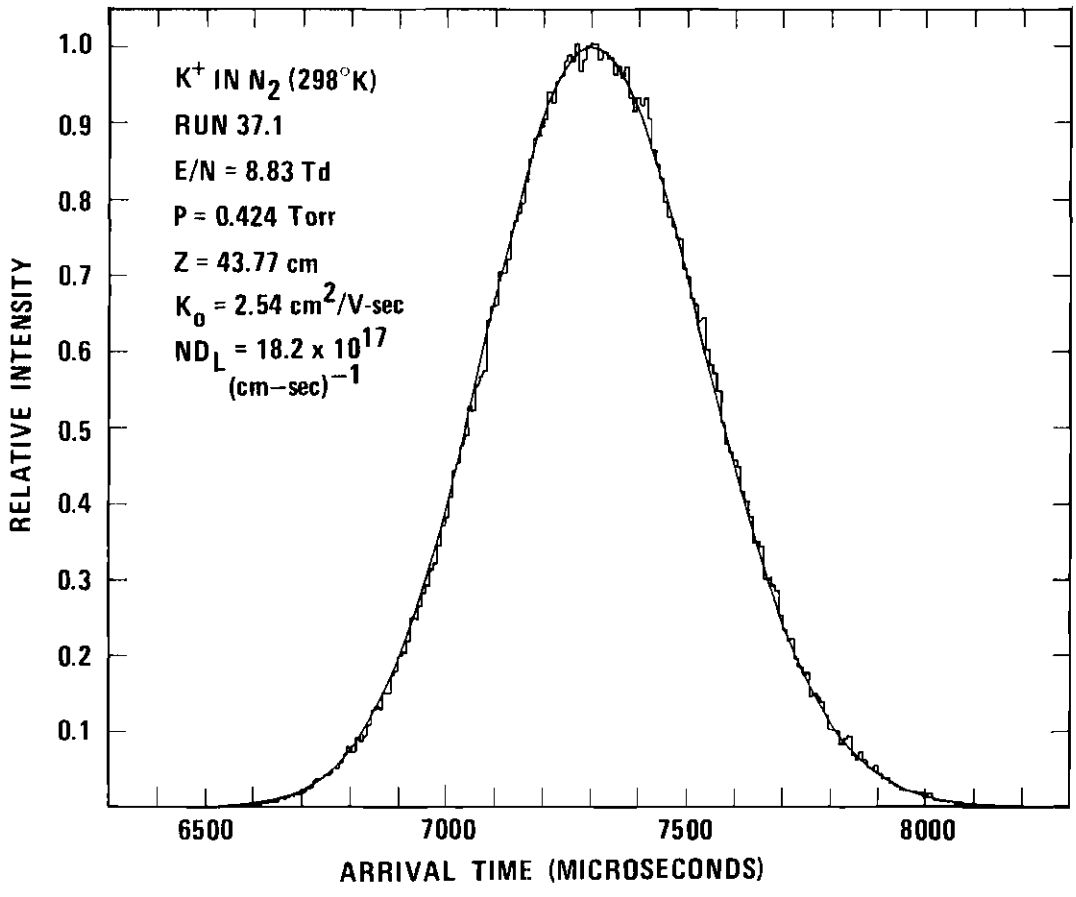

Figure 3. Sample Arrival Time Spectrum with Theoretical Fit for D_L

CHAPTER III

THEORETICAL CONSIDERATIONS

Review of Past Theory

The earliest work in the theory of mobility was carried out by Langevin. His first calculation in 1903[28] considered the ions and molecules to be solid elastic spheres in which the only interaction accounted for was the hard sphere repulsion occurring at impact. The theory was intended for low E/N and low ion densities. With the assumption that the mean free path of the ion was the same as that of the molecule and considering the crude nature of the calculation, it is not surprising that the predicted mobilities were systematically much higher than experiment. Also the variation of K with ionic charge, mean free path, and temperature was found to be incorrect.

Langevin was aware of the problems with his simple mean free path calculations and in 1905[29] published a much more rigorous theory based on the momentum transfer method developed earlier by Maxwell. This theory also applied only to low fields, but it accounted for not only the rigid sphere repulsive interaction, but also an attractive inverse fifth power force between the ions and molecules. An ion will induce a dipole moment in a nonpolar gas molecule, and the resulting attractive polarization force will have the form[30]

$$f = - 2\alpha e^2/r^5 , \qquad (3\text{-}1)$$

where α is the polarizability of the molecule, e is the electronic charge, and r is the ion-molecule separation distance. Of course if the gas is polar, there is direct attraction of the permanent dipoles. Equation (3-1) applies if r is large compared to the charge separation of the dipole.

Langevin's exhaustive treatment of this subject was frequently neglected and sometimes misunderstood by other workers in the field for about twenty years until Hassé[31] in 1926 made a recalculation of the numerical part of the paper. During the time when Langevin's work lay unnoticed two contrasting theories concerning the polarization attraction force arose. The "cluster-ion theory" proposed that the neutral molecules became permanently bound to the ions, and that the increased mass and size of the charge carrier were responsible for the low measured values of the mobilities. The other concept was the "small-ion theory" in which the size of the ion was relatively unimportant. Momentum transfers due to the attractive forces were thought to be mainly responsible for the slowing down of the ions in their motion through the gas.

In the notation of Hassé the expression for the mobility derived by Langevin for the case when the molecules are perfectly elastic spheres experiencing attractive forces of the form (3-1) is

$$K = \frac{A}{[\rho(K - 1)]^{\frac{1}{2}}} \left[1 + \frac{M}{m}\right]^{\frac{1}{2}}, \qquad (3\text{-}2)$$

where ρ is the mass density of the gas, K is the dielectric constant, M is the molecular mass, m is the ionic mass, and A is a numerical coefficient. A is a function of the parameter λ (not to be confused with the mean free path) where

$$\lambda^2 = \frac{8\pi P D_{12}^4}{(K - 1)e^2} . \qquad (3\text{-}3)$$

Here P is the gas pressure and D_{12} is the sum of the radii of the ion and molecule. The calculation of A in terms of λ is quite complicated and is one of the most important features of Langevin's 1905 paper. There are two limiting cases for the mobility. For the case of large λ where hard sphere scattering is the dominant interaction, the value of λA approaches 0.75 in the limit, and the mobility becomes

$$K_e = \frac{0.75e}{D_{12}^2[8\pi\rho P]^{\frac{1}{2}}}\left[1 + \frac{M}{m}\right]^{\frac{1}{2}} . \qquad \text{(elastic sphere limit)} \qquad (3\text{-}4)$$

At the other extreme $\lambda = 0$ and the polarization force prevails. The resulting mobility is

$$K_p = \frac{0.5105}{[\rho(K - 1)]^{\frac{1}{2}}}\left[1 + \frac{M}{m}\right]^{\frac{1}{2}} . \qquad \text{(polarization limit)} \qquad (3\text{-}5)$$

The result in (3-5) is independent of both ionic charge and gas temperature. The momentum loss of the ion due to collisions produced by the polarization forces is directly proportional to the ionic charge. Since the external electric force also varies as the charge, the two effects cancel giving a mobility which is charge independent. An increase in temperature increases the thermal motion of the ions and tends to decrease the mobility. However, the corresponding decrease in momentum loss raises the mobility just enough to cancel out any temperature dependence. The zero-field reduced mobility in (cm^2/V-sec) derived from Equation (3-5) is

$$K_0(0) = 35.9/[\mu\alpha]^{\frac{1}{2}} , \qquad (3\text{-}6)$$

where μ is the reduced mass given in units of the proton mass, and α is the polarization expressed in atomic units (a_0^3; a_0 = 1 Bohr radius).

The use of the complete Langevin equation (3-2) is hampered by the difficulty in estimating the sum of the ionic and molecular radii (D_{12}) which appears through the calculation of λ^2 in (3-3). Hence the polarization limit form has been a much more useful equation for the mobility, and in many cases the agreement with experiment is quite satisfactory. Wannier[17] has treated the high-E/N situation and has demonstrated that (3-6) is valid for the reduced mobility at any E/N provided that the polarization force is dominant.

In the years 1916-17 Chapman and Enskog[32] developed a rigorous kinetic theory for unionized monatomic gases. Although their original calculations applied only to neutral gases and not ions, the low-field mobility of an ion may be obtained from the mutual diffusion coefficient $\mathcal{D}_{12}$ which they derived by using the relation

$$K = \frac{e\mathcal{D}_{12}}{kT} . \qquad (3\text{-}7)$$

The Chapman-Enskog theory gives for the mutual diffusion coefficient

$$\mathcal{D}_{12} = \frac{3\sqrt{\pi}}{16}\left[\frac{2kT}{\mu}\right]^{7/2} \frac{1 + \epsilon_0}{(N_1 + N_2)P_{12}} , \qquad (3\text{-}8)$$

where

$$P_{12} = \int_0^\infty v_0^5 Q_d(v_0) e^{-\mu v_0^2/2kT} \, dv_0 \tag{3-9}$$

$$Q_d(v_0) = 2\pi \int_0^\infty (1 - \cos\theta) I_s(\theta) \sin\theta d\theta \, . \tag{3-10}$$

Q_d is just the cross section for momentum transfer, often called the diffusion cross section, with θ as the center of mass scattering angle and $I_s(\theta)$ the differential elastic scattering cross section. The quantity v_0 is the relative velocity of approach of the two particles. N_1 and N_2 are the gas and ionic number densities, respectively, with N_2 usually negligible compared to N_1. ϵ_0 is a small second order correction which may be neglected for many applications. P_{12} can be related to the omega or collision integral $\bar{\Omega}^{(1,1)}$ which frequently appears in kinetic theory. A familiar form of the omega integral is

$$\bar{\Omega}^{(1,1)}(T) = \frac{1}{2(kT)^3} \int_0^\infty Q_d(E) E^2 e^{-E/kT} \, dE \, . \tag{3-11}$$

Making the substitution $E = \frac{\mu v_0^2}{2}$ in (3-9) for P_{12} results in the relation

$$P_{12} = \left[\frac{2kT}{\mu}\right]^3 \bar{\Omega}^{(1,1)} \, .$$

If Q_d is independent of v_0, the omega integral is no longer a function of the temperature, and $\mathcal{D}_{12}$ then varies as $(T/\mu)^{\frac{1}{2}}$. By dimensional analysis[33] it can be shown that for a potential of the form $V(r) \sim r^{-n}$, Q_d varies as $v_0^{-4/n}$, which implies that $\mathcal{D}_{12}$ varies as $T^{2/n} T^{\frac{1}{2}}$. Hence the mobility is proportional to $T^{2/n} T^{-\frac{1}{2}}$. Thus the variation of mobility with temperature

can give useful information about the ion-molecule interaction.

As mentioned in Chapter I, Wannier[17] made vital contributions to both mobility and diffusion theory in his epic 1953 paper. Although he emphasized the high-E/N case, he also considered intermediate and to some extent low fields. He assumed the ion density to be small so that ion-ion interactions could be neglected, and all collisions were taken to be elastic. In the high-field case Wannier showed by dimensional analysis that the mobility for the model of a constant mean free path (for example, hard spheres) was proportional to $E^{-\frac{1}{2}}$, where E is the magnitude of the electric field strength. Similar reasoning gave a constant mobility for the constant mean free time model (constant τ) at both high and low fields. Wannier's formal treatment of the high-field case resulted in his obtaining a general expression connecting velocity averages derived from moments of the Boltzmann Equation. Using this moment equation it was possible to calculate the drift velocity, total energy, and energy partition for the constant τ case. The mobility so calculated was a constant and numerically equal to the value obtained for low fields. For this model at high fields Wannier's expression for the total energy of the ion was

$$E_{total} = \frac{1}{2}(m + M)v_d^2 + \frac{3}{2}kT \ , \qquad (3\text{-}12)$$

where m is the ionic mass and M the mass of the molecule. The first term on the right of (3-12) is the energy gained from the field which is divided into two parts, the visible drift energy $mv_d^2/2$, and the random field energy $Mv_d^2/2$. The ratio of the random field to the drift energy is thus M/m which reflects the ability of light ions to store energy in the form

of random motion. At sufficiently high E/N the thermal energy can be neglected.

Wannier also investigated the intermediate field region where he obtained a complete solution for the constant mean free time model as a convolution of the high-field and Maxwellian solutions. The calculated mobility was again, as expected, a constant. For the pure polarization attraction model ($V \sim r^{-4}$) and constant τ, Wannier found the mobility to be a constant, which is exact for both high and low fields. The constant mean free time model along with isotropic scattering yielded nearly the same results as the polarization case, which led Wannier to conclude that scattering is very nearly isotropic for the polarization force.

Recall that for an ion swarm of number density n moving in steady-state through a gas under the influence of a uniform electric field, the ionic flux density $\vec{j}$ is given by

$$\vec{j}(\vec{r},t) = n(\vec{r},t)\vec{v}_d - \overline{\overline{D}} \cdot \vec{\nabla} n(\vec{r},t), \qquad (2\text{-}3)$$

where the diffusion tensor has the form

$$\overline{\overline{D}} = \begin{bmatrix} D_T & 0 & 0 \\ 0 & D_T & 0 \\ 0 & 0 & D_L \end{bmatrix}. \qquad (1\text{-}6)$$

The first two components of the tensor are equal and are called the transverse diffusion coefficient. They apply to diffusion perpendicular to the

field. The third component, the longitudinal diffusion coefficient, describes diffusion parallel to the field.

In the limit of vanishing E/N, the ionic velocity distribution is Maxwellian and isotropic. Then D_T and D_L are equal and are related to the zero-field mobility K(0) by the Einstein equation (1-5):

$$D_T = D_L = D(0) = \frac{kT}{e} K(0) . \qquad (3\text{-}13a)$$

Here k is Boltzmann's constant. A useful form of the Einstein equation is

$$ND(0) = 2.315 \times 10^{15} K_0(0)T , \qquad (3\text{-}13b)$$

where ND(0) is in $cm^{-1}sec^{-1}$; $K_0(0)$, the zero-field reduced mobility, is in $cm^2/V\text{-}sec$; and T is in degrees Kelvin. At higher E/N the field causes the ionic velocity distribution to be skewed in the field direction. Some of the energy imparted to the swarm by the field is also manifest in increased transverse ionic motion due to the randomizing action of the ion-molecule collisions. Since collisions broaden both the transverse and longitudinal velocity distributions, one expects both D_L and D_T to increase with increasing E/N.

In addition to mobilities Wannier has also described diffusion at high E/N in terms of several different ion-molecule scattering models. One model, which has been tested by McDaniel and Moseley[34] with experimental data from various sources, is that of isotropic scattering and a constant mean free time between collisions. Another model, which will be

used here, assumes the ion-molecule interaction to consist of only the attractive polarization force (3-1) of which a constant mean free time between collisions is a consequence. As stated before, the results obtained for the two models are quite similar. Wannier's original equations for D_L and D_T based on the polarization model, which are numbered (149) and (150) in his paper, are

$$D_L = \frac{M + m}{Mm} 0.905\tau_s kT + \frac{1}{3} \frac{(M + m)^3 (M + 3.72m)}{M^2 m(M + 1.908m)} \left[\frac{eE}{m}\right]^2 (0.905\tau_s)^3 \quad (3\text{-}14)$$

$$D_T = \frac{M + m}{Mm} 0.905\tau_s kT + \frac{1}{3} \frac{(M + m)^4}{M^2 m(M + 1.908m)} \left[\frac{eE}{m}\right]^2 (0.905\tau_s)^3. \quad (3\text{-}15)$$

Here the mass of the ion is denoted by m, that of the molecule by M; τ_s is the ionic mean free time for spiralling collisions[17,35] and is a constant for this model. However τ_s is not a measurable quantity, but it can be expressed in terms of the experimentally determined mobility in the following manner. As E/N tends to zero the terms involving E in Equations (3-14) and (3-15) vanish. Since the Einstein equation governs diffusion in this limit, the remaining constant term can be equated to the Einstein value. Hence we have

$$\frac{M + m}{mM} 0.905\tau_s kT = D(0) = \frac{kT}{e} K(0) \quad (3\text{-}16)$$

using (3-13a). In terms of the zero-field reduced mobility we get

$$0.905\tau_s = \frac{mM}{m + M} \frac{K_0(0)}{e} \frac{N_0}{N} \quad (3\text{-}17)$$

which demonstrates that τ_s is indeed a constant at a given number density N. The number density at standard temperature and pressure is $N_o = 2.687 \times 10^{19}$ cm^{-3}. Substituting (3-17) into (3-14) and (3-15) one gets after putting in the values of the constants

$$ND_L = 2.315 \times 10^{15} K_0(0) T + 6.701 \times 10^{11} \frac{M(M + 3.72m)}{(M + 1.908m)} \left(\frac{E}{N}\right)^2 \left[K_0(0)\right]^3 \quad (3\text{-}18)$$

$$ND_T = 2.315 \times 10^{15} K_0(0) T + 6.701 \times 10^{11} \frac{(M + m)M}{(M + 1.908m)} \left(\frac{E}{N}\right)^2 \left[K_0(0)\right]^3, \quad (3\text{-}19)$$

where $K_0(0)$ is the zero-field reduced mobility in cm^2/V-sec; T the gas temperature in degrees Kelvin; m and M the ion and molecule masses in amu; and E/N expressed in Td. Equations (3-18) and (3-19) are the original, unmodified Wannier equations for the constant mean free time case.

Improved agreement with experimental data can be achieved if the original Wannier equations are modified to remove some of the model dependence. A natural change to make in (3-18) and (3-19) is to replace the zero-field reduced mobility $K_0(0)$ in the field dependent term by the reduced mobility measured at the particular E/N being considered. Thus τ_s is now in effect being allowed to vary as a function of E/N. The resulting equation for the longitudinal diffusion coefficient is then

$$ND_L(E) = 2.315 \times 10^{15} K_0(0) T + \quad (3\text{-}20)$$

$$6.701 \times 10^{11} \frac{M(M + 3.72m)}{(M + 1.908m)} \left(\frac{E}{N}\right)^2 \left[K_0\left(\frac{E}{N}\right)\right]^3 .$$

The $ND_L(E)$ signifies the additional field dependence in the modified form

of the Wannier equation. $K_0(E/N)$ indicates the functional dependence on E/N. Using (1-3) K_0 can be eliminated in favor of the drift velocity to get

$$ND_L(E) = 2.315 \times 10^{15} K_0(0) T + \qquad (3\text{-}21)$$

$$0.3455 \times 10^{17} \frac{M(M + 3.72m)}{(M + 1.908m)} \frac{v_d^3}{E/N},$$

where v_d is in units of 10^4 cm/sec and E/N in Td. The effect has been to transform from the constant τ_s to the observable variable v_d. This technique has been discussed by McDaniel and Moseley[34] and McDaniel and Mason[24]; the latter reference discusses in greater detail the theoretical implications of the procedure. The results (3-20) and (3-21) are sometimes called the "free flight" ND_L values due to the use of the mean free time concept.

Also in 1953[21] Kihara published a paper on the general theory of ion mobility which was not restricted to a particular ion-neutral interaction or mass ratio. Kihara assumed only binary collisions between ions and neutrals and sufficiently low ion densities to ensure that the use of a Maxwell velocity distribution for the neutral gas was justified. The theory is valid for all field strengths, but the expansion of the mobility in a power series in the square of the field strength limits the practical application to low E/N.

Whealton and Mason[36] have extended the general theory of ion mobility formulated by Kihara to include ion diffusion and mixtures of neutral gases. The results are valid for any mass ratio and all ion-neutral

potentials provided the scattering is elastic. They have solved the linearized Boltzmann equation by a moment expansion method to obtain the mobilities and diffusion coefficients as functions of the electric field strength and temperature. Successive iterations of the moment equations lead to an expansion of the longitudinal diffusion coefficient in terms of $(E/N)^2$. The result, to first order, may be put in the form

$$D_L = D_L(E)\left[1 + \frac{d\ell nK}{d\ell n(E/N)}\right], \tag{3-22}$$

where $D_L(E)$ is the free flight value given by Equation (3-20). The first order correction to the transverse diffusion coefficient vanishes. Robson,[37] using arguments based on nonequilibrium thermodynamics, has obtained results similar to those of Whealton and Mason. Viehland and Mason[23] have also obtained (3-22) using the approach to be discussed in the next section.

The Viehland-Mason Transport Theory

The prediction and interpretation of most phenomena involving ions in neutral gases depends on knowledge of the ion-neutral interaction potential. Since ab initio calculations are extremely difficult for most systems, the usual method employed to get the interaction potential is the careful analysis of accurate measurements of a property which depends on it in a well established way. Such a procedure has been followed for the mobility of trace amounts of ions in neutral gases under the influence of very weak electric fields, the only case for which the transport theory is highly developed. The success of this method depends, of course, on

the fact that all transport phenomena depend on the scattering properties of the particles involved and hence on the interaction potentials. Clearly, if low-field ionic mobility data are to be utilized for this purpose, it is desirable to obtain the data over the widest possible range of gas temperature. However, there are substantial experimental difficulties associated with reliably measuring ionic mobilities at temperatures far above or below room temperature. Very few good experimental data are available on the low field mobility of ions as a function of the gas temperature, and the temperature range of the data is limited--usually to a few hundred ^{o}K. Hence, this approach has been of very limited utility.

However, variation of the electric field has roughly the same effect as variation of the gas temperature, and it permits the average ionic energy to be varied from the thermal value up to about 10 eV in drift velocity measurements. For a long time it has been realized that if mobility data covering such a wide range of ionic energy could be quantitatively and accurately analyzed, information on the ion-neutral interaction potential could be derived that would span a very wide range of ion-neutral separation distance. The snag has been that up to now accurate mobility theory for arbitrary mass ratios and interaction potentials has been available only for the region of very low E/N, where the ions are close to being in thermal equilibrium with the gas molecules. Viehland and Mason[23] have recently developed the first rigorous kinetic theory for the mobility of gaseous ions which applies at electric fields of arbitrary strength. A brief description of this theory and how it can be used to obtain ion-neutral interaction potentials follows.

The starting point for the theory is the Boltzmann Equation, in which the neutral gas molecules are assumed to have a Maxwellian velocity distribution function. It is not assumed however, as in weak-field treatments, that the ionic distribution function f_i is only slightly perturbed from equilibrium. Hence the standard Chapman-Enskog procedure is not applicable. Since the Boltzmann Equation itself is not amenable to direct solution except in a few special cases which unfortunately do not apply here, another approach is necessary. One usually attacks the problem via the moment method in which an equation relating moments of f_i is derived from the Boltzmann Equation. This procedure is acceptable because macroscopic quantities of interest, such as the drift velocity, can be expressed as moments of the ionic distribution. The solution to the moment equation requires the choice of a basis set of functions $\psi_{\ell m}^{(r)}$ which are themselves functions of the ionic velocity. A series expansion is made in terms of the $\psi_{\ell m}^{(r)}$ and the resulting set of algebraic equations are solved by a method of successive approximations. Rapid convergence of the successive solutions naturally depends upon the choice of the basis functions. It has been customary to use Burnett functions for the $\psi_{\ell m}^{(r)}$ since they are eigenfunctions for the Maxwell model of the inverse 4th power potential.[21] The use of these functions however leads to a power series or a ratio of polynomials in the field strength E, and the result is then necessarily limited to low E because of divergence difficulties. The source of the difficulty is that at high fields the ionic temperature is different from the gas temperature and the Burnett functions fail to take this into account. Viehland and Mason chose to use a different basis

set, namely the (Burnett-like) spherical polar functions which have the form

$$\psi_{\ell m}^{(r)} = W^{\ell} S_{\ell+\frac{1}{2}}^{(r)}(W^2) P_{\ell}^{|m|}(\cos\theta) e^{im\phi} , \qquad (3\text{-}23)$$

where

$$W^2 = \frac{mv^2}{2kT_i} . \qquad (3\text{-}24)$$

Here v is the ion velocity, $S_{\ell+\frac{1}{2}}^{(r)}$ are the Sonine (Generalized Laguerre) polynomials, $P_{\ell}^{|m|}$ are the associated Legendre polynomials with θ and ϕ the polar and azimuthal angles with respect to the field direction. The essential difference between this treatment and previous ones is the appearance of the parameter T_i having the dimension of a temperature. T_i is allowed to vary in order to effect the quickest convergence of the successive solutions to the moment equation. All choices of T_i should lead to the same result. The quantity T_i is the temperature associated with the total energy of the ions. At low fields the appropriate choice is $T_i = T$ which is consistent with results from the usual theories of ion mobility and diffusion. In this case the $\psi_{\ell m}^{(r)}$ reduce to the ordinary Burnett functions which are identical to (3-23) and (3-24) with the parameter T_i replaced with the gas temperature T. At high fields it is assumed that the ionic energy is entirely derived from the field, implying that T_i should be proportional to v_d^2. This dependence of T_i at high fields is the property which enables the Viehland-Mason results to be valid at all values of E/N. When the ion temperature is allowed to be different from

the gas temperature, it is then possible to define an "effective ion temperature" T_{eff} by the relation

$$T_{eff} = \frac{mT + MT_i}{m + M} . \tag{3-25}$$

At low fields the choice $T_i = T$ yields $T_{eff} = T = T_i$ and for high E, T_{eff} varies as v_d^2.

In the solution of the moment equation to obtain the mobility and diffusion coefficients, it is necessary to specify T_i more precisely. In keeping with the assumptions above, the natural choice is

$$\frac{3}{2} kT_i = \frac{3}{2} kT + \frac{1}{2} mv_d^2 + \frac{1}{2} Mv_d^2 , \tag{3-26}$$

where $mv_d^2/2$ is the drift energy of the ion derived from the field and $Mv_d^2/2$ is the memory energy or the random field energy. This form is the same as that derived by Wannier for the total ion energy at high fields. Substituting (3-26) into (3-25) results in

$$\frac{3}{2} kT_{eff} = \frac{3}{2} kT + \frac{1}{2} Mv_d^2 \tag{3-27}$$

which describes T_{eff} as the temperature associated with the total random energy of the ion. Using (3-26) as the choice of T_i, Viehland and Mason derive a first order expression for the drift velocity as a function of E and the omega integral. The equation is identical to that obtained by free flight methods with the exception of the appearance of T_{eff} in the omega integral in place of the usual gas temperature T.

To check convergence of their approximate solutions, Viehland and Mason compare their results to four special cases for which the mobility is rigorously known. The four cases are:

(1) $m \ll M$ with a rigid sphere potential for which the mobility may be determined exactly by numerical integration;

(2) $m = M$ with a rigid sphere interaction for which the mobility has been done by Monte Carlo methods;

(3) arbitrary mass ratio and rigid spheres for the high field limit only. For $m \ll M$, this problem can be solved numerically; the case $m \gg M$ can be solved exactly, since the ionic velocity distribution function is a delta function. Monte Carlo calculations exist for the finite arbitrary mass ratios;

(4) arbitrary mass ratios and a repulsive r^{-n} potential at high fields where Monte Carlo results are also available.

In all cases the approximation scheme appears to converge and the first approximation is never in error by more than about 10%. The success achieved by using (3-26) for the choice of the parameter T_i gives further justification for calling T_{eff} an effective ion temperature.

By rearranging their first order approximation for the drift velocity, Viehland and Mason obtain an expression for the omega integral as a function of the effective temperature. They derived the result

$$\bar{\Omega}^{(1,1)}(T_{eff}) = 497.4 \frac{z}{v_d} \left(\frac{1}{\mu T_{eff}}\right)^{\frac{1}{2}} \frac{E}{N} , \qquad (3\text{-}28)$$

where

$$T_{eff} = T + 0.4009Mv_d^2 \ . \qquad (3\text{-}29)$$

Here $\bar{\Omega}^{(1,1)}$ is expressed in $\mathring{A}^2$, z is the number of electric charges, μ is the reduced mass in g/mole or amu, E/N in Td, v_d in units of 10^4 cm/sec, and both T and T_{eff} in degrees Kelvin. Here T_{eff} is a function of E/N through the drift velocity, v_d. Experimental mobility data can be used to calculate the omega integral as a function of the effective temperature. Then an appropriate form such as

$$V(r) = Ae^{-\alpha r} + \frac{B}{r^4} + \frac{C}{r^6} + \frac{D}{r^8} \ , \qquad (3\text{-}30)$$

where B is usually known, is chosen for the interaction potential from which a numerical calculation of the diffusion cross section and the omega integral is then made. The parameters are systematically varied to obtain the best agreement between theory and experiment. The enormous range of temperature covered by this method, typically 300 to 20,000 degrees Kelvin or more, yields information about the potential over a much wider range of separation distances than can be achieved by beam experiments. Accurate interaction potentials over a wide range of separation distance are important since V(r) must be known (or assumed) to make many theoretical predictions. For example, both the classical and quantal calculation of cross sections for various atomic processes requires knowledge of the potential. Plots of $\bar{\Omega}^{(1,1)}$ versus T_{eff} for the mobility data of this experiment appear in Chapter IV. Short range repulsive potentials have been determined for a number of ion-molecule combinations from high energy beam scattering experiments. Omega integrals calculated from such

potentials serve as a check on the validity of the Viehland-Mason theory. Comparison with the beam data is quite favorable.

The emergence of an effective temperature T_{eff} leads to an important concept concerning the variation of mobility with temperature. Once the field variation of the mobility or drift velocity is known, Equation (3-29) can be used to find the effective temperature corresponding to a particular E/N. The omega integral at T_{eff} may be found from (3-28). Thus we now have a method of getting the collision integral as a function of temperature by knowing the field dependence of the drift velocity at a single value of T which is usually low (room temperature). The Chapman-Enskog[24,32] formula for the mobility as a function of temperature is valid at low field strengths and is given in the first approximation by

$$K = \frac{3}{16}\frac{e}{N}\left(\frac{2\pi}{\mu kT}\right)^{\frac{1}{2}}\frac{1}{\bar{\Omega}^{(1,1)}_{(T)}} \quad . \tag{3-31}$$

We can substitute into this equation the $\bar{\Omega}^{(1,1)}(T_{eff})$ at the temperature T_{eff} to obtain the mobility at <u>low fields</u>, but corresponding to a gas temperature T_{eff}. Hence, it is possible through the Viehland-Mason theory to convert high-field mobility data at low temperatures to zero-field mobilities at high temperatures. This procedure is made possible by allowing the low density ions in a gas subjected to medium and strong electric fields to have an ion temperature different from that of the surrounding gas.

This equivalence property is not too surprising when one looks at the collision process itself. The scattering properties depend upon the interaction potential between an ion and neutral particle and also upon

the relative velocity. It should make no difference in the details of a particular collision and ultimately to the mobility whether the relative velocity of approach is caused by thermal motion at a high temperature (and low field) or by a large electric field at low temperature. Hence we may think of a mobility measurement in either context. As an example of this duality consider Equation (3-31) derived by Chapman and Enskog for the low field mobility. If one solves for $\bar{\Omega}^{(1,1)}$ and replaces the gas temperature T by the effective temperature T_{eff}, one obtains exactly the result (3-28) derived by Viehland and Mason, where now the mobility must be associated with high fields and low temperatures of the laboratory measurement.

The transformation from field dependence to temperature dependence allows one to obtain the zero-field reduced mobility as a function of temperature through the omega integral. The intermediate step of actually calculating $\bar{\Omega}^{(1,1)}$ may be circumvented by substituting (3-28) directly into (3-31). The result is for singly charged ions

$$K_0(0) = 37.214 \frac{v_d}{(E/N)} , \qquad (3\text{-}32)$$

for E/N in Td, v_d in 10^4 cm/sec, and $K_0(0)$ in cm^2/V-sec. Table 1 gives some typical values of the zero-field reduced mobilities. The effective temperature T_{eff} is calculated from Equation (3-29) using the experimentally determined drift velocities measured as a function of E/N. The zero-field reduced mobility is then determined from (3-32). The K^+-D_2 experimental data are that of Miller, et al.[12] The K^+-N_2 and K^+-CO drift velocities are from Thomson, et al.[3] All other data are from the present experiment

Table 1. Zero-field Reduced Mobilities of K^+ Ions in Various Gases as a Function of the Effective Temperature. The mobilities are reduced to the standard gas number density $2.69 \times 10^{19}/cm^3$ and expressed in $cm^2/V\text{-}sec$. T_{eff} is expressed in degrees Kelvin.

T_{eff}	$K_0(E/N \rightarrow 0)$									
	K^+-H_2	K^+-D_2	K^+-He	K^+-Ne	K^+-CO	K^+-N_2	K^+-NO	K^+-O_2	K^+-Ar	K^+-CO_2
300	13.1	9.35	21.5	7.43	2.31	2.53	2.28	2.72	2.67	1.45
400	13.5	9.60	21.8	7.62	2.33	2.58	2.29	2.75	2.74	1.42
500	14.0	9.90	21.7	7.75	2.35	2.62	2.33	2.85	2.85	1.39
600	14.5	10.3	21.6	7.82	2.38	2.66	2.37	2.94	2.96	1.37
800	15.4	11.0	21.1	7.84	2.43	2.72	2.44	3.09	3.09	1.35
1,000	16.0	11.6	20.5	7.78	2.48	2.78	2.50	3.20	3.18	1.34
1,200	16.5	12.1	20.0	7.69	2.52	2.84	2.56	3.27	3.23	1.34
1,500	17.0	12.5	19.3	7.53	2.57	2.89	2.63	3.34	3.29	1.36
1,800	17.1	12.6	18.6	7.36	2.62	2.93	2.70	3.39	3.31	1.37
2,000	17.2	12.7	18.2	7.25	2.65	2.95	2.73	3.42	3.32	1.39
2,500	17.1	12.6	17.3	6.98	2.70	2.99	2.79	3.46	3.28	1.43
3,000	16.8	12.5	16.6	6.72	2.73	3.02	2.83	3.48	3.24	1.46
3,500	16.5	12.3	15.9	6.48	2.75	3.03	2.87	3.49	3.21	1.49

Table 1. (Continued)

T_{eff}	$K_0(E/N \rightarrow 0)$									
	K^+-H_2	K^+-D_2	K^+-He	K^+-Ne	K^+-CO	K^+-N_2	K^+-NO	K^+-O_2	K^+-Ar	K^+-CO_2
4,000	16.2	12.1	15.3	6.28	2.76	3.05	2.88	3.48	3.18	1.51
5,000	15.6	11.5	14.4	5.94	2.77	3.04	2.89	3.45	3.10	1.56
6,000	15.0	10.9	13.7	5.70	2.76	3.03	2.88	3.37	3.03	1.60
8,000	13.8	9.75		5.4	2.72	2.96	2.84	3.24	2.90	1.66
10,000	13.1	8.8			2.67	2.89	2.80	3.13	2.79	1.70
12,000	12.6	8.1			2.63	2.82	2.75		2.69	1.72
15,000	12.2				2.55	2.72	2.68		2.57	1.73
18,000	12.0				2.48	2.63	2.62		2.47	1.73
20,000					2.44	2.57	2.58		2.41	1.73

and are reported in Chapter IV. It is interesting to note that reduced mobility data plotted as a function of the parameter E/N also represent the zero-field reduced mobility values as a function of temperature if the appropriate effective temperature scale is added. The mobilities on the graph do not change their ordinate value. Only the abscissa scale need be altered. Hence we are essentially saying that a mobility measurement is only a number subject to either of two interpretations. The Viehland-Mason theory enables us to write the following equation:

$$K_0(0,T_{eff}) = K_0(E/N,T) \tag{3-33}$$

where $K_0(0,T_{eff})$ is the reduced mobility in the zero-field limit at temperature T_{eff} given by (3-29); $K_0(E/N,T)$ is the reduced mobility at the E/N corresponding to T_{eff} and T is the gas temperature.

The theoretical work discussed above has been strictly classical in nature. Quantum effects are usually important only when the de Broglie wavelength of the ions is comparable to the separation distance between molecules, for example when the number density is very large ($N \gg 10^{19}$ cm^{-3}) or the temperature is extremely low. Also if the ion and gas molecules have identical cores, symmetry effects such as resonant charge transfer require quantal treatments. The essential difference between classical and quantal results lies in the calculation of the differential cross section $I_s(\Theta)$ which depends on the ion-molecule interaction. The success of the classical theory is in part due to the appearance of the factor $(1 - \cos\Theta)$ in the diffusion cross section Q_d. This factor decreases the effect of small angle scattering where $I_s(\Theta)$ makes the largest contribution to the integral.

CHAPTER IV

MOBILITIES

In this chapter the reduced mobilities of K^+ ions in the seven gases He, Ne, Ar, H_2, O_2, NO, and CO_2 are presented as functions of the parameter E/N. The temperature of the neutral gases was in each case within 5 degrees of 300^oK, so the data are stated to be at a nominal temperature of 300^oK for convenience. The measured values of T are tabulated for each E/N in Appendix I. It should be noted again that to compare data with other experiments a number density normalization must be made. The number density an ideal gas assumes at 0^oC and 760 Torr is the Loschmidt Number, $N_0 = 2.69 \times 10^{19}$ particles/cm^3. Elementary theory shows that the mobility K varies as 1/N, which allows the definition of a reduced mobility K_0 given by the expression

$$K_0 = K \frac{N}{N_0} = K \frac{P}{760} \frac{273.16}{T} . \qquad (4\text{-}1)$$

Even though T appears in this formula, it is strictly a number density normalization and the resulting K_0 refers to the original temperature T at which the measurement was made and not to the standard temperature of 273.16^oK. T and P, which can be experimentally measured, enter the expression only to calculate the number density using the ideal gas law. The normalization is carried out holding the temperature constant, with no assumption about how the mobility varies with T. The result is that

K_0 is still an explicit function of T, i.e., $K_0 = K_0(E/N,T)$. When comparing zero-field mobilities taken at different T, one must assume that K_0 does not vary appreciably with temperature over some small range of T which may be as large as 10 to 15°K. To make reasonable comparisons, the variation probably should not be more than about 1% since experimental errors are typically less than 2%. Indications are that in some cases there may be as much as 1% or more variation, especially in gases where there is resonant charge transfer.

Also in this chapter are plots of the omega or collision integrals, $\bar{\Omega}^{(1,1)}$, versus effective ion temperature. The longitudinal diffusion coefficient data are found in the next chapter.

Ion Production and Boundary Effects

As mentioned in Chapter II, the potassium ions were produced thermionically by directly heating a platinum mesh filament coated with potassium feldspar. The ions so created are singly charged and in the ground state. Trace amounts of other alkali ions were detected, the most abundant of which was Na^+, but their intensities were not consistently high enough to permit a thorough investigation of their transport properties. The presence of alkalis other than potassium should have no effect on the measurement of the K^+ ions, since the number densities of each ionic species is very much less than that of the neutral gas. However, to ensure that ion-ion interactions or space charge effects do not influence the data, the source current is varied to see if there is any change in the arrival time spectrum.

Since the alkali ions possess a closed shell electronic structure

($1s^2\ 2s^2\ 2p^6\ 3s^2\ 3p^6$ for K^+), ion-molecule reactions involving the breaking of chemical bonds and the formation of new bonds are not likely to be significant in this experiment. There was no distortion or unusual structure to the arrival time spectrum which would indicate any appreciable reactions. However, it is known that clustering reactions of the form

$$K^+ + 2M \rightleftarrows K^+ \cdot M + M\,, \qquad (4\text{-}2)$$

where M is a neutral gas molecule or impurity ion, are possible. Thomson[3] reported the existence of K^+ clusters for CO_2, NO, CO, N_2, O_2, Ar, D_2, Ne, and He in order of decreasing abundances. Clusters are expected to form at low E/N and high pressures; hence for each gas studied checks for cluster formation were made. Operation of the drift tube was restricted to conditions where the intensity ratio of clustered to unclustered K^+ ions was usually less than about 1%, with the exception of CO_2 which will be discussed later in this chapter. The presence of clusters (or dimers as they are sometimes known) are not always an evil, although they have confused matters for drift tube experimenters without mass spectrometers for quite some time. In certain cases it is possible to determine the reaction rate for (4-2), as was done in the case of $CO^+ \cdot CO$ in this laboratory.[38]

Another problem associated with ion production involves the Tyndall gate which admits the ion pulse into the drift region. Sometimes 20 to 40 volts on this grid are necessary to have sufficient ion intensity to permit a data run. These setups usually occur at the extremes of the E/N range where control of the ions is most difficult. The effect of high

Tyndall grid voltages is to inject or throw the ions into the drift region with a non-zero initial drift velocity thus violating the source boundary condition of the mathematical model. There is then some distance inside the drift chamber where the ions are not in a condition of steady-state drift within the gas. Hence the drift length becomes uncertain by the same amount, which is undoubtedly at least several mean free paths. As the mean free path at 0.1 Torr is about 0.06 cm, even two or three collisions to randomize the ionic motion mean a 0.5 to 0.75% error in the drift distance at 25 cm corresponding to position 4. Due to the use of a differencing technique made possible by the movable ion source, the mobilities are not appreciably affected by the injection of the ions. However, the longitudinal diffusion coefficients would be erroneously high in this case since the ion cloud would initially diffuse at a greater rate than it normally should. The effect was apparent in the gas CO_2 where ND_L in the zero-field region was consistently higher than the Einstein value when relatively high Tyndall grid voltages were used. It was found that good agreement with the Einstein value could be obtained if great care was taken to set up the runs at lower gate voltages, meaning a decrease in ion intensity and hence substantially longer data accumulation times. This compromise was made throughout in an attempt to obtain higher quality data.

Another type of boundary condition which arises in drift tubes is due to the radial extent of the electric field uniformity. Beyond a certain radius (6 cm in the Georgia Tech apparatus) the electric field becomes appreciably nonuniform, resulting in either a sweeping away of ions to the guard ring walls or a reflection of particles back into the drift

region where they stand a chance of being detected. Since the analysis model does not account for this type of reflection, checks must be made to see that this fraction of ions is negligible. Schummers[39] and Graham[40] have shown that for $4D_T t < 30$ cm^2, fewer than 1% of the detected ions have diffused radially past 6 cm and back on axis. For each gas $4D_T t$ was calculated at a low, intermediate, and high value of E/N. The Wannier free flight D_T was used, and the drift times were in each case those for position 7 which gave the largest value. The worst cases occur at the low E/N's. When the values of $4D_T t$ are normalized to 0.1 Torr for comparison, only NO, Ne, and H_2 with values of 30.9, 36.0, and 45.9 cm^2, respectively, exceed 30 cm^2. To force $4D_T t$ below 30 would require pressures of at least 0.103, 0.120, and 0.153 Torr, respectively; at low E/N's the real pressures used in the drift tube for the runs easily surpassed these limits. Thus radial diffusion effects should present no difficulties in these measurements.

Experimental Data

The reader is again referred to Appendix I for a tabulated listing of all mobility and diffusion data. In these measurements an attempt was made to cover the widest possible range of E/N without compromising the quality of the data. Theory predicts that the mobility will become a constant in the limit of vanishing E/N, that is when zero-field conditions exist. In practice the zero-field state is typically reached at E/N's below about 5 to 10 Td for K^+ ions in the gases considered in this experiment, as evidenced by a flattening out of the reduced mobility curves for this range of E/N. Mobility measurements at E/N's lower than about 1 Td

are usually very difficult to take due to a lack of sufficient ion intensity. However, this circumstance frequently does not present a problem since the reduced mobility generally has attained its constant value at this E/N, and hence only enough measurements in the low E/N range to obtain a good average zero-field value are necessary.

At high E/N there are two experimental difficulties which ultimately limit the measurements for the Georgia Tech drift tube. For high E/N runs E is generally quite large (5 to 6 V/cm) and P fairly low (0.025 to 0.100 Torr). Depending upon the gas and its pressure, a glow discharge, originating from the high voltage connections inside the drift tube, will occur as E is increased to around 7 V/cm. The glow permeates the entire drift region, and the avalanche of ions saturate the detection equipment. Of course it is impossible to take data under such conditions. Attempts to shield the high voltage feedthroughs from ground were not successful in eliminating the glow discharge. It became obvious that to correct the problem major changes in the design of the drift tube would be necessary. Hence, the decision was made not to modify the apparatus and to take data at the highest E/N's attainable without setting off the glow. These E/N's, although limited to a degree, still cover a significantly wide range.

A second problem at high E/N arises when neutral gas pressures less than about 0.050 Torr are used. Mean free paths of the molecules at 0.025 Torr and 300^{o}K are then of the order 0.25 cm. Thus there may be problems associated with conventional swarm analysis for paths that large. In fact, pronounced distortion of the arrival time spectrum has been observed as the pressure was lowered to less than 0.005 Torr. However, all data presented here were taken at pressures of 0.025 Torr or greater where there

was little or no distortion apparent. Nevertheless, the experimental error at high E/N and low pressures must be somewhat larger than that at the low and intermediate E/N where higher pressures could be used. An estimate of the experimental error at high E/N is discussed in the error analysis section following the presentation of the data.

K^+ in Ar

In Fig. 4 are the results of the mobility measurements for K^+ ions in Ar taken at nominally 300°K. The limits of the parameter E/N were 1.00 Td at the low side and 610 Td at the high end, where the pressures were 0.984 and 0.0246 Torr, respectively. There is a pronounced hump in the mobility curve which peaks at about 125 Td. Using Equation (3-12) the average energy of the ion ranged from the thermal value of 0.039 eV at 1 Td to 6.0 eV at the highest E/N. The peak occurred at an energy of roughly 0.55 eV. The number on the graph next to the arrow is the zero-field reduced mobility which was measured to be (2.66 ± 0.05) cm^2/V-sec by averaging the low E/N points. This value may be compared to that measured by Tyndall[4] who obtained 2.63 cm^2/V-sec; the Langevin polarization limit as given by Equation (3-6) yields a $K_0(0)$ of 2.43 cm^2/V-sec. Elford[10] obtained (2.64 ± 0.02) cm^2/V-sec at pressures of 1.4 to 190 Torr which are considerably higher than those used in this experiment. In an earlier paper[8] Elford reported mobilities up to an E/N of 183.8 Td. Agreement with his data is excellent for E/N's less than about 40 Td, above which his data are lower than the Georgia Tech data by about 2%. Creaser,[20] who got a $K_0(0)$ of 2.67 cm^2/V-sec, also agrees well with the present data. The mobility at very high E/N may be compared to that of Skullerud[16] who covered the range from 22.9 to 793 Td with pressures from

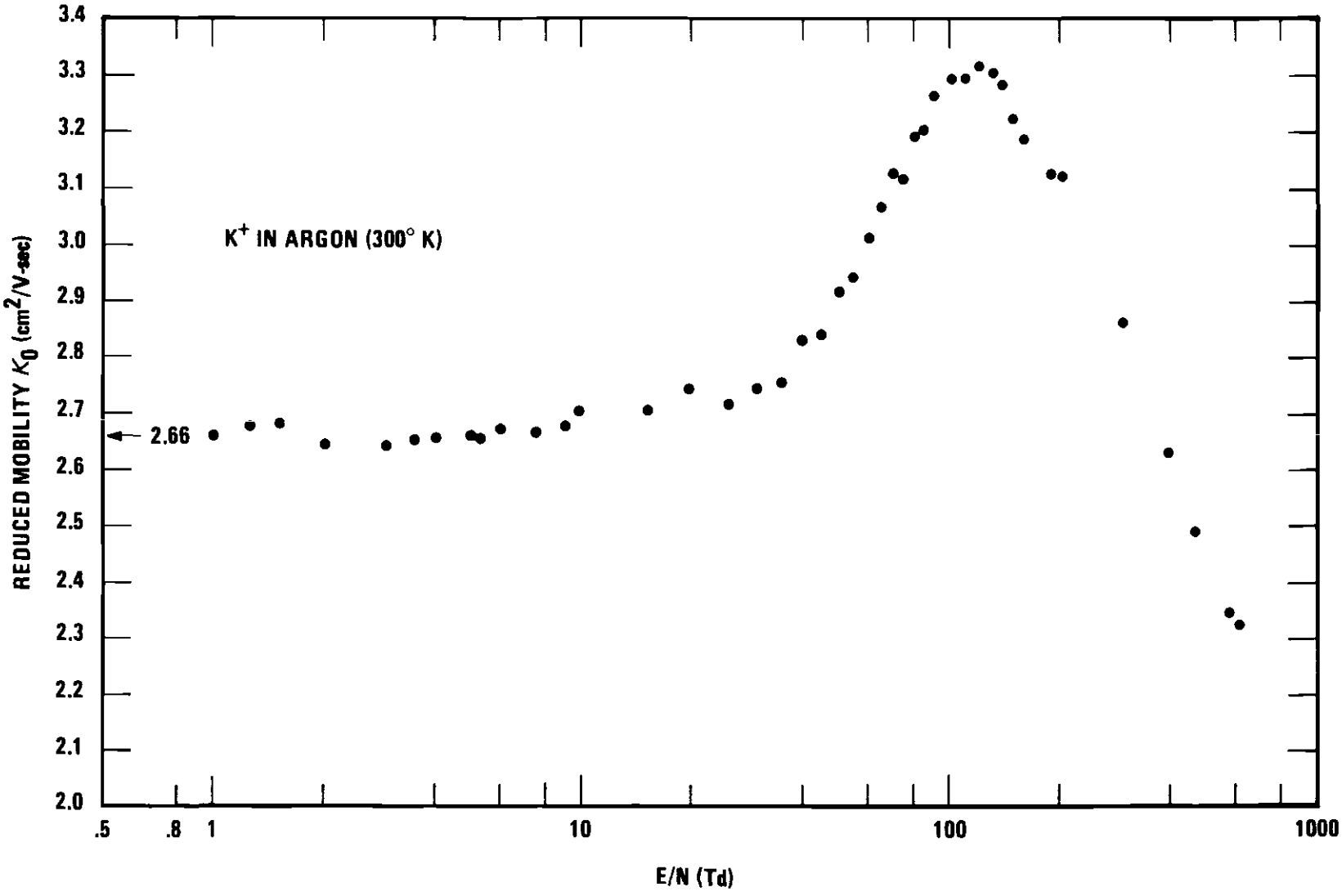

Figure 4. Reduced Mobilities for K^+ Ions in Argon as a Function of E/N at $300^{\circ}K$

0.14 to 1.0 Torr. For all E/N, and especially for those over 150 Td, agreement with Skullerud's data is excellent. Keller, Beyer, and Colonna-Romano[19] did not measure the mobility as a function of E/N, but did obtain a zero-field reduced mobility of (2.73 ± 0.06) cm^2/V-sec. The zero-field reduced mobilities obtained in this work are compared with previous measurements in Table 2.

K^+ in He

The solid circles of Fig. 5 represent the reduced mobilities of K^+ ions drifting in He. For this set of measurements the lowest E/N was 1.01 Td and the highest was 152 Td. The pressures ranged from 0.0982 Torr at the higher E/N's to 0.491 Torr at the low end. A zero-field reduced mobility of (21.6 ± 0.4) was determined from the flat part of the curve. The characteristic rise in the mobility curve as the E/N is increased just past the thermal region is barely visible in the He data at approximately 18 Td.

Tyndall's value of 21.5 cm^2/V-sec for $K_0(0)$ is in good agreement with the present data. The polarization limit of 16.1 cm^2/V-sec however is too low by more than 25%. Creaser[20] also obtained 21.5 cm^2/V-sec and his points lie consistently lower than the Georgia Tech data over the range of 9 to 82 Td covered by his experiment. However, all the points lie within the range of overlap of uncertainties. Elford and Milloy[10] measured (21.3 ± 0.2) cm^2/V-sec for $K_0(0)$ after corrections for the pressure effect discussed earlier in Chapter I had been made.

K^+ in H_2

The open circles in Fig. 5 show the variation of K_0 with E/N for

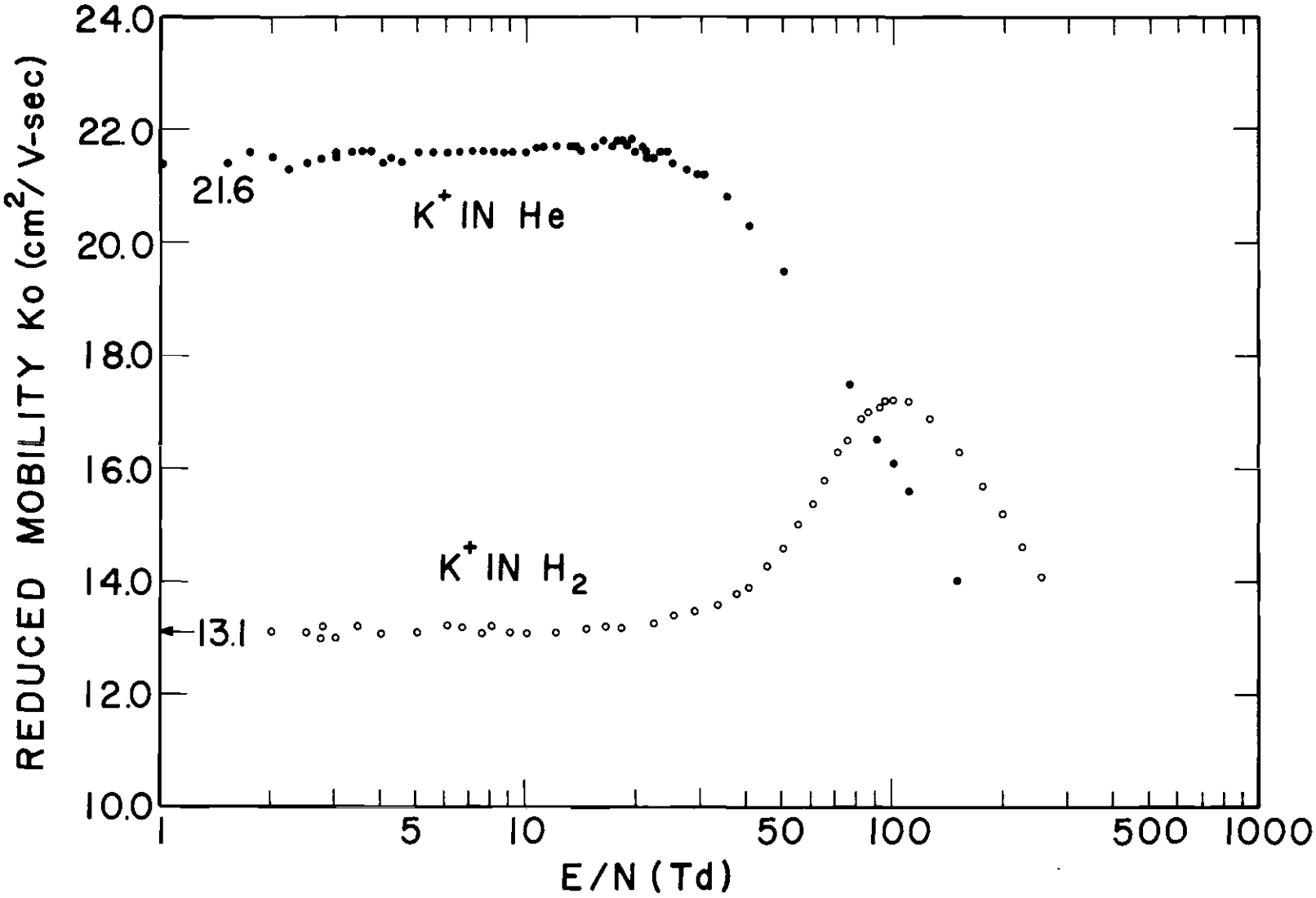

Figure 5. Reduced Mobilities for K^+ Ions in He and H_2 as Functions of E/N at 300^oK

K^+ ions in H_2 in the range 2.03 to 254 Td. Pressures used for this set of runs were between 0.0739 and 0.394 Torr. The zero-field reduced mobility was found to be (13.1 ± 0.3) cm^2/V-sec. There is a pronounced hump in the curve at an E/N of 100 Td. The zero-field reduced mobility may be compared to that of Tyndall[4] who determined it to be 12.7 cm^2/V-sec. The polarization limit of 11.2 cm^2/V-sec is again below the measured values. A further comparison is afforded by Elford's data[7] in which he measured $K_0(0)$ to be 12.75 cm^2/V-sec. Elford operated at pressures from 1 to 50 Torr and his E/N covered the range 0.6 to 91 Td. His points generally lie 2 to 3% below the present Georgia Tech data. Fleming, Tunnicliffe, and Rees[11] investigated the mobility over a larger range of E/N than Elford, 3 to 200 Td, with pressures reported at 0.63 to 13.3 Torr. The data of Fleming, et al., agree well with Elford's data at E/N below about 70 Td and hence are also lower than the current Georgia Tech data. Above 70 Td the measurements by Fleming, et al., fall below those of Elford and at the peak of the mobility hump, the Georgia Tech data is roughly 6.4% higher than Fleming's. At the higher E/N the points of Fleming fall systematically lower than the Georgia Tech data and are as much as 12.5% lower at an E/N of 200 Td.

A final set of data for comparison is that of Miller[12] whose measurements were made in the same drift tube as were the new data reported by the Georgia Tech group here. Improvements in the apparatus and analysis warranted another look at K^+ in H_2. Miller's zero-field reduced mobility of (12.8 ± 0.6) cm^2/V-sec compare favorably with the current value of (13.1 ± 0.3) cm^2/V-sec. Below about 30 Td there is considerable scatter in Miller's points which extend down to an E/N of 1.41 Td. In

the present measurements care was taken to set up the runs with low source voltages to try to minimize scatter in the data. It was possible to achieve less than 1% random scatter in the low E/N range which is a slight improvement over the previous work. There is good agreement over the remaining range of E/N. Miller's data extended to 422 Td which is well above the 254 Td limit of the more recent work.

K^+ in Ne

The third inert gas to be studied was Ne. The mobility results appear in Fig. 6 as the solid circles. The zero-field reduced mobility of (7.43 ± 0.15) cm^2/V-sec is indicated on the figure. The experimental parameters used for this gas were $1.26 \leq E/N \leq 203$ Td and $0.0736 \leq P \leq 0.393$ Torr. The rise in the mobility spectrum is well defined, being less pronounced than the large Ar peak, but considerably more than the slight rise occurring in He. Thus, we may assume that the relative peak heights for the inert gases increase with increasing mass of the atomic gas.

The Tyndall mobility of 7.50 cm^2/V-sec and the value 7.42 cm^2/V-sec of Crompton and Elford[5] are in good agreement with the present result. The Langevin polarization value of 6.07 cm^2/V-sec deviates considerably from the measured value. The Crompton-Elford data for $4.25 \leq E/N \leq 31$ Td, and pressures of 3.3, 4.6, and 12.5 Torr match up well with the Georgia Tech data. Creaser,[20] who obtained a zero-field reduced mobility of 7.41 cm^2/V-sec, carried the range of E/N up to around 82 Td, where there is also excellent agreement.

K^+ in O_2

Fig. 6 also presents the K^+ in O_2 mobility data for E/N in the

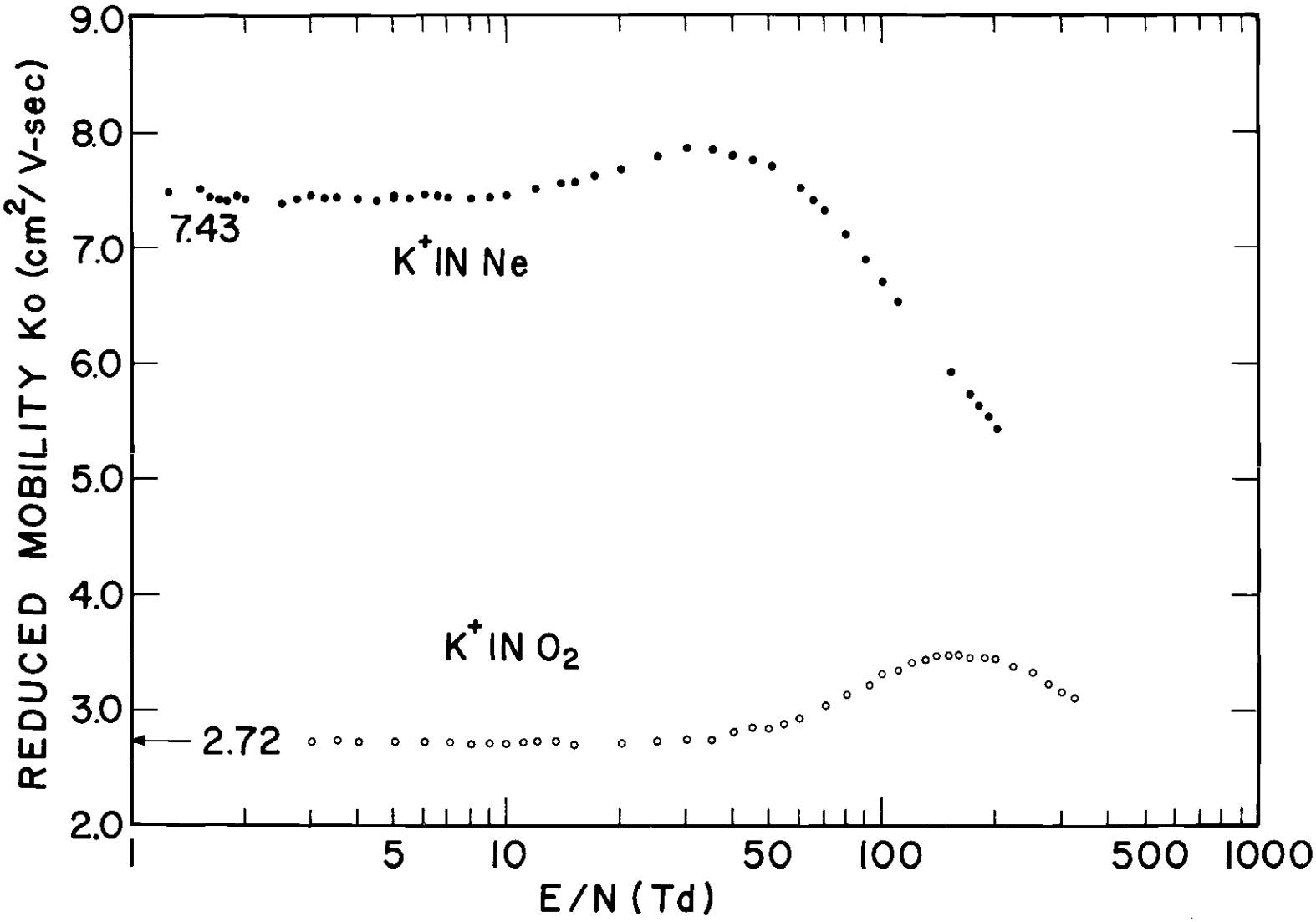

Figure 6. Reduced Mobilities for K^+ Ions in Ne and O_2 as Functions of E/N at 300°K

range from 3.04 to 328 Td and pressures varying from 0.0491 to 0.491 Torr. As indicated on the graph $K_0(0)$ was (2.72 ± 0.05) cm^2/V-sec. The only previous measurements were those of Snuggs[14] in work done in this lab. Snuggs covered roughly the same range of E/N, but his measurements at the lowest E/N's included pressures of 6.27 Torr; his $K_0(0)$ was (2.68 ± 0.07) cm^2/V-sec. Despite the use of high gas pressures, Snuggs' data appears unaffected by clustering, and there is excellent agreement throughout the entire spectrum. The polarization limit this time agrees somewhat better at 2.61 cm^2/V-sec.

K^+ in NO

The other curve on Fig. 7 is for CO_2 having a $K_0(0)$ of (1.45 ± 0.03) cm^2/V-sec. Measurements were made over a range of E/N from 10.1 to 708 Td, where pressures of 0.0295 to 0.0982 Torr were used. Cluster formation was monitored by counting the number of clustered ions arriving at the detector during a fixed time interval. By comparing this number to the counts registered by the dominant K^+ ions for an identical time period, one can arrive at an intensity ratio of clustered to unclustered ions. This ratio varied from 1.0% at 70 Td to as much as 3.4% at 10 Td. Pressures used in this range were nominally 0.050, 0.075, and 0.100 Torr. Above 70 Td the cluster percentage was less than 1%; it decreased to 0.11% at an E/N of 125 Td. All other results were below the 3.4% level and in each case there was no visible distortion of the arrival time spectrum. It is believed that clustering had no appreciable effect on the results for CO_2. No other data on CO_2 which are unaffected by clustering are known at this time.

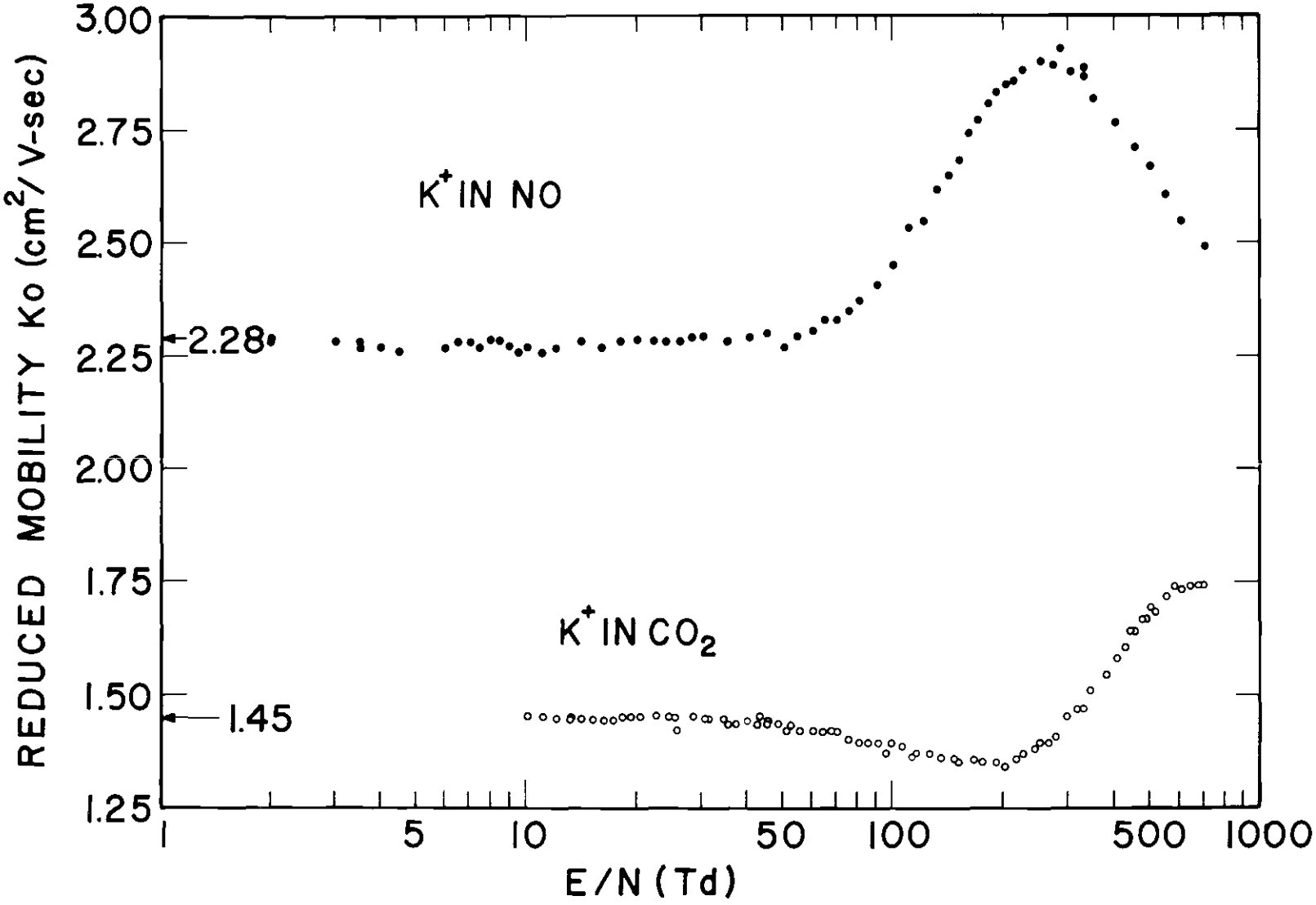

Figure 7. Reduced Mobilities for K^+ Ions in NO and CO_2 as Functions of E/N at 300°K

From about 50 to 200 Td there is a slight but unmistakable dip in the mobility curve, a structure not observed before in other gases investigated by this laboratory. This depression of the mobility occurs between the zero-field range and the characteristic rise exhibited by the other curves. The dip bottoms out at about 200 Td where the mobility is 7.6% below the zero-field value. The energies corresponding to 50 and 200 Td are, from the Wannier theory, 0.054 and 0.266 eV, respectively. It is known that the CO_2 molecule possesses a large cross section for vibrational excitation by electron impact at electron energies of the order 0.1 eV.[41] Therefore, it is possible that vibrational excitation of CO_2 by ionic impact may cause the dip in the mobility. A similar effect has been observed by Takata[52] for Li^+ ions in N_2. Although he admits the presence of clusters, he maintains that they could not explain such a large effect on the mobility curve. He also postulates that the phenomenon is caused by details of the molecular structure. To justify this hypothesis a rigorous calculation of the mobility as a function of E/N is needed. Such a treatment is not expected for sometime, although work in this direction is anticipated.

Table 2 summarizes the zero-field reduced mobility results obtained in this laboratory and compares them to previously measured values.

Error Analysis

The determination of the experimental error of a mobility measurement requires an analysis of the parameters z, t, V, P, and T as they appear in the equation for the reduced mobility,

Table 2. Zero-field Reduced Mobilities of K^+ Ions in Various Gases Expressed in $cm^2/V\text{-}sec$

Gas	Reduced Mobility	Reference	E/N Range Covered (Td)
He	21.6 ± 0.4	This Work (48)	1.01-152
	21.5	Creaser (20)	9 - 82
	21.3	Elford and Milloy (10)	1 - 28
	21.5	Tyndall (4)	
Ne	7.43 ± 0.15	This Work (48)	1.26-203
	7.41	Creaser (20)	9 - 82
	7.42	Crompton and Elford (5)	4.25- 31
	7.50	Tyndall (4)	
Ar	2.66 ± 0.05	This Work (48)	1 -610
	2.67	Creaser (20)	9 -107
	2.64	Elford and Milloy (10)	1 - 28
	2.73	Keller, et al. (19)	
	2.63	Tyndall (4)	
H_2	13.1 ± 0.3	This Work (48)	2.03-254
	12.8	Elford and Milloy (10)	1 - 28
	12.70	Fleming, et al. (11)	3 -200
	12.8	Miller, et al. (12)	1.41-422
	12.9	Albritton, et al. (2)	1.59-143
	12.75	Elford (7)	0.6 - 91
	12.7	Tyndall (4)	
O_2	2.72 ± 0.05	This Work (48)	3.04-328
	2.68	Snuggs, et al. (14)	1.53-308
NO	2.28 ± 0.05	This Work (48)	2.03-703
	2.245	Volz, et al. (15)	2.88-345
CO_2	1.45 ± 0.03	This Work (48)	10.1 -708

$$K_0 = \frac{\Delta z/\Delta \bar{t}}{V/z} \frac{P}{760} \frac{273.16}{T} . \qquad (4\text{-}3)$$

The mobility K has been replaced by the quantity v_d/E. The drift velocity is calculated by the differencing technique to get $\Delta z/\Delta \bar{t}$ and the electric field intensity is given by V/z, where V is the potential applied across the guard rings.

Drift Distance

Drift distances are known to within ± 0.008 cm and positioning of the source is repeatable to within ± 0.003 cm. The difference between any two adjacent source positions is about 6.25 cm. Since there are two lengths involved, the individual errors must be doubled. Hence the uncertainty in Δz is 0.26% systematic and 0.096% random. However, another factor of length appears due to the electric field intensity. For a drift distance of 25 cm corresponding to position 4, the errors in the measurement of z are 0.032% systematic and 0.012%random. Since the z and Δz are present as a product, the total error for the length may be found by adding up the respective uncertainties, resulting in a ± 0.29% systematic and ± 0.11% random errors.

Time

Systematic errors in the measurement of the drift times have been discussed in detail in references 25 and 43, where the error due to diffusion for times obtained in the differencing method was found to be no more than ± 0.1%. The scatter of experimental times about the least squares fit straight line was never more than 0.5% and frequently it was 0.2% or less. However, the random error will be taken to be ± 0.5%. Uncertainties in the time produced by reactions are negligible since care

was exercised to operate under conditions where reactions were insignificant.

Pressure

It has been the practice in this laboratory to calibrate the pressure measuring device (MKS Baratron) using the method proposed by McDaniel and Martin.[44] The procedure involves comparing the measured value of the zero-field reduced mobility of K^+ ions in N_2 to the accepted "standard" value of 2.54 $cm^2/V\text{-sec}$ which has been established by several laboratories throughout the world. A pressure calibration factor is adjusted to eliminate the discrepancy between the two values. Several such calibrations have indicated that the systematic error in pressure measurement has been no more than ± 1.5%. A random error of ± 0.3% is caused by fluctuations and drift of the Baratron pressure controller.

Temperature

Chromel-alumel thermocouples on the top, center, and bottom guard rings in the drift region monitor the temperature. At each source position three readings are made, so that in most cases there are 12 measurements associated with a run. The final temperature for the run is found by averaging the individual readings. The predominant error propagated is from a thermal gradient in the drift region due to uneven heating of the gas by the source. No data were taken when the gradient exceeded 3 degrees out of 300°K which represents a 1% systematic error. Fluctuations about the average value were such that the random error is determined to be ± 0.5%.

It was previously mentioned that high E/N mobility measurements at low pressures were subject to an additional error due to a slight deviation of the arrival time spectrum from the mathematically predicted shape.

The curve is skewed toward earlier times which is opposite to the expected behavior. A Monte Carlo calculation of the drift velocity of K^+ in Ar for an E/N of 600 Td and pressure of 0.025 Torr at 300^oK indicated that the mean free path of an ion was of the order of 0.5 cm. When the pressure was increased to 0.100 Torr, the drift velocity from the computer simulation was found to increase about 10%. Hence, the experimentally measured v_d's and K_0's may be in error by as much as 10% at high E/N where pressures on the order of 0.025 Torr were used. The lowest pressures in Torr for each gas were: 0.0982(He), 0.0736(Ne), 0.0246(Ar), 0.0739(H_2), 0.0491(O_2), 0.0344(NO), and 0.0295(CO_2). At the following E/N's and higher values (in Td) the skewness should be taken into account: 102(He), 172(Ne), 75(Ar), 203(O_2), 152(NO), and 268(CO_2). The spectra for K^+ in H_2 were skewed less than those in the other gases. Hence, with the exception of H_2, an error of ± 10% will be assigned to the mobilities in the high E/N range defined by the above values of E/N. We assign an error of ± 5% to H_2. It should be noted that this is a rough estimate. These values were determined by inspection of the arrival time spectra compared to the computer generated fit for determining D_L. We do not believe our mobility results are in serious error since, as shown in the next section, omega integrals calculated from our data using Equation (3-28) agree well with omega integrals determined from beam scattering data at high effective temperatures. The E/N's listed above fall in the high field region. They occur well past the K_0 peak for Ne, O_2, and He; for Ar and NO they are just below the peak and in CO_2 the value lies just before the rise in K_0 as E/N is increased. A cutoff for H_2 could not be easily determined.

Table 3 summarizes the above error estimates. The various

Table 3. Uncertainties in the Measurement of Mobilities

		Systematic	Random
	Length	± 0.29%	± 0.11%
	Time	0.1 %	0.5 %
	Pressure	1.5 %	0.3 %
	Voltage	0.11%	0.05%
	Temperature	1.0 %	0.5 %
Total Error:	Low and Intermediate E/N		± 2.0%
	High E/N, H_2		± 5%
	High E/N, Other Gases		± 10%

uncertainties apply to the data for each gas. The overall error was found by taking the square root of the sum of the squares of all the errors, since they are presumed independent. Thus, the uncertainty in any given measurement of the reduced mobility is ± 2% at low and medium fields. Of course, there is an error associated with each value of E/N since both E and N are subject to experimental error. Making estimates like those above one finds the uncertainty in the determination of E/N to be ± 1.9%.

Omega Integrals

As mentioned in Chapter III, the omega integral provides the necessary intermediate link between converting ion mobility data into useful information about the ion-neutral interaction potential. The mechanics of the link have been supplied by Mason and Viehland.[23] Using the concept of the omega integral, they have demonstrated a fundamental equivalence

between the mobility at high electric fields and relatively low temperatures (the order of $300^{o}K$) and the low-field mobility at high temperatures. By substitution of an effective ion temperature for the neutral gas temperature T, field-dependent quantities may be transformed to obtain their behavior with temperature variation. Of course, this is not just an ad hoc procedure; it has been rigorously justified from first principles in their paper.

In Fig. 8 the omega integral $\bar{\Omega}^{(1,1)}$ in units of $\mathring{A}^2$ is presented as a function of the effective temperature T_{eff} for K^+ ions in the three inert gases studied in this research, He, Ne, and Ar. The circles represent reduced mobility data which have been converted to the omega integral via Equation (3-28). The experimental values are taken from this laboratory and from references 48 and 49. Notice the extremely wide range of temperatures made possible by the high-field variation of mobility. There are two independent checks on the validity of the theory afforded by experiment. First are the mobility data as functions of E/N taken at different gas temperatures which are in excellent agreement with the calculated omega integrals. Also omega integrals for the zero-field reduced mobilities as functions of temperature can be found from the Chapman-Enskog theory, which is undoubtedly correct for low fields; agreement in this case is again quite good.

Secondly the scattering of fast ion beams in gas targets provide another important test of the theory.[45] Numerical integration using the potentials obtained from the beam data gives a value for the omega integral which is independent of the Viehland-Mason theory. These results are

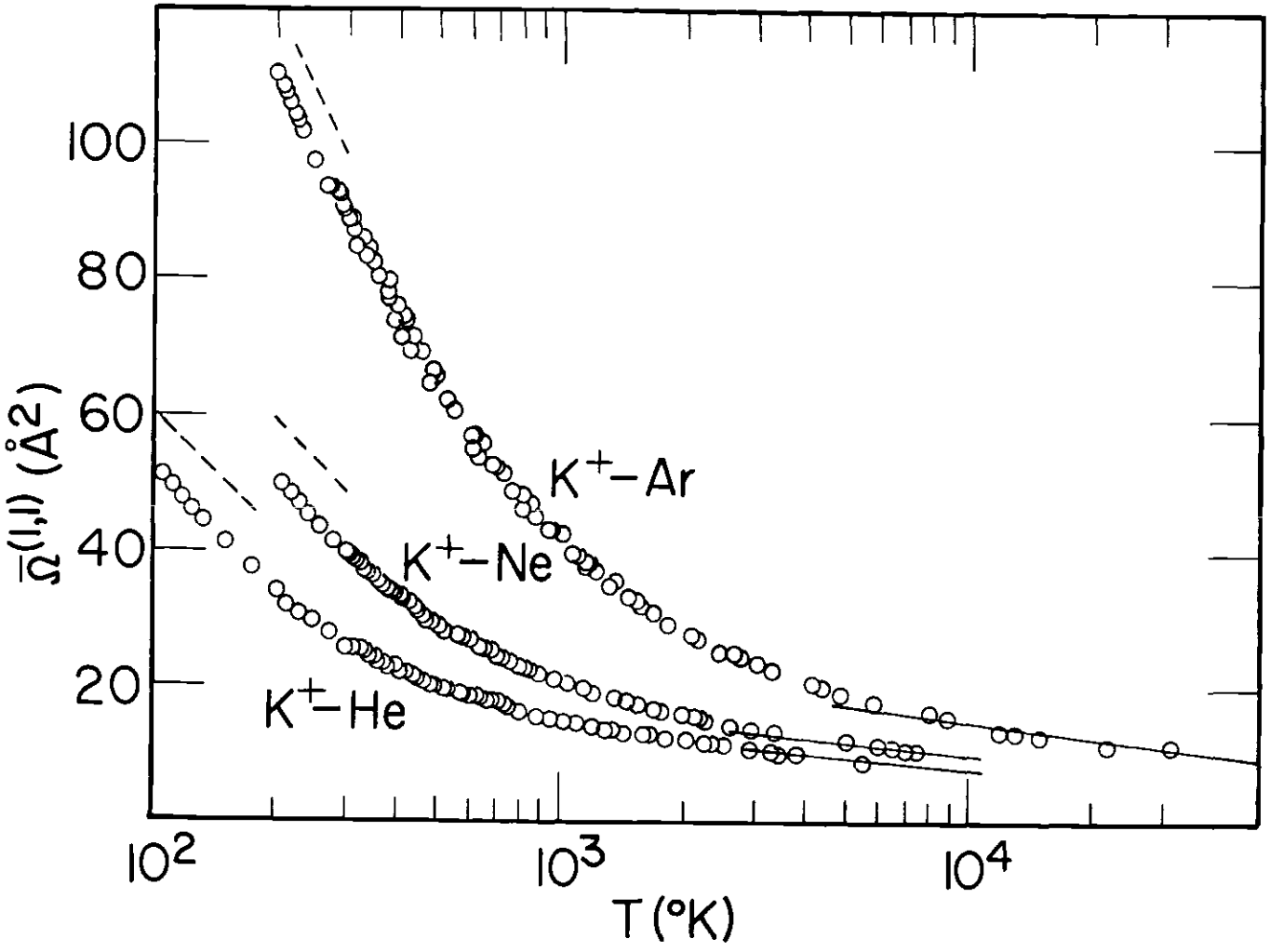

Figure 8. Omega Integrals for K^+ in He, Ne, and Ar as Functions of Effective Temperature; ---- Polarization Limit; —— Beam Data(Ref. 45)

shown as the solid lines at the high temperatures; the agreement is exceptionally good for the inert gases. The dashed lines at the upper end of the graph are the polarization asymptotes. The points are seen to lie below these limits due to the additional repulsive part of the potential being added in which tends to somewhat cancel the polarization attraction and hence lower the omega integral.

Figure 9 depicts the collision integrals for K^+ ions in NO, O_2, and H_2 obtained from (3-28). The solid circles represent the values of $\bar{\Omega}^{(1,1)}$ for K^+ in O_2. The dashed lines at low T (below 1000 degrees Kelvin) are the polarization limits; the longest dashed line belongs with the NO data. At high T the data are again compared with omega integrals calculated from beam scattering results. The long dashed line corresponds to K^+ in NO; the solid line belongs with O_2, and the short dashes are for K^+ in H_2. The repulsive potentials used in the calculation of the omega integrals for the beam data may be found in Reference 45.

Figure 10 shows $\bar{\Omega}^{(1,1)}$ as a function of T for the cases K^+ in CO_2, CO, and N_2. The lines again refer to the polarization limit at low T and beam scattering omega integrals at high T (see Reference 45). The solid lines correspond to K^+ in CO.

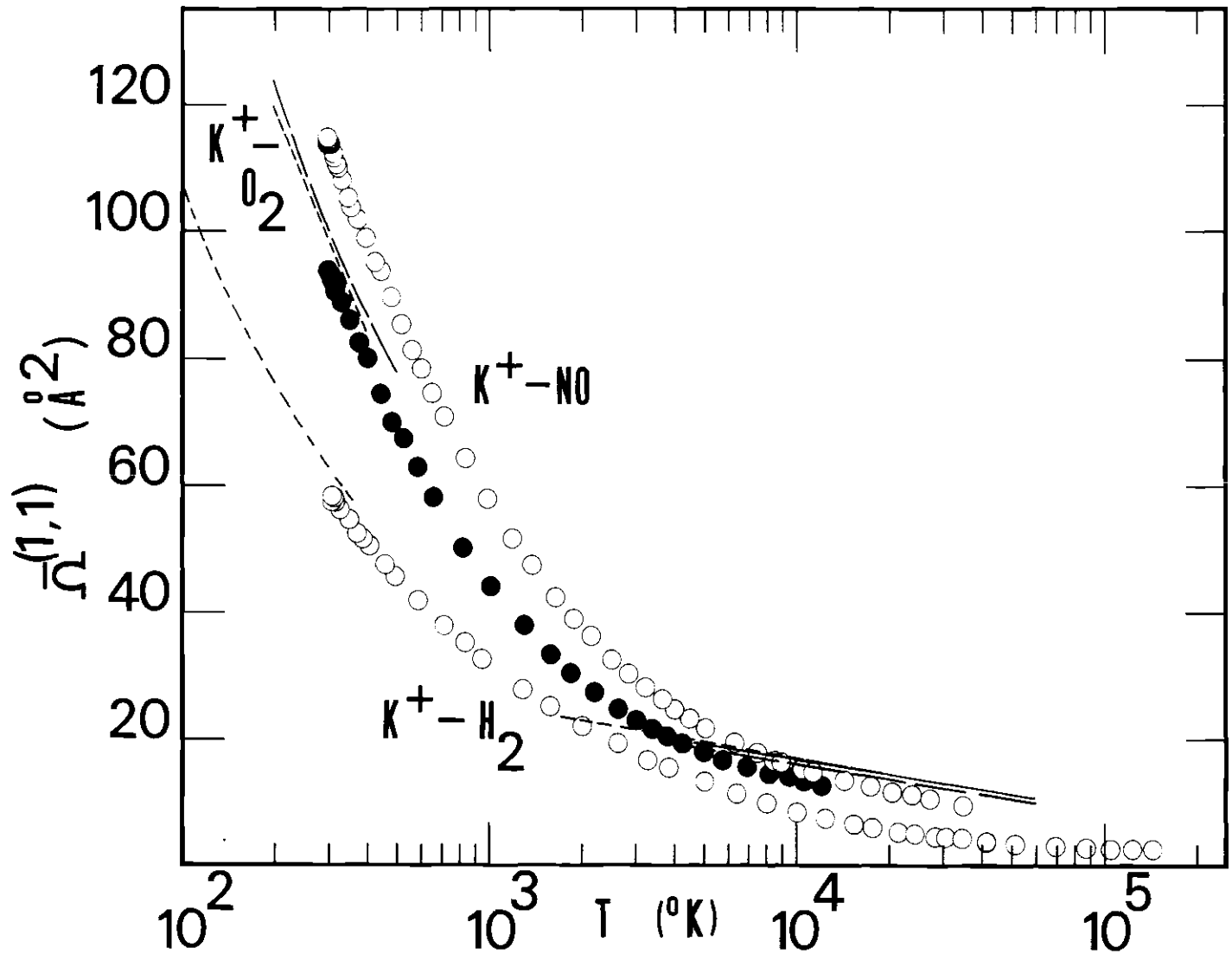

Figure 9. Omega Integrals for K^+ in H_2, NO, and O_2 as Functions of Effective Temperature. Beam Data at High T (Ref. 45): ---- H_2; — — NO; ——— O_2

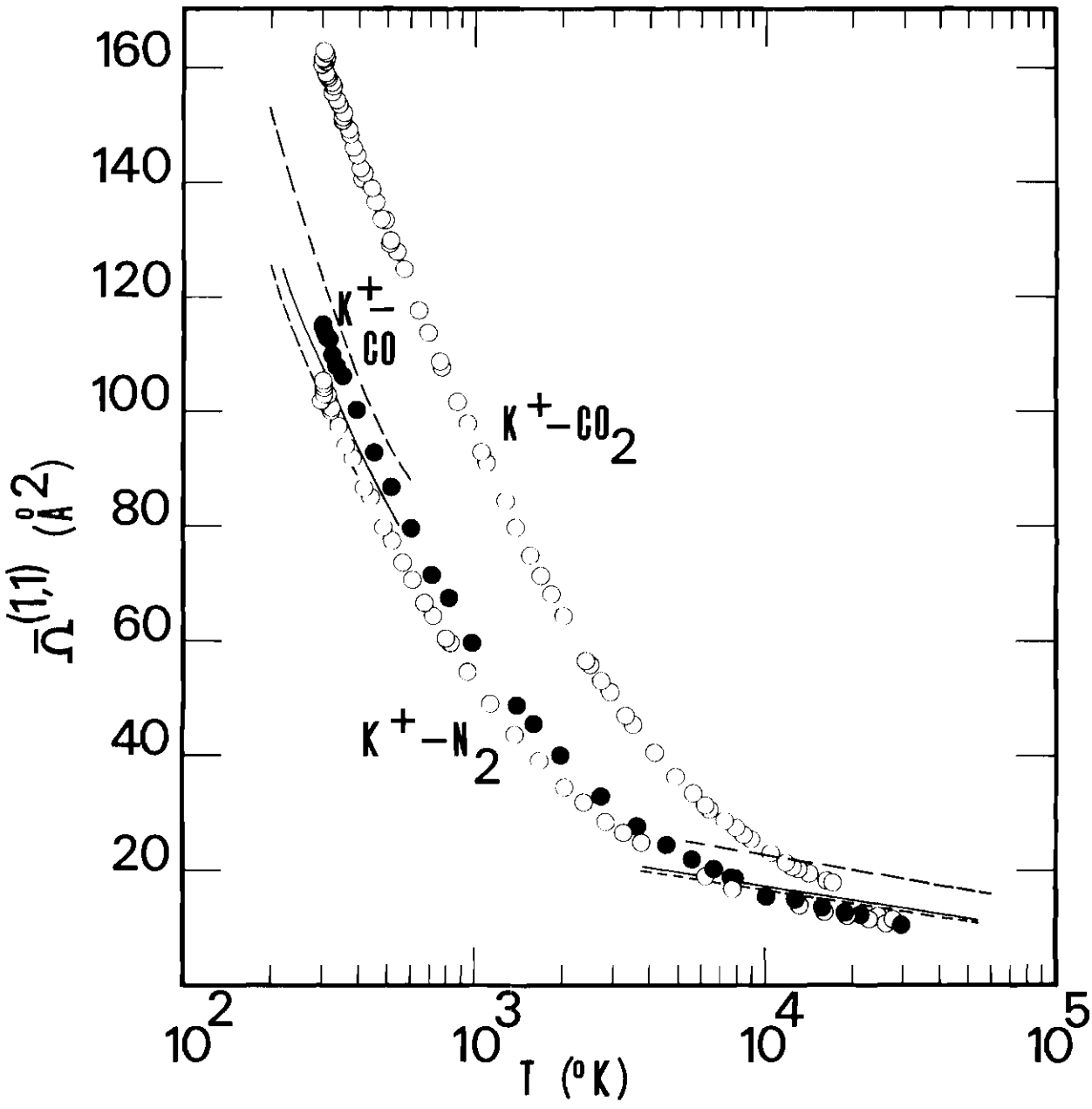

Figure 10. Omega Integrals for K^+ in N_2, CO, and CO_2 as Functions of Effective Temperature. Solid Lines for Polarization Limit and Beam Data(Ref. 45) Correspond to CO.

CHAPTER V

LONGITUDINAL DIFFUSION COEFFICIENTS

The longitudinal diffusion coefficients which describe diffusion parallel to the electric field have been determined from an analysis of the arrival time spectra at a given E/N. At present the only method for obtaining D_L is by comparison to predictions from mathematical models of drift tubes, such as the one developed by Gatland.[24,26,27] Of course each model must incorporate the boundary conditions characteristic of the drift tube to which it applies. The ultimate accuracy of a diffusion coefficient measurement depends upon how well the model describes the arrival time spectrum, or conversely, how well the equipment conforms to the mathematical model. Since boundary effects must be approximated by mathematical functions, for example the ion source term being represented as a delta function as in Equation (2-2), there are inherent errors just due to the model alone. In addition purely experimental errors further complicate the problem. Therefore one cannot hope to achieve the same degree of accuracy in measuring diffusion coefficients that one has been able to obtain for mobilities. Moseley, et al.[13] in 1969 were the first to report measurements of longitudinal coefficients (N^+, N_2^+, and K^+ ions in N_2), but his low-field values were substantially higher than the value calculated from the Einstein equation. With subsequent refinements in experimental techniques and analysis, not to mention a greater understanding of the problems involved, we now have the ability to determine longi-

tudinal diffusion coefficients to within about 5%. This gain in accuracy now makes possible more useful comparisons with theories like those of Wannier and those of Whealton and Mason.

Longitudinal Diffusion Coefficient Data

Ar, N_2, and CO

The longitudinal diffusion coefficients for the motion of K^+ ions in Ar, N_2, and CO are shown in Fig. 11. The data on N_2 and CO are those of Thomson, et al.,[3] and are included for completeness. The solid circles are the experimental diffusion coefficients. As described in Chapter II, the D_L values were obtained by curve fitting the Gatland expression, Equation (2-5), to the experimental arrival time spectra. Since D_L is inversely proportional to the number density N, it is convenient to present the data in the form ND_L to eliminate the explicit dependence on N. In Ar the range of E/N covered was from 1 to 610 Td with pressures at the low E/N's of 0.984 Torr decreasing to 0.0246 Torr at the opposite extreme. The N_2 data extend over a range of E/N from about 4 to 636 Td, the corresponding pressure limits being 0.636 and 0.0246 Torr. The CO measurements also cover a wide range of parameters, $3.94 \leqq E/N \leqq 640$ Td and $0.026 \leqq P \leqq 0.795$ Torr. Note the broken scales on the two vertical axes. The dashed curve is the theoretical prediction of Wannier for the constant mean free time case as prescribed by Equation (3-18) in Chapter III. In each case the agreement with this calculation at low E/N is good, but for intermediate and high values the theory and experiment differ substantially. Better agreement in the medium field case is provided by the solid curve which is the free flight theory given by Equation (3-20). Recall that in

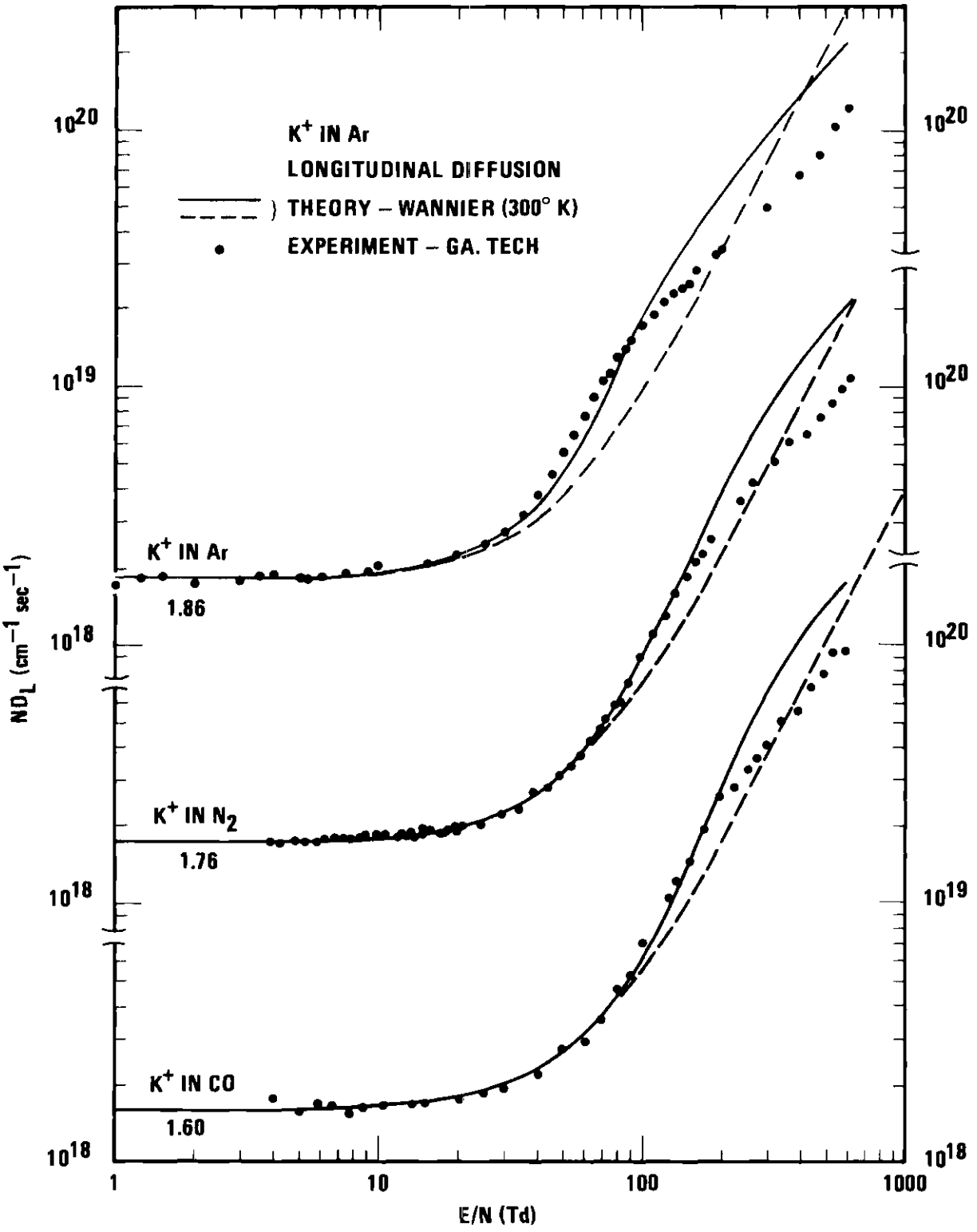

Figure 11. Longitudinal Diffusion Coefficients for K^+ in Ar, N_2, and CO Compared to Original and Modified Wannier Predictions

the free flight case the mean free time between collisions is not taken to be a constant, but is allowed to vary with E/N. One check of the diffusion measurements is to compare the low field coefficients with the prediction of the Einstein equation. These values, shown on the face of the graph below each curve, are 1.86×10^{18}, 1.76×10^{18}, and 1.60×10^{18} $cm^{-1}sec^{-1}$ for K^+ in Ar, N_2, and CO, respectively. In each case agreement with these predictions is within the experimental error of 5%. However there is still a discrepancy at high E/N where the predicted diffusion is too large by as much as a factor of 2. The divergence of the data from the theory may in part be due to the failure of the model to account for forces other than that of polarization. Using Wannier's expression for the ionic energy, Equation (3-12), one finds the average energy to be 6 eV at the highest E/N for Ar. At these energies it is reasonable to assume the the ion is certainly seeing some of the effects of the medium and short range forces; hence the breakdown of the theory is not surprising. Experimental errors for all diffusion coefficients except those at extremely high E/N are taken to be about 5%. Due to the use of low pressures in the region above about 200 Td, the uncertainty in a measurement in this range may be substantially higher than 5%, but there are no indications that the entire discrepancy between theory and experiment can be explained by this effect. More about the error induced at high E/N appears in the error analysis section at the end of the chapter.

Skullerud[16] has also measured the longitudinal diffusion coefficient for K^+ in Ar over a range of E/N from 85 to 793 Td, where his experimental error was quoted as ± 10%. His measurements were made at pressures of 0.14, 0.2, 0.3, and 0.5 Torr with the temperature in the range

$284 \leqq T \leqq 286°K$. A comparison with his data is given in reference 18 which shows good agreement throughout the range of E/N and even at the high E/N where Skullerud's values fall slightly below the Georgia Tech data. The solid curve in reference 18 is the theoretical prediction of Whealton and Mason[36]; the behavior of the theory at high E/N is not quite correct due to a mathematical error discovered after publication, and hence the exceptionally good agreement with the data above about 100 Td is misleading. The error, which was a factor of 3/2 instead of 1 multiplying the correction term in Equation (3-22), has been corrected and accurate graphs appear in Fig. 14. The agreement with Skullerud's diffusion measurements give added confidence to the validity of the high E/N values obtained in this laboratory.

As mentioned before, Moseley's[13] longitudinal diffusion data for K^+, N^+, and N_2^+ ions in N_2 were the first quantitative results to be reported. However, he used relatively short drift distances and there was appreciable scatter in his low-field data. Milloy[47] in 1973 published values for the longitudinal diffusion coefficient of K^+ in N_2 over a range of E/N from 2.83 to 28.3 Td. His measurements were made without a mass spectrometer, and at his highest pressure of 9.82 Torr, the formation of the $K^+ \cdot N_2$ cluster could have been significant. Milloy's results are in poor agreement with the work of Thomson.[3] At Milloy's lowest E/N his value of ND_L is 6% above the Einstein value, and at 14 Td his ND_L is 11% above the prediction from the Wannier equation.

H_2, H_e, and Ne

Figure 12 shows the longitudinal diffusion results for these gases.

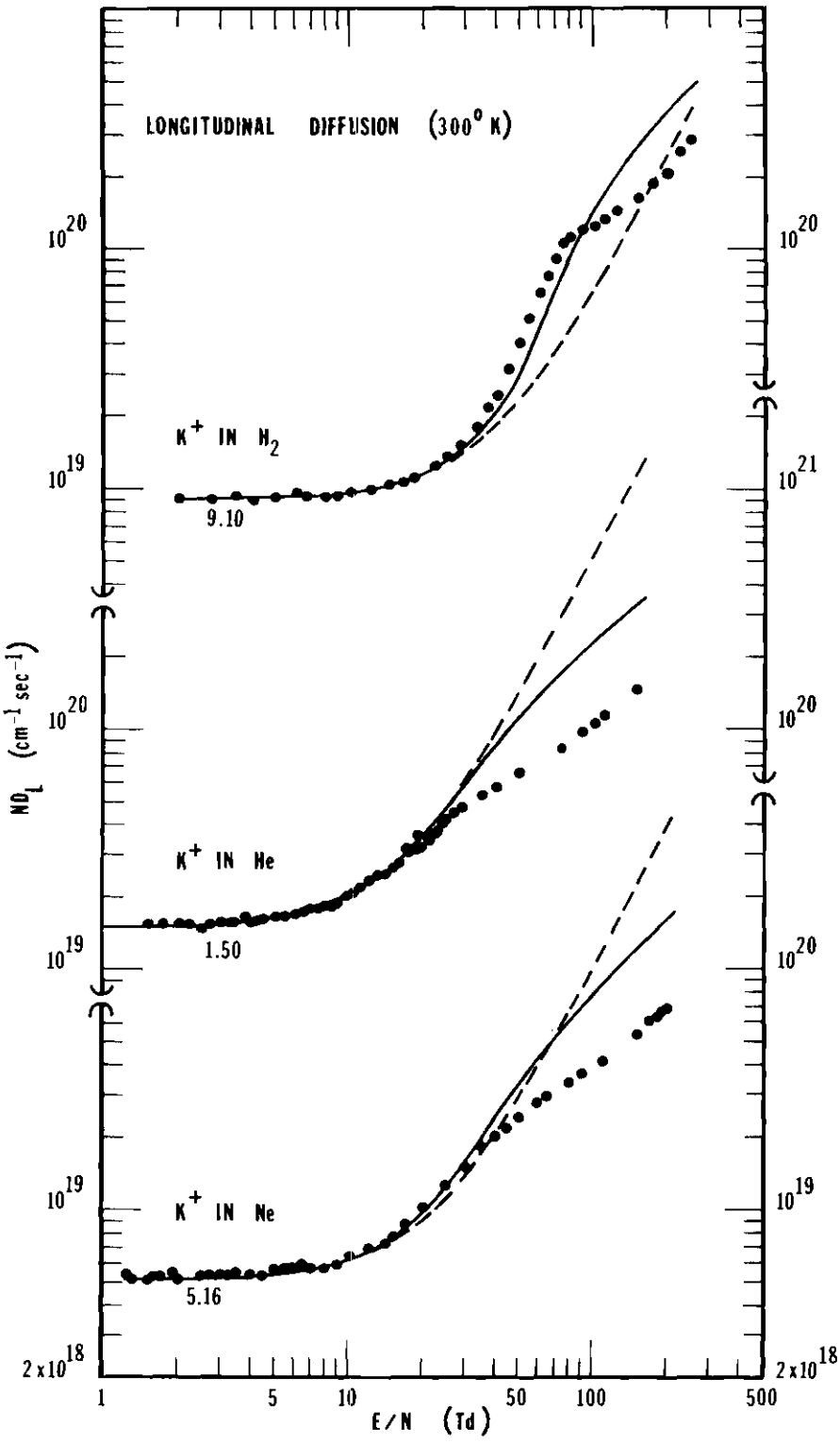

Figure 12. Longitudinal Diffusion Coefficients for K^+ in H_2, He, and Ne Compared to Wannier Predictions

The theoretical curves have the same meaning as in the previous figure. The numbers below the curves are the Einstein diffusion coefficients calculated from the zero-field mobilities; they are 9.10×10^{18}, 1.50×10^{19}, and 5.10×10^{18} $cm^{-1}sec^{-1}$ for H_2, He, and Ne, respectively. The experimental values are seen to be in good agreement. There is again the high-field "breakaway" from the theory. The lowest pressure used in the H_2 and He work was 0.0739 Torr at the high E/N and in He the lowest pressure was 0.0982 Torr, where the mean free path is about 0.06 cm. These pressures represent a factor of 3 and 4 increase over the pressures used in the Ar, N_2, and CO work at high E/N, and there is still a significant discrepancy between the theory and the experimental values. Hence from this fact alone it appears that any pressure effect at high E/N could not account for an appreciable portion of the divergence from the theory.

O_2, NO, and CO_2

This set of diffusion data appears in Fig. 13. The dashed line is again the constant mean free time Wannier curve, and the solid curve is the free flight theory. The same pattern at high E/N is seen for these gases also. The experimental points are as much as a factor of 2 lower than the theory in the region of high E/N. In the O_2 and NO graphs the measurements do not extend into the zero-field regime, where the Einstein values for O_2 and NO are 1.89×10^{18} and 1.58×10^{18} $cm^{-1}sec^{-1}$, respectively. There was considerably more scatter in the low-field diffusion coefficients for O_2 and NO than in the other 7 gases, and it was not possible to obtain data consistent with the Einstein values to within the experimental error of 5%. This discrepancy has also been observed by

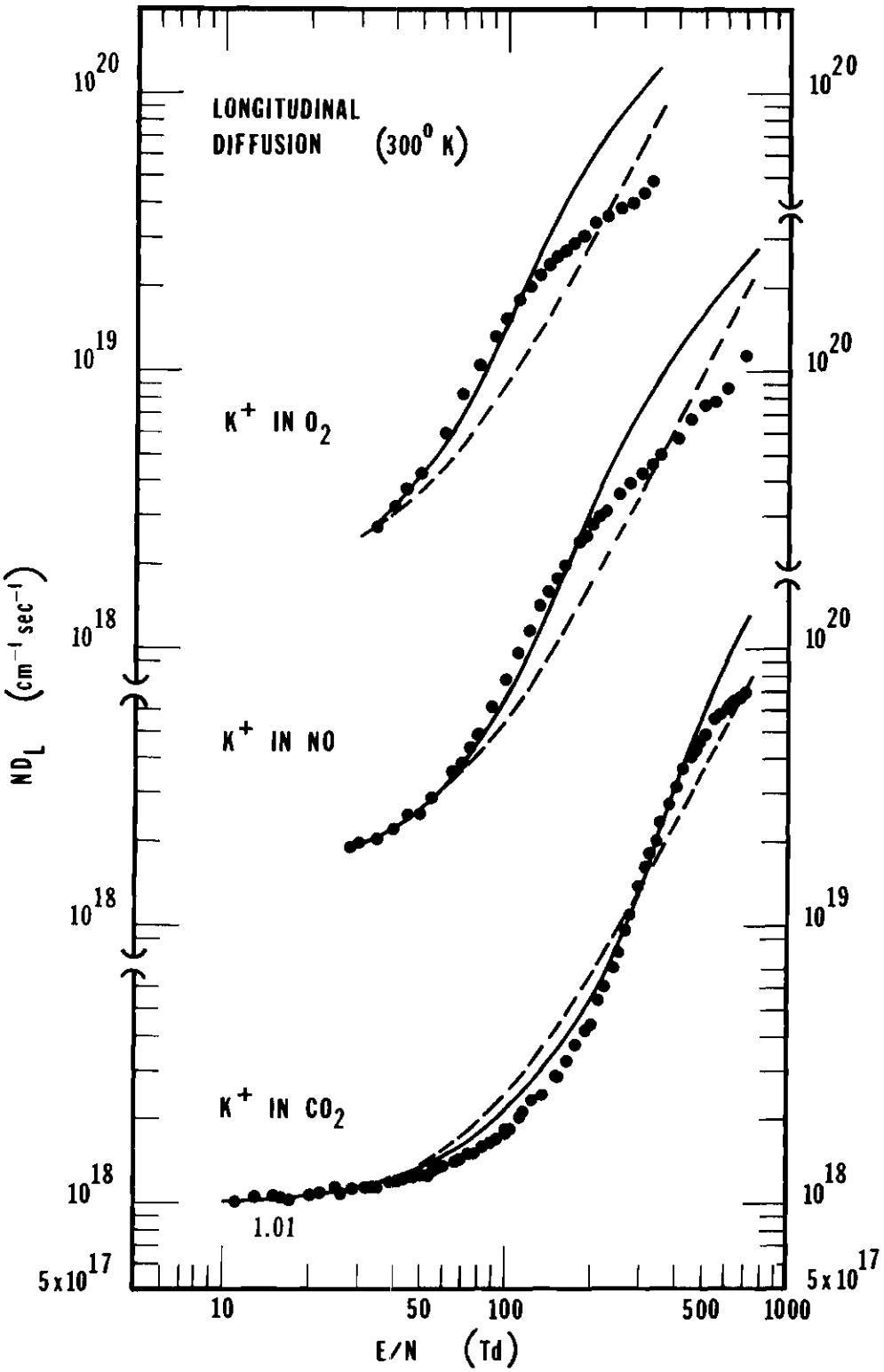

Figure 13. Longitudinal Diffusion Coefficients for K^+ in O_2, NO, and CO_2 Compared to Wannier Predictions

Snuggs[14] for K^+ in O_2 whose low-field diffusion coefficients were an average of 8.4% higher than the Einstein value calculated from his zero-field reduced mobility of 2.68 $cm^2/V\text{-}sec$. Volz's data[15] on NO also showed a large amount of scatter in the low field region and some of his values were as much as 25% above the Einstein value. These divergences probably arise from the fact that NO and O_2 are particularly difficult gases to work on at pressures of 0.3 to 0.5 Torr used at low E/N. These gases tend to inhibit the proper setup of the source pulsing, perhaps due to their highly corrosive and reactive characteristics. Since the Einstein equation is known to be rigorously correct at low E/N, and since the zero-field reduced mobilities are available to calculate the Einstein values, actual experimental measurements of the low-field diffusion coefficients are redundant. However the measurements are performed when possible to provide a check on the experimental procedures.

The third curve on Fig. 13 is for K^+ ions drifting in CO_2. Good agreement with the Einstein value of 1.01×10^{18} $cm^{-1}sec^{-1}$ was obtained in this case. The Wannier theory again fails above about 400 Td at the high E/N. There is also a depression of the diffusion coefficient in the range of intermediate E/N from about 50 to 200 Td, which corresponds to a similar effect found in the mobility curve in Fig. 7. It is expected that excitations of the CO_2 molecule are responsible for this discrepancy, since the ionic energy varies between 0.055 and 0.27 eV in this range.

Figures 14-16 show the longitudinal diffusion coefficients for the same nine gases, except this time the dashed curve is the diffusion coefficient with the Whealton-Mason first order correction term given in

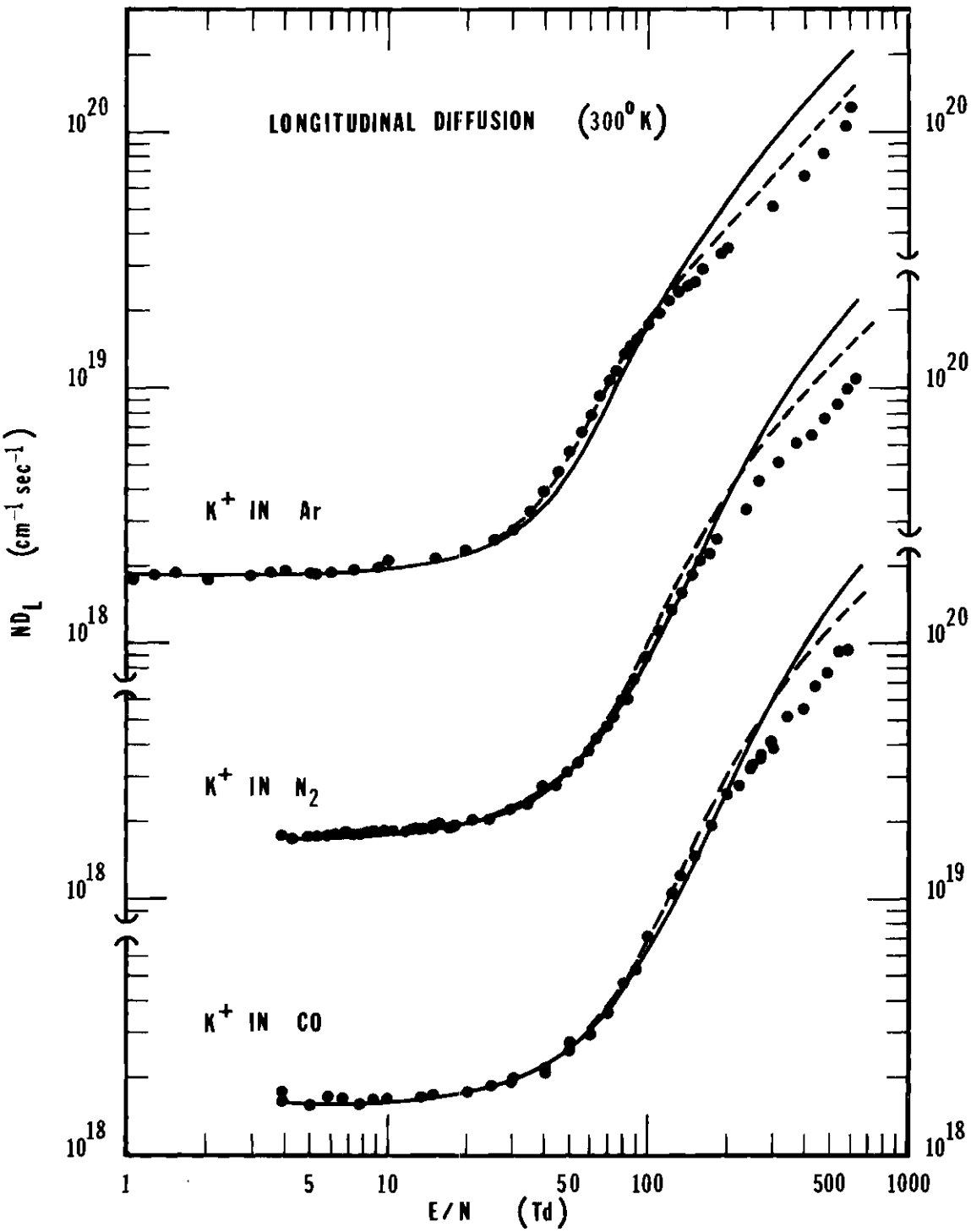

Figure 14. Longitudinal Diffusion Coefficients for K^+ in Ar, N_2, and CO Showing Modified Wannier Prediction with Whealton-Mason First Order Correction

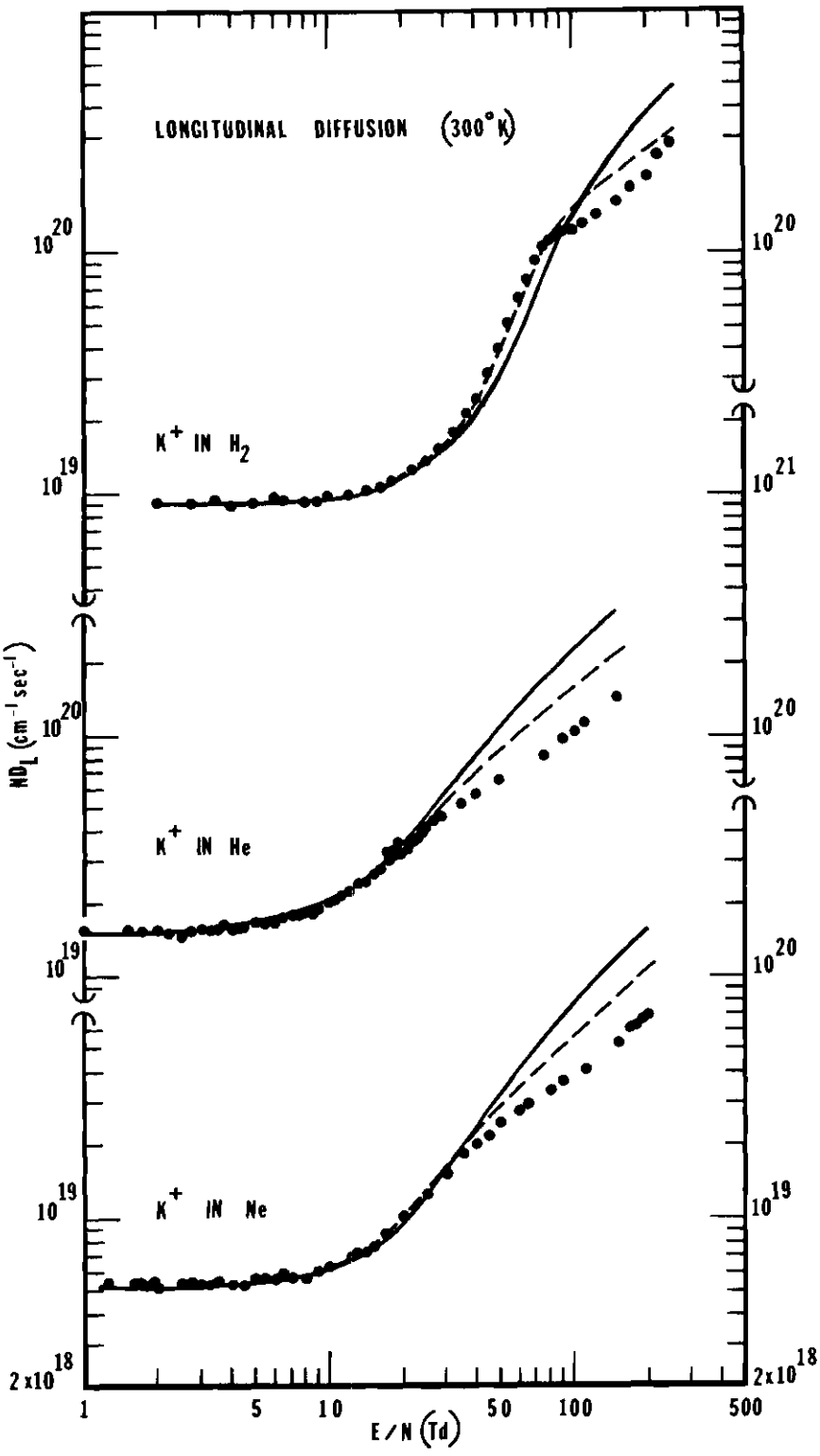

Figure 15. Longitudinal Diffusion Coefficients for K^+ in H_2, He, and Ne Compared to Modified Wannier Prediction with Whealton-Mason First Order Correction

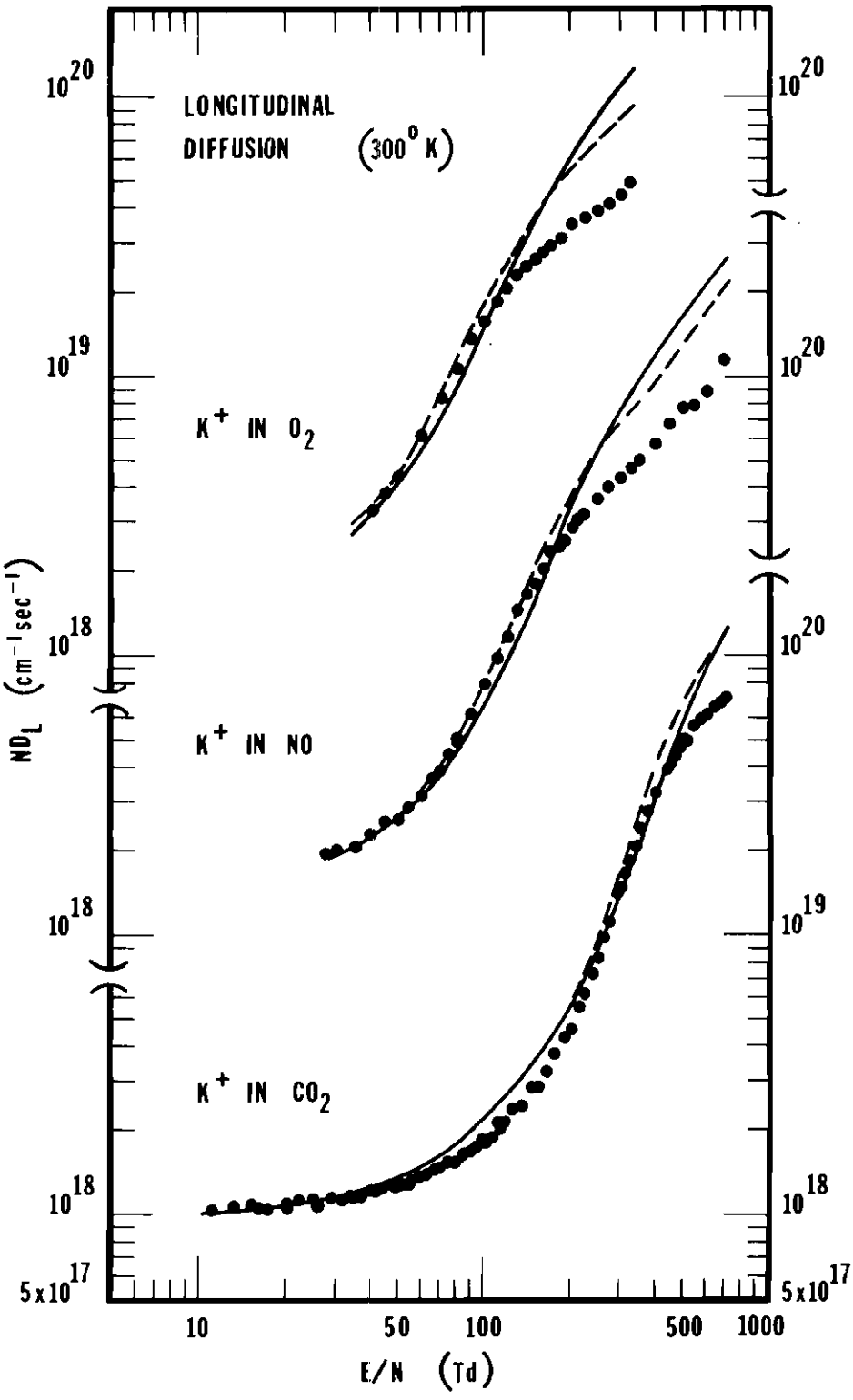

Figure 16. Longitudinal Diffusion Coefficients for K^+ in O_2, NO, and CO_2 Compared to Modified Wannier Expression with Whealton-Mason First Order Correction

Equation (3-22). When modified slightly to incorporate the reduced mobility K_0, (3-22) becomes

$$ND_L = ND_L(E)\left[1 + \frac{d\ell nK_0}{d\ell n(E/N)}\right] \tag{4-1}$$

where $D_L(E)$ is the Wannier free flight value from (3-20) and is plotted as the solid curve. In all cases we see that the correction improves the fit at intermediate fields except for CO_2 which is possibly distorted by inelastic collisions. At high E/N the correction is in the right direction but is not large enough to account for all of the discrepancy. In the case of CO_2 the correction appears to be actually worse than the free flight model; however, the data do not extend in E/N beyond the peak in the mobility curve, and presumably if they did, the corrected curve would cross the solid line and eventually fall below it. Higher order corrections might possibly result in still better agreement, but at present they have not been carried out.

It is interesting to note the correlation between the peak in the mobility curve and the point where the longitudinal diffusion coefficients start to diverge from the free flight theory. Table 4 gives for each gas the approximate E/N where the breakaway of the diffusion coefficient first occurs along with the E/N at the peak of the mobility curve. Also included are the energy at the peak and the energy associated with the highest E/N. The Wannier energy formula (3-12) was used for this purpose. It is seen from the table that the breakaway occurs at roughly the same E/N, and hence energy, as the peak of the K_0 data. Of course this is to be expected, since other forces besides polarization start to influence

the drift parameters at these energies.

Table 4. Energies Associated with K_0 Peak and ND_L Breakaway

Gas	Breakaway E/N	K_0 Peak E/N	Energy at K_0 Peak	Maximum Energy
Ar	100 Td	100 Td	0.55 eV	6.0 eV
N_2	160-200	200	1.4	6.6
CO	200	225	1.3	6.3
H_2	100	100	4.7	19.7
He	20-25	18	0.3	7.3
NO	200	250	1.4	7.9
O_2	125	151	0.8	2.8
CO_2	500	700	4.8	4.8
	depression in CO_2:			
	start	50 Td	(0.055 eV)	
	minimum	200 Td	(0.27 eV)	
Ne	38	31	0.2	2.7

Diffusion Error Analysis

As mentioned in Chapter III the measurement of the longitudinal diffusion coefficient involves a computerized curve fitting of the experimental arrival time spectrum. The theoretical expression used is

$$\phi(z,t) = \frac{Ase^{-\alpha t}}{4[\pi D_L t]^{\frac{1}{2}}} \left(v_d + \frac{z}{t}\right)\left[1 - \exp\left(-\frac{r_0^2}{4D_T t}\right)\right]\exp\left[-\frac{(z - v_d t)^2}{4D_L t}\right], \quad (4\text{-}2)$$

where $\phi(z,t)$ is the ionic flux density, A the area of the exit aperture, s the planar density of ions gated out of the source, and r_0 the radius of the entrance aperture. The quantity α is a depletion reaction frequency and v_d is the drift velocity previously measured for the current value of E/N. The drift distance z depends upon the source position, which in all but a few cases corresponded to the four longest drift distances. Since the theoretical curve does not include the time ions spend in the analysis region, the experimental distribution is shifted along the time axis until both peaks are aligned. Then both peak heights are normalized to unity. The unknown values A and s in Equation (4-2) are not needed. Moseley[25] has shown that the term $(1 - \exp(r_0^2/4D_T t))$ affects only the magnitude of the spectrum, leaving the shape unchanged over a variation in D_T of as much as 0.01 D_L to 10 D_L. Hence in the absence of any direct measurements of D_T, one may invoke the Wannier free flight theory value from Equation (3-20) for a reasonable estimate of D_T.

The sources of error in determining ND_L are then v_d, z, α, and the uncertainty in the curve fitting procedure itself. The reaction frequency α may produce a substantial error if reactions are present, but in the present case of K^+ ions the degree of ion-molecule reactions was insignificant; hence, α was set to zero.

In order to estimate the systematic error in a determination of D_L the low-field diffusion coefficients for each gas have been analyzed and compared to the Einstein value calculated from the zero-field reduced mobilities for that gas. At the lowest values of E/N for each gas except NO and O_2, the curve of ND_L vs. E/N flattens out and the diffusion coefficients tend to a constant value which should be those obtained using

the Einstein relation. However, due to experimental errors there is usually some discrepancy between the measured limit and the predicted number. Since the Einstein relation is rigorously correct, the ND calculated from it may be taken to be the true value in the low-field limit. There is of course an error even in the Einstein value due to the uncertainty in the zero-field reduced mobility used, but as mobilities are much more accurately and precisely measured than diffusion coefficients, this error of 2% should not seriously prohibit comparisons. The average values of the diffusion coefficients in this flat region for each gas and the corresponding RMS fractional deviations from this average are given in the first and second columns of Table 5. The percentages give some idea of the random scatter involved. The table also shows the Einstein values using the mobilities from Chapter IV. Also given is the percent discrepancy between the low-field average and the Einstein value. The plus sign indicates that the measured value was higher than the predicted and the opposite is true for the minus sign. The numbers for NO and O_2 are omitted since diffusion coefficients in the low-field region were not reported for these gases, due to experimental difficulties which precluded getting good agreement with the Einstein values. In each case except Ar the measured ND_L was higher, confirming the belief that any systematic errors in the experiment nearly always cause the diffusion coefficient to be too high. The agreement with the Ar data is probably fortuitous, because the same techniques were used in these measurements that were used for all the other gases.

The error in the drift velocity may be calculated from the individual errors in the Δz and $\Delta \bar{t}$ as discussed in the error analysis for the

Table 5. Comparison of Measured Low-field ND_L with Einstein Value

Gas	Ave. Low-field ND_L ($\times 10^{18} cm^{-1} sec^{-1}$)	% RMS Dev.	Einstein ND ($\times 10^{18} cm^{-1} sec^{-1}$)	% Discrepancy
He	15.3	1.8	15.0	+2.0
Ne	5.34	1.7	5.16	+3.5
Ar	1.84	3.3	1.85	-0.5
H_2	9.28	2.5	9.10	+2.0
O_2	--	--	1.89	--
NO	--	--	1.58	--
CO_2	1.06	1.5	1.01	+4.6

mobilities in the previous chapter. The uncertainty in v_d is then 0.58%. Schummers[46] has found that the error in a value of D_L is approximately three times the error in the drift velocity. Hence the overall contribution to the error is 1.74% at low and intermediate E/N's.

Another explicit source of error is in the value of z itself. Compared to the other errors this uncertainty of 0.034% is practically negligible. However, there is a substantial error in the determination of the neutral gas number density N which multiplies D_L. Since the diffusion coefficient varies inversely with N, the width of the time profile also reflects in a qualitative way the value of N. The width is an indication of the "true" number density as the ions see it. The instruments, subject to the fluctuations and calibration errors, measure the pressure and temperature, and the ideal gas law is used to calculate N, which has corresponding experimental errors in it. Hence the product ND_L is not independent of experimental pressure and temperature errors, since the implicit value of the number density associated with D_L is not the same as the explicit N as calculated. The uncertainty in N found by combining the errors in P and T from Table 3 is 1.9%.

At each E/N, spectra were obtained for several source positions, usually the four longest. For each distance a diffusion coefficient was determined with all parameters the same except for the drift distance. The values obtained exhibited a random scatter which is perhaps the best indication of the error available. The scatter was found to be significantly larger at the higher E/N's. The region of "high" E/N is taken to be those values of E/N at the peak of the mobility curve and higher. This

region also corresponds to the region where the experimental ND_L begin to break away from the Wannier theory. Medium or intermediate fields lie between the low field characterized by the flat part of the mobility spectrum and the high fields. The RMS deviations of the ND_L are indicated in Table 6.

Table 6. Error Estimates in the Measurement of ND_L (all errors expressed in percent)

	He	Ne	Ar	H_2	O_2	NO	CO_2
Systematic							
Low-Med. E/N	2.0	3.5	0.5	2.0	2.0	2.0	2.6
High E/N	10-15	10-15	10-15	10	10-15	10-15	10-15
RMS Deviation							
Low-Med. E/N	4.0	3.0	4.0	3.0	3.0	3.0	3.0
High E/N	3.0	3.6	6.4	7.5	3.0	3.7	3.0
Drift Velocity							
Low-Med. E/N	1.7	1.7	1.7	1.7	1.7	1.7	1.7
High E/N	30	30	30	15	30	30	30
Number Density	1.9	1.9	1.9	1.9	1.9	1.9	1.9
Total Error							
Low-Med. E/N	5.2	5.3	4.8	4.5	5.3	5.3	6.1
High E/N	30-35	30-35	30-35	15-20	30-35	30-35	30-35

A further complication in estimating the error occurs at high E/N where it was necessary to use relatively low gas pressures, the lowest being 0.0246 Torr in Ar. Diffusion data using these low pressures exhibited a definite systematic skewness of the arrival time spectrum which was evident from the curve fitting analysis. The departure from the theo-

retical model was relatively slight and an assessment of the error associated with the effect is difficult to make. There is no evidence to indicate that the discrepancy between the measured and Wannier ND_L's is entirely due to experimental error. In the case of K^+ in Ar there is good agreement in the high-E/N range with the data of Skullerud[16] whose lowest pressure was 0.140 Torr. Hence it is believed that the high-E/N diffusion coefficients cannot be in serious error. In the measurements the pressure was varied in the high-E/N range to ensure that an anomalous pressure effect was not the cause of the divergence from the theory. In Ar the breakaway trend was unaffected when pressures of 0.0492 and 0.0984 Torr were used at E/N slightly lower than the maximum. This represents a factor of 2 and 4 above the lowest pressure used in that gas. In H_2 the discrepancy persisted when the pressures were varied from 0.0739 to 0.148 Torr over a range of 101 to 254 Td. Similar findings occur for the other gases. Despite these observations the fact that the arrival time spectra at high E/N do not conform exactly to the predicted mathematical model is cause for concern. The experimental points of the spectrum are slightly higher than the predicted values on the early time side of the peak and lower on the late side. The discrepancy may be due in part to the in-increased mean free path and correspondingly lower cross sections at the lower pressures. There may also be an intrinsic skewness of the ionic velocity distribution function at these high E/N. Much of the discrepancy with the Wannier theory is probably due to interactions other than pure polarization becoming important.

A crude estimate of the minimum systematic error in D_L at high E/N

is about 10-12% based on the fact that Moseley was able to discern differences in an arrival time spectrum when D_L was varied by about 12%.[25] This type of error is not exactly the same as a skewness type error, but it does provide some guidance. Another contributing factor to the error at high E/N is the error associated with the drift velocity at high E/N from Chapter IV. It was concluded that for all gases except H_2 which had an error of ± 5%, there was a possible uncertainty of ± 10% in v_d at high fields. This would, according to Schummers,[46] cause an error of about ± 30% in D_L. A systematic error of roughly ± 10-15% due to the skewness problem will be assigned as a reasonable guess. The error propagated by the drift velocity is taken to be about ± 30%. The total error then at high fields is approximately ± 30-35%.

The systematic error at low and intermediate fields is just the discrepancy from the Einstein value appearing in Table 5. The values of 2.0% for H_2 and O_2 apply to the intermediate field region only, as low field ND_L's were not reported for these gases. The estimate of 4.6% for CO_2 is probably too conservative since some of the points used for the calculation were on the borderline between the low and medium fields. Hence an overall error of ± 5% at low and intermediate fields is a sensible compromise for the uncertainty in a measurement of ND_L for K^+ ions in each gas.

CHAPTER VI

CONCLUSIONS

It is important to consider whether the goals set forth in the beginning of this research effort were achieved. The aims as stated at the end of Chapter I were to measure the mobilities and longitudinal diffusion coefficients over the widest range of E/N the experimental apparatus would permit. While obtaining these data it was also the hope to achieve an improved level of accuracy and precision over that attained by previous investigators. With the exception of measurements of K^+ in H_2 by Miller[12] and K^+ in Ar by Skullerud,[16] the range of E/N covered in this work has exceeded that of other workers. One can consult Table 2 for more detailed information. It is believed that the quality of the present Georgia Tech data probably exceeds that of Miller, who stated errors for his alkali measurements of ± 5% at low E/N and + 20, - 15% at high E/N. The K^+ in Ar work of Skullerud was done without mass analysis and he did not obtain a zero-field reduced mobility. As for diffusion measurements, there have been only a few determinations of the longitudinal diffusion coefficients made outside the Georgia Tech laboratory. Only Skullerud[16] for K^+ in Ar has been able to obtain reasonably good values for ND_L. All things taken into consideration, it is believed that the quality and the quantity, in the sense of the large ranges of E/N covered, of the Georgia Tech data are among the best available. To this extent the goals of the research have been satisfactorily accomplished.

The longitudinal diffusion coefficient data have been compared to the theories of Wannier,[17] Whealton and Mason,[36] and to the Einstein equation (3-13a). Several conclusions can be drawn about the results of the comparisons. First of all is the fact that all diffusion data should agree to within experimental error with the value obtained from the Einstein equation. Any systematic discrepancy is a direct indication of experimental errors in the measurement process, provided of course that the zero-field mobility one uses in (3-13a) is good. Referring to Table 5 the low-field ND_L's in each case are less than 5% from the Einstein value, but the diffusion coefficients are systematically higher. This tendency is incorporated into the error analysis as indicated in Table 6.

It has been demonstrated that the Wannier pure polarization model, Equation (3-14), works well only at the low and slightly higher E/N, whereas the modified equations (3-20) work well all the way up to the high E/N regime. At high fields a "breakaway" from the Wannier predictions is observed in each of the nine gases studied. There is an increase in the experimental error at high E/N, but it is concluded that the discrepancy from the theory is not caused by experimental error alone, since forces other than the pure polarization force undoubtedly begin to become important at high E/N. The Whealton-Mason first order correction to the diffusion coefficient given by (3-22) is seen to be in the right direction but not large enough in magnitude to obtain the type of agreement observed at low and intermediate fields. Higher order corrections might improve agreement further.

The mobility data obtained for K^+ in the various gases as a function of E/N all exhibit the same characteristic shape, that is a flat region at

low E/N followed by a pronounced rise in K_0 to a peak at medium field strengths and then a swift fall off at the high E/N. In He the peak is barely perceptible; in CO_2 a peak was observed, but the data did not extend to a large enough E/N to see the high-field fall off. A new, additional structure to the K_0 versus E/N plot for CO_2 appeared as a depression of the mobility at low to intermediate E/N. A similar depression of the ND_L was also observed. It was concluded that clustering could not account for the effect, nor could any systematic experimental error be held responsible. Hence it is interesting to speculate that inelastic collisions could possibly be causing the structure.

Perhaps the most important application of the mobility results has been in conjunction with the Viehland-Mason theory.[23] New developments in the theory now make it possible to convert the field-dependent mobility data to a temperature-dependent omega integral. This conversion provides an experimental set of omega integrals which can be compared to ones calculated by assuming a parameterized form of the potential. By varying the parameters to obtain a good match, one can determine quite a bit about the nature of the potential. It is fortunate that the theory is now available to take advantage of the extensive package of data that now exists.

APPENDIX I

TABULATION OF MOBILITIES AND LONGITUDINAL DIFFUSION COEFFICIENTS

In this appendix are tabulated the mobility and longitudinal diffusion coefficient results for K^+ ions drifting in the nine gases: He, Ne, Ar, H_2, N_2, O_2, CO, NO, and CO_2. The tabulated data on Ar, N_2, and CO have been published in a Technical Report of the Georgia Institute of Technology entitled: "The Mobility, Diffusion, and Clustering of K^+ Ions in Gases, Report II," by D. R. James, E. Graham IV, G. M. Thomson, J. H. Schummers, I. R. Gatland, and E. W. McDaniel, Dec. 1, 1972. The data on these three gases are included again here for completeness.

The reduced mobility K_0, drift velocity v_d, ND_L, and D_L are listed with the corresponding E/N, pressure, and gas temperature at which the measurements were made. The appropriate units are given at the head of each column. E/N, where E is the electric field intensity and N the number density of the gas, is expressed in units of the Townsend (Td), with 1 Td = 10^{-17} V-cm^2. The conversion between E/P_0 and E/N is given in Appendix II, number (2).

At the given value of E/N appearing in the tables, the drift velocity v_d was determined from Equation (2-1). The mobility K is then the ratio v_d/E, where E is the magnitude of the electric field intensity. Equation (1-2) is used to find the reduced mobility K_0, which is the quantity reported in the table. The longitudinal diffusion coefficient

D_L is found by curve fitting the expression (2-5) to the experimental arrival time spectrum.

Table 7. Transport Data for K^+ Ions in Helium

E/N (Td)	Reduced Mobility ($\frac{cm^2}{V\text{-}sec}$)	Drift Velocity ($10^4 \frac{cm}{sec}$)	ND_L (10^{19}/cm-sec)	D_L (cm^2/sec)	Pressure (Torr)	Temp. (°K)
1.01	21.4	0.583	1.55	979	0.491	298.8
1.53	21.4	0.878	1.54	971	0.491	299.1
1.77	21.6	1.03	1.54	1620	0.295	298.0
2.04	21.5	1.18	1.54	970	0.491	299.1
2.28	21.3	1.30	1.51	1580	0.295	297.9
2.53	21.4	1.45	1.47	1150	0.393	297.8
2.78	21.5	1.61	1.53	1610	0.295	298.1
3.05	21.5	1.76	1.58	997	0.491	299.3
3.05	21.6	1.77	1.53	965	0.491	299.4
3.34	21.6	1.93	1.54	1610	0.295	298.0
3.56	21.6	2.07	1.56	986	0.491	299.7
3.79	21.6	2.21	1.65	1300	0.393	297.8
4.07	21.4	2.34	1.57	992	0.491	299.5
4.30	21.5	2.49	1.59	1250	0.393	298.0
4.57	21.4	2.63	1.60	1680	0.295	299.0
5.09	21.6	2.95	1.65	1740	0.295	299.8
5.58	21.6	3.24	1.63	1710	0.295	298.9
6.10	21.6	3.54	1.67	1760	0.295	299.2
6.59	21.6	3.82	1.71	1350	0.393	298.7
7.12	21.6	4.13	1.79	1890	0.295	299.6
7.61	21.6	4.41	1.79	1410	0.393	299.0
8.15	21.6	4.72	1.83	1930	0.295	299.7
8.70	21.6	5.04	1.80	1890	0.295	298.1
9.16	21.6	5.33	1.89	1990	0.295	299.8
10.0	21.6	5.81	2.00	2110	0.295	299.5
10.6	21.7	6.19	2.06	2160	0.295	298.5
11.2	21.7	6.52	2.18	2290	0.295	299.0
12.2	21.7	7.12	2.24	2350	0.295	299.6
13.2	21.7	7.72	2.41	2530	0.295	299.4
13.7	21.7	8.02	2.47	2600	0.295	299.4
14.2	21.6	8.23	2.46	2580	0.295	298.3
15.3	21.7	8.89	2.63	2770	0.295	299.8
16.2	21.8	9.49	2.76	2900	0.295	298.6
17.2	21.7	10.0	3.21	3360	0.295	298.3
17.8	21.8	10.4	3.02	3170	0.295	298.8
18.3	21.8	10.7	3.33	3500	0.295	298.7
18.8	21.7	11.0	3.14	3300	0.295	299.0

Table 7. Continued

E/N (Td)	Reduced Mobility ($\frac{cm^2}{V\text{-}sec}$)	Drift Velocity ($10^4 \frac{cm}{sec}$)	ND_L (10^{19}/cm-sec)	D_L (cm^2/sec)	Pressure (Torr)	Temp. (°K)
19.3	21.8	11.3	3.60	3780	0.295	299.0
19.7	21.6	11.5	3.20	3360	0.295	298.0
20.8	21.7	12.1	3.43	3600	0.295	298.4
21.2	21.5	12.3	3.38	3540	0.295	297.8
21.3	21.6	12.4	3.55	3730	0.295	299.1
22.3	21.5	12.9	3.62	3790	0.295	298.3
23.3	21.6	13.5	3.75	3940	0.295	298.7
24.3	21.6	14.1	3.96	4160	0.295	299.0
25.2	21.4	14.5	4.18	4380	0.295	297.5
27.3	21.3	15.6	4.45	4650	0.295	297.7
29.3	21.2	16.7	4.67	4890	0.295	298.0
30.6	21.2	17.4			0.295	299.5
35.6	20.8	19.9	5.21	8230	0.196	299.5
40.6	20.3	22.1	5.70	5990	0.295	298.7
50.8	19.5	26.6	6.53	10300	0.196	299.5
76.4	17.5	35.8	8.43	13300	0.196	299.8
91.6	16.5	40.5	9.70	15300	0.196	299.4
102	16.1	44.0	10.5	33200	0.0982	299.5
112	15.6	46.9	11.4	35900	0.0982	299.8
152	14.0	57.1	14.5	104000	0.0982	298.2

Table 8. Transport Data for K^+ Ions in Neon

E/N (Td)	Reduced Mobility ($\frac{cm^2}{V\text{-}sec}$)	Drift Velocity ($10^4 \frac{cm}{sec}$)	ND_L (10^{18}/cm-sec)	D_L (cm^2/sec)	Pressure (Torr)	Temp. (°K)
1.26	7.48	0.254	5.41	425	0.393	298.0
1.53	7.50	0.308	5.18	546	0.295	299.7
1.62	7.44	0.323	5.35	559	0.295	297.3
1.72	7.42	0.343	5.35	421	0.393	298.2
1.82	7.41	0.362	5.26	549	0.295	296.9
1.92	7.45	0.385	5.46	572	0.295	298.0
2.03	7.41	0.404	5.13	538	0.295	298.4
2.53	7.38	0.502	5.36	561	0.295	298.1
2.78	7.42	0.554	5.40	567	0.295	298.4
3.04	7.44	0.609	5.34	561	0.295	298.8
3.30	7.42	0.657	5.32	559	0.295	298.6
3.55	7.43	0.708	5.43	569	0.295	298.4
4.05	7.41	0.806	5.38	563	0.295	297.7
4.55	7.40	0.905	5.29	554	0.295	297.7
5.06	7.43	1.01	5.62	589	0.295	298.3
5.07	7.45	1.02	5.66	595	0.295	298.9
5.58	7.41	1.11	5.66	594	0.295	298.6
6.07	7.47	1.22	5.69	596	0.295	297.9
6.60	7.45	1.32	5.90	621	0.295	299.2
7.06	7.43	1.41	5.67	592	0.295	297.2
8.07	7.41	1.61	5.64	589	0.295	296.9
9.07	7.42	1.81	5.98	624	0.295	296.8
10.1	7.44	2.03	6.41	672	0.295	298.6
12.2	7.50	2.46	6.82	717	0.295	299.1
14.2	7.55	2.88	7.26	765	0.295	299.4
15.2	7.56	3.09	7.73	812	0.295	298.9
17.2	7.61	3.52	8.62	905	0.295	298.6
20.3	7.69	4.19	10.1	1060	0.295	298.8
25.4	7.78	5.31	12.5	1310	0.295	299.1
30.5	7.86	6.43	15.0	1580	0.295	299.1
35.6	7.84	7.49	18.2	1920	0.295	299.5
40.5	7.80	8.49	20.0	2100	0.295	298.2
45.6	7.75	9.49	21.5	2250	0.295	298.3
50.8	7.70	10.5	24.1	3800	0.196	299.0
60.9	7.51	12.3	27.7	4360	0.196	299.0
66.0	7.40	13.1	29.4	4630	0.196	299.2
70.8	7.31	13.9			0.196	298.0
81.1	7.11	15.5	33.9	7110	0.147	298.1

Table 8. Continued

E/N (Td)	Reduced Mobility ($\frac{cm^2}{V\text{-}sec}$)	Drift Velocity ($10^4 \frac{cm}{sec}$)	ND_L (10^{18}/cm-sec)	D_L (cm^2/sec)	Pressure (Torr)	Temp. (°K)
91.2	6.89	16.9	36.6	7690	0.147	298.5
101	6.71	18.3			0.147	299.0
111	6.52	19.5	41.1	12900	0.0982	298.0
152	5.92	24.2	52.9	16600	0.0982	298.1
172	5.74	26.6	60.1	25300	0.0736	298.8
182	5.63	27.6	62.9	26400	0.0736	298.6
192	5.54	28.6	66.8	28000	0.0736	298.4
203	5.43	29.6	69.0	28900	0.0736	298.1

Table 9. Transport Data for K^+ Ions in Argon

E/N (Td)	Reduced Mobility ($\frac{cm^2}{V\text{-}sec}$)	Drift Velocity ($10^4 \frac{cm}{sec}$)	ND_L (10^{18}/cm-sec)	D_L (cm^2/sec)	Pressure (Torr)	Temp. (°K)
1.00	2.66	0.072	1.72	54.3	0.984	301.0
1.26	2.68	0.090	1.84	58.4	0.984	301.4
1.51	2.68	0.109	1.87	59.3	0.984	301.9
2.01	2.65	0.143	1.75	55.4	0.984	300.9
2.95	2.64	0.209	1.81	74.9	0.750	299.8
3.50	2.66	0.250	1.89	79.4	0.738	300.0
4.00	2.66	0.286	1.91	80.5	0.738	300.2
5.01	2.66	0.359	1.87	78.9	0.738	300.8
5.28	2.66	0.377	1.82	95.4	0.591	298.3
6.02	2.67	0.432	1.88	79.4	0.738	301.1
7.47	2.67	0.535	1.91	78.8	0.750	298.7
9.04	2.68	0.651	1.97	83.3	0.738	301.3
9.80	2.71	0.713	2.10	661	0.0984	299.9
15.0	2.71	1.09	2.13	337	0.197	300.3
19.6	2.74	1.44	2.30	725	0.0984	299.9
25.2	2.72	1.84	2.52	400	0.197	302.3
30.0	2.75	2.21	2.78	439	0.197	300.2
35.0	2.75	2.59	3.23	508	0.197	299.7
39.8	2.83	3.03	3.90	612	0.197	298.4
45.0	2.84	3.44	4.68	739	0.197	300.1
50.0	2.92	3.91	5.64	1780	0.0984	299.9
55.1	2.95	4.36	6.73	1060	0.197	300.6
60.0	3.01	4.86	7.83	2470	0.0984	300.0
65.0	3.07	5.36	9.33	5890	0.0492	300.1
70.2	3.13	5.90	10.6	3360	0.0984	300.8
75.0	3.12	6.29	11.5	7260	0.0492	300.1
80.3	3.19	6.89	13.3	4220	0.0984	301.3
85.1	3.20	7.33	14.0	8840	0.0492	300.5
90.3	3.27	7.92	15.3	9650	0.0492	300.9
100	3.29	8.87	17.5	5540	0.0984	300.8
110	3.29	9.76	19.2	12200	0.0492	300.7
120	3.32	10.7	21.7	13700	0.0492	301.2
130	3.31	11.6	23.4	14800	0.0492	300.3
140	3.28	12.3	24.6	15500	0.0492	299.7
150	3.23	13.0	25.6	16200	0.0492	299.3

Table 9. Continued

E/N (Td)	Reduced Mobility ($\frac{cm^2}{V\text{-}sec}$)	Drift Velocity ($10^4 \frac{cm}{sec}$)	ND_L (10^{18}/cm-sec)	D_L (cm^2/sec)	Pressure (Torr)	Temp. (°K)
160	3.19	13.7	28.9	9080	0.0984	299.3
190	3.13	15.9	33.4	10500	0.0984	299.4
200	3.12	16.8	34.8	22000	0.0492	299.7
300	2.86	23.0	50.2	63300	0.0246	299.6
399	2.63	28.2	67.4	84900	0.0246	299.2
475	2.49	31.8	81.1	102000	0.0246	298.4
581	2.35	36.7	103	130000	0.0246	298.8
610	2.32	38.0	122	155000	0.0246	301.9

Table 10. Transport Data for K^+ Ions in Hydrogen Gas

E/N (Td)	Reduced Mobility ($\frac{cm^2}{V\text{-}sec}$)	Drift Velocity ($10^4 \frac{cm}{sec}$)	ND_L (10^{18}/cm-sec)	D_L (cm^2/sec)	Pressure (Torr)	Temp. (°K)
2.03	13.1	0.714	9.09	716	0.394	299.7
2.53	13.1	0.894			0.296	299.7
2.78	13.0	0.974	9.00	707	0.394	299.0
3.04	13.0	1.07			0.296	300.0
3.48	13.2	1.23	9.47	1490	0.197	299.5
4.06	13.1	1.42	8.95	1410	0.197	300.2
5.05	13.1	1.78	9.16	1450	0.197	300.4
6.11	13.2	2.17	9.68	1530	0.197	300.3
6.72	13.2	2.38	9.35	1470	0.197	300.0
7.60	13.1	2.68			0.345	299.8
8.10	13.2	2.86	9.34	1180	0.246	299.7
9.11	13.1	3.21	9.46	1490	0.197	299.5
10.1	13.1	3.57	9.84	1550	0.197	299.6
12.2	13.1	4.32	9.90	1560	0.197	299.8
14.6	13.2	5.17	10.4	1630	0.197	299.4
16.7	13.2	5.89	10.7	1670	0.197	298.8
18.2	13.2	6.47	11.2	1770	0.197	299.8
22.3	13.3	7.99	12.4	1950	0.197	299.5
25.3	13.4	9.08	13.8	1450	0.296	299.2
28.9	13.5	10.5	15.2	1200	0.394	300.0
33.4	13.6	12.2	18.0	1410	0.394	299.0
37.4	13.8	13.9	21.7	1700	0.394	299.4
40.5	13.9	15.1	24.2	2540	0.296	299.3
45.6	14.3	17.5	31.4	2470	0.394	299.6
50.6	14.6	19.9	40.1	4210	0.296	299.6
55.6	15.0	22.4	51.2	5360	0.296	299.2
60.8	15.4	25.2	65.0	6820	0.296	299.8
65.6	15.8	27.8	77.2	9710	0.246	299.0
71.0	16.3	31.1	91.4	14400	0.197	299.9
75.7	16.5	33.5	105	13200	0.246	299.0
81.3	16.9	36.8	111	17400	0.197	300.2
85.9	17.0	39.2	116	18300	0.197	299.1
92.2	17.1	42.4	120	19000	0.197	299.7
95.9	17.2	44.2	125	22500	0.172	298.9
101	17.2	46.9	122	25600	0.148	300.2
111	17.2	51.4	132	27600	0.148	298.9
127	16.9	57.3	143	30100	0.148	299.7

Table 10. Continued

E/N (Td)	Reduced Mobility ($\frac{cm^2}{V\text{-}sec}$)	Drift Velocity (10^4 $\frac{cm}{sec}$)	ND_L (10^{18}/cm-sec)	D_L (cm^2/sec)	Pressure (Torr)	Temp. (°K)
152	16.3	66.6	162	40800	0.123	300.2
177	15.7	74.7	186	58600	0.0985	299.4
202	15.2	82.2	207	65300	0.0985	300.3
227	14.6	89.1	256	94700	0.0838	299.3
254	14.1	95.9	284	120000	0.0739	300.4

Table 11. Transport Data for K^+ Ions in Nitrogen

E/N (Td)	Reduced Mobility ($\frac{cm^2}{V\text{-}sec}$)	Drift Velocity ($10^4 \frac{cm}{sec}$)	ND_L (10^{18}/cm-sec)	D_L (cm^2/sec)	Pressure (Torr)	Temp. (°K)
3.95	2.53	.268	1.74	84.9	0.636	300.2
4.26	2.53	.289	1.70	89.6	0.591	300.4
4.92	2.51	.332	1.74	84.9	0.636	299.2
5.28	2.53	.360	1.74	91.1	0.591	298.9
5.90	2.53	.401	1.75	127	0.424	298.8
6.36	2.54	.433	1.78	140	0.394	299.5
6.87	2.53	.467	1.80	262	0.212	298.4
7.41	2.53	.503	1.78	280	0.197	298.8
7.88	2.54	.538	1.76	129	0.424	299.4
8.48	2.54	.579	1.80	142	0.394	299.7
8.84	2.53	.601	1.81	132	0.424	298.5
9.80	2.54	.669	1.84	268	0.212	298.0
9.86	2.55	.675	1.85	135	0.424	299.8
10.5	2.54	.717	1.83	287	0.197	298.7
10.6	2.54	.725	1.82	144	0.394	300.6
11.8	2.54	.806	1.80	132	0.424	299.2
12.3	2.55	.839	1.86	271	0.212	297.9
12.8	2.56	.880	1.82	144	0.394	301.0
13.2	2.54	.901	1.83	293	0.197	298.1
13.8	2.55	.944	1.83	134	0.424	299.2
14.8	2.54	1.01	1.96	572	0.106	299.0
14.8	2.55	1.02	1.86	147	0.394	299.6
15.8	2.55	1.08	1.92	141	0.424	299.3
15.9	2.54	1.08	1.92	603	0.098	298.4
17.1	2.54	1.17	1.87	272	0.212	297.7
17.8	2.55	1.22	1.89	139	0.424	299.9
18.4	2.54	1.26	1.93	302	0.197	297.8
19.7	2.56	1.35	1.98	578	0.106	298.8
19.8	2.55	1.36	1.95	143	0.424	300.1
21.1	2.54	1.44	2.04	629	0.0984	298.1
24.5	2.55	1.68	2.04	296	0.212	297.5
29.5	2.56	2.03	2.22	650	0.106	298.7
34.3	2.56	2.35	2.31	335	0.212	297.5
39.3	2.60	2.74	2.72	795	0.106	298.7
44.1	2.57	3.04	2.77	402	0.212	297.5
49.1	2.61	3.45	3.14	918	0.106	298.7
54.0	2.60	3.77	3.41	496	0.212	298.3
59.1	2.61	4.15	3.74	1090	0.106	299.4
63.8	2.62	4.49	4.21	614	0.212	298.2
68.9	2.65	4.91	4.75	1390	0.106	298.9

Table 11. Continued

E/N	Reduced Mobility ($\frac{cm^2}{V\text{-}sec}$)	Drift Velocity ($10^4 \frac{cm}{sec}$)	ND_L (10^{18}/cm-sec)	D_L (cm^2/sec)	Pressure (Torr)	Temp. (°K)
73.6	2.65	5.24	5.09	741	0.212	298.1
78.7	2.68	5.67	5.87	1710	0.106	298.9
83.3	2.64	5.91	5.97	870	0.212	297.9
88.5	2.72	6.46	7.23	2110	0.106	298.9
98.4	2.77	7.32	8.95	2620	0.106	299.0
110	2.81	8.32	11.1	3240	0.106	298.1
123	2.86	9.43	13.2	3860	0.106	298.3
135	2.91	10.6	15.8	4600	0.106	298.7
147	2.94	11.6	18.5	5390	0.106	298.0
159	2.99	12.8	21.0	6110	0.106	298.0
172	2.99	13.8	22.6	6630	0.106	298.0
184	3.01	14.9	25.7	7480	0.106	298.2
239	3.05	19.6	36.6	23200	0.0492	300.4
266	3.06	21.9	43.1	27200	0.0492	300.3
318	2.95	25.2	51.0	32200	0.0492	299.8
372	2.88	28.8	60.8	38400	0.0492	300.1
426	2.81	32.2	65.2	82500	0.0246	300.9
478	2.73	35.0	75.2	95100	0.0246	300.4
531	2.67	38.0	86.3	109000	0.0247	300.7
584	2.61	41.0	98.8	125000	0.0246	300.2
636	2.54	43.4	108	137000	0.0246	299.7

Table 12. Transport Data for K^+ Ions in Oxygen Gas

E/N (Td)	Reduced Mobility ($\frac{cm^2}{V\text{-}sec}$)	Drift Velocity ($10^4 \frac{cm}{sec}$)	ND_L (10^{18}/cm-sec)	D_L (cm^2/sec)	Pressure (Torr)	Temp. (°K)
3.04	2.72	0.222			0.491	298.5
3.55	2.73	0.260			0.491	298.7
4.05	2.72	0.296			0.491	298.4
5.06	2.73	0.370			0.491	298.3
6.09	2.73	0.446			0.295	299.1
7.10	2.73	0.520			0.295	298.6
8.10	2.72	0.592			0.295	298.5
9.12	2.71	0.665			0.295	298.5
10.1	2.72	0.739			0.295	298.4
11.2	2.73	0.818			0.295	298.6
12.2	2.74	0.895			0.295	298.7
13.7	2.75	1.01			0.295	299.2
15.1	2.71	1.10			0.295	297.6
20.2	2.72	1.48			0.295	297.3
25.3	2.74	1.86			0.295	297.6
30.4	2.76	2.25			0.295	298.1
35.2	2.76	2.60	2.76	288	0.295	296.4
40.3	2.82	3.05	3.31	345	0.295	296.9
45.1	2.86	3.47	3.81	396	0.295	295.4
50.4	2.85	3.85	4.39	458	0.295	297.1
55.3	2.89	4.30			0.295	297.0
60.7	2.95	4.81	6.06	634	0.295	297.9
70.9	3.06	5.82	8.45	1328	0.196	298.2
80.9	3.13	6.80	10.7	1680	0.196	298.0
92.1	3.23	7.99	13.5	2120	0.196	298.1
101	3.32	9.05	15.7	3310	0.147	298.9
111	3.36	10.0	18.3	2880	0.196	297.3
121	3.41	11.1	20.4	4270	0.147	297.4
131	3.45	12.2	22.8	4770	0.147	297.6
141	3.47	13.2	24.6	5150	0.147	297.6
151	3.49	14.1	26.2	8170	0.0982	295.7
161	3.47	15.0	27.6	8650	0.0982	296.9
172	3.46	16.0	29.3	9170	0.0982	297.2
187	3.47	17.4	31.3	9820	0.0982	297.4
203	3.46	18.8	35.1	11000	0.0982	298.4
227	3.39	20.7	36.8	15400	0.0736	298.0
253	3.32	22.6	39.1	16400	0.0736	298.3
279	3.24	24.3	41.9	17600	0.0736	298.6
302	3.18	25.8	44.5	27900	0.0491	297.1
328	3.13	27.6	49.6	31100	0.0491	297.2

Table 13. Transport Data for K^+ Ions in Carbon Monoxide

E/N (Td)	Reduced Mobility ($\frac{cm^2}{V\text{-}sec}$)	Drift Velocity ($10^4 \frac{cm}{sec}$)	ND_L (10^{18}/cm-sec)	D_L (cm^2/sec)	Pressure (Torr)	Temp. (°K)
3.94	2.31	0.245	1.76	69	0.795	301.4
5.02	2.29	0.310	1.53	89	0.530	299.9
5.91	2.31	0.366	1.69	66	0.795	301.0
6.70	2.30	0.414	1.64	96	0.530	300.0
7.87	2.29	0.483	1.52	60	0.795	300.4
8.83	2.29	0.545	1.61	63	0.795	300.0
10.0	2.31	0.623	1.66	97	0.530	299.7
10.0	2.28	0.616	1.62	237	0.212	299.7
13.4	2.30	0.830	1.68	99	0.530	300.4
15.0	2.31	0.930	1.70	248	0.212	298.3
20.1	2.31	1.25	1.73	255	0.212	300.3
20.1	2.31	1.25	1.76	104	0.530	300.5
25.1	2.31	1.56	1.85	270	0.212	299.6
30.1	2.31	1.86	1.91	278	0.212	299.4
30.2	2.32	1.88	1.99	117	0.530	300.5
40.1	2.30	2.48	2.15	314	0.212	299.1
40.2	2.32	2.50	2.09	307	0.212	300.0
50.2	2.32	3.12	2.72	399	0.212	299.5
50.2	2.33	3.14	2.52	369	0.212	299.5
60.2	2.32	3.75	2.93	428	0.212	299.4
70.1	2.35	4.42	3.59	524	0.212	299.1
80.2	2.39	5.16	4.63	677	0.212	299.3
90.2	2.38	5.77	5.29	772	0.212	299.0
100	2.45	6.60	7.12	4170	0.053	299.6
125	2.51	8.42	10.5	6130	0.053	298.4
134	2.54	9.13	12.2	7160	0.053	299.8
151	2.58	10.43	14.7	8590	0.053	299.5
175	2.65	12.47	19.2	11200	0.053	298.6
201	2.73	14.69	25.9	15200	0.053	299.3
225	2.74	16.59	27.9	16300	0.053	298.8
248	2.74	18.24	32.8	38500	0.026	300.4
251	2.78	18.76	33.9	19800	0.053	299.4
275	2.75	20.35	36.4	21200	0.053	298.9
275	2.74	20.32	35.2	20600	0.053	299.2
298	2.74	21.95	40.3	47200	0.026	300.1
301	2.74	22.13	38.5	23300	0.053	299.6
344	2.73	25.23	51.4	60000	0.026	298.6
395	2.68	28.48	55.4	64900	0.026	299.7
442	2.66	31.56	68.1	80900	0.026	298.8
493	2.61	34.58	76.3	89300	0.026	299.7
541	2.54	36.95	92.9	109000	0.026	299.3
593	2.48	39.54	94.2	111000	0.026	300.1
640	2.46	42.21			0.026	299.5

Table 14. Transport Data for K^+ Ions in Nitric Oxide

E/N (Td)	Reduced Mobility ($\frac{cm^2}{V\text{-}sec}$)	Drift Velocity ($10^4 \frac{cm}{sec}$)	ND_L (10^{18}/cm-sec)	D_L (cm^2/sec)	Pressure (Torr)	Temp. (°K)
2.03	2.29	0.125			0.491	299.2
2.03	2.28	0.124			0.491	298.7
3.05	2.28	0.187			0.491	298.9
3.54	2.27	0.216			0.491	298.2
3.55	2.28	0.218			0.295	298.7
4.05	2.27	0.248			0.491	298.6
4.55	2.26	0.277			0.491	298.0
5.21	2.20	0.308			0.491	298.6
6.09	2.27	0.372			0.491	299.2
6.58	2.28	0.402			0.295	298.2
7.10	2.28	0.435			0.491	298.8
7.58	2.27	0.462			0.295	297.7
8.11	2.28	0.496			0.491	298.5
8.59	2.28	0.526			0.295	297.5
9.11	2.27	0.556			0.491	298.4
9.58	2.26	0.582			0.295	297.3
10.1	2.27	0.617			0.295	298.3
11.1	2.26	0.676			0.295	297.7
12.1	2.27	0.741			0.295	298.1
14.2	2.28	0.868			0.295	298.1
16.2	2.27	0.990			0.295	298.3
18.3	2.28	1.12			0.295	298.7
20.3	2.28	1.24			0.295	299.0
22.3	2.28	1.36			0.295	298.4
24.3	2.28	1.49			0.295	298.6
26.4	2.28	1.62			0.295	298.7
28.4	2.29	1.75	1.94	204	0.295	299.1
30.6	2.29	1.89	2.00	210	0.295	299.3
35.5	2.28	2.18	2.07	217	0.295	298.5
40.6	2.29	2.49	2.27	239	0.295	298.6
45.7	2.30	2.82	2.52	265	0.295	298.8
50.5	2.27	3.08	2.52	395	0.196	297.4
55.6	2.29	3.42	2.89	454	0.196	297.8
60.7	2.31	3.77	3.15	495	0.196	298.1
65.9	2.33	4.12	3.65	574	0.196	298.6
70.8	2.33	4.43	3.89	611	0.196	298.1
76.0	2.35	4.79	4.41	693	0.196	298.3
81.1	2.37	5.16	4.97	782	0.196	298.5
91.5	2.41	5.91	6.22	980	0.196	298.9

Table 14. Continued

E/N (Td)	Reduced Mobility ($\frac{cm^2}{V\text{-}sec}$)	Drift Velocity ($10^4 \frac{cm}{sec}$)	ND_L (10^{18}/cm-sec)	D_L (cm^2/sec)	Pressure (Torr)	Temp. (°K)
101	2.45	6.67	7.94	2500	0.0982	298.2
112	2.53	7.57	9.80	3090	0.0982	298.8
122	2.55	8.34	11.7	3680	0.0982	298.3
132	2.62	9.28	14.3	4500	0.0982	298.8
142	2.65	10.1	16.2	5090	0.0982	298.5
152	2.68	10.9	18.0	5660	0.0982	298.5
162	2.74	11.9	20.3	6370	0.0982	298.0
172	2.77	12.8	23.5	7390	0.0982	298.7
182	2.81	13.7	24.2	7610	0.0982	298.2
193	2.83	14.7	26.0	8200	0.0982	299.2
203	2.85	15.5	28.3	8900	0.0982	298.4
215	2.86	16.5	30.6	9630	0.0982	298.4
228	2.88	17.6	32.0	10100	0.0982	298.7
253	2.90	19.7	36.3	22900	0.0491	298.5
277	2.89	21.5	40.2	25200	0.0491	297.1
289	2.93	22.8			0.0491	299.1
304	2.88	23.6	43.7	27500	0.0491	298.8
330	2.89	25.7			0.0491	299.4
331	2.87	25.5	47.0	29300	0.0491	295.5
353	2.82	26.7	50.3	31500	0.0491	297.3
404	2.77	30.1	57.9	36400	0.0491	297.5
455	2.71	33.1	68.4	43000	0.0491	297.9
503	2.67	36.1	77.8	70000	0.0344	298.6
556	2.61	38.9	79.7	71500	0.0344	297.7
609	2.55	41.7	89.3	80500	0.0344	299.1
703	2.49	47.1	116.0	104000	0.0344	299.3

Table 15. Transport Data for K^+ Ions in Carbon Dioxide

E/N (Td)	Reduced Mobility ($\frac{cm^2}{V\text{-}sec}$)	Drift Velocity ($10^4 \frac{cm}{sec}$)	ND_L (10^{17}/cm-sec)	D_L (cm^2/sec)	Pressure (Torr)	Temp. (°K)
10.1	1.45	0.395			0.0982	300.1
11.2	1.45	0.435	10.4	439	0.0736	300.2
12.2	1.44	0.471			0.0736	299.7
12.2	1.44	0.471			0.0982	299.5
13.2	1.44	0.509	10.7	451	0.0736	299.2
13.3	1.45	0.515			0.0982	300.6
14.2	1.44	0.552			0.0736	299.4
14.3	1.44	0.555			0.0982	301.1
15.2	1.44	0.590	10.8	456	0.0736	299.9
15.3	1.45	0.598			0.0736	300.4
16.3	1.43	0.627	10.4	329	0.0982	300.1
16.4	1.44	0.635			0.0982	301.4
17.3	1.43	0.665	10.4	330	0.0982	299.7
17.4	1.45	0.675			0.0736	300.8
18.4	1.45	0.720			0.0736	301.5
19.4	1.45	0.755			0.0736	300.9
19.4	1.45	0.755			0.0982	300.4
20.2	1.45	0.789	10.6	669	0.0491	299.2
20.4	1.45	0.797	11.0	468	0.0736	301.2
20.9	1.45	0.816	11.0	466	0.0736	300.7
22.6	1.45	0.879	11.1	471	0.0736	302.0
23.0	1.46	0.898			0.0736	301.0
24.5	1.44	0.949			0.0736	300.9
24.5	1.45	0.958			0.0736	301.6
25.5	1.45	0.991	11.3	479	0.0736	300.6
26.6	1.42	1.02	10.7	452	0.0736	301.0
28.6	1.45	1.11			0.0736	301.2
29.6	1.45	1.15	11.4	484	0.0736	300.9
30.7	1.44	1.19			0.0982	301.4
31.6	1.45	1.23			0.0982	300.7
32.8	1.44	1.27	11.3	479	0.0736	302.0
34.3	1.44	1.33	11.5	489	0.0736	301.4
35.6	1.43	1.37	11.4	483	0.0736	299.7
37.7	1.43	1.45	11.4	481	0.0736	299.9
40.4	1.44	1.56			0.0736	301.2
40.7	1.43	1.57	12.1	510	0.0736	300.1
42.8	1.43	1.65	12.0	509	0.0736	300.5
43.9	1.45	1.71	12.2	517	0.0736	300.9
45.9	1.44	1.78	12.4	522	0.0736	300.6

Table 15. Continued

E/N (Td)	Reduced Mobility ($\frac{cm^2}{V\text{-}sec}$)	Drift Velocity ($10^4 \frac{cm}{sec}$)	ND_L (10^{17}/cm-sec)	D_L (cm^2/sec)	Pressure (Torr)	Temp. (°K)
47.9	1.43	1.85			0.0736	300.8
49.0	1.43	1.88	12.5	395	0.0982	300.3
50.6	1.42	1.93	12.4	524	0.0736	299.4
53.0	1.42	2.03	12.8	405	0.0982	300.2
53.1	1.43	2.04			0.0982	301.2
55.9	1.42	2.13	12.8	404	0.0982	300.1
57.2	1.42	2.18			0.0982	301.1
57.2	1.42	2.19	13.2	419	0.0982	300.9
61.4	1.42	2.34	13.7	436	0.0982	301.0
64.3	1.42	2.45	14.0	446	0.0982	301.0
68.5	1.42	2.61	14.5	460	0.0982	301.3
71.7	1.42	2.73	14.7	468	0.0982	301.7
75.9	1.40	2.85	15.2	478	0.0982	298.3
81.0	1.39	3.03	15.3	482	0.0982	298.7
86.1	1.39	3.22	16.3	512	0.0982	298.7
91.7	1.39	3.42	16.9	532	0.0982	299.0
96.2	1.37	3.54	17.4	274	0.196	298.8
99.8	1.39	3.72	18.7	588	0.0982	298.9
101	1.38	3.74	18.1	570	0.0982	298.6
107	1.38	3.94	18.8	593	0.0982	299.2
115	1.36	4.20	20.0	629	0.0982	298.7
115	1.37	4.22	20.6	649	0.0982	299.0
115	1.37	4.22	20.4	643	0.0982	299.0
115	1.36	4.20	19.7	622	0.0982	300.0
115	1.37	4.23	20.3	642	0.0982	299.4
117	1.37	4.31	21.4	676	0.0982	299.7
127	1.37	4.67	23.6	746	0.0982	300.0
137	1.36	5.01	24.6	776	0.0982	299.4
149	1.36	5.44	28.2	888	0.0982	298.8
152	1.36	5.56	28.6	902	0.0982	299.4
152	1.35	5.51	28.6	900	0.0982	298.5
167	1.36	6.07	32.7	1030	0.0982	298.8
178	1.35	6.45	37.9	1200	0.0982	299.7
193	1.35	6.98	42.7	1350	0.0982	298.7
202	1.34	7.26	45.7	1440	0.0982	298.2
218	1.36	7.92	55.2	2320	0.0736	298.1
228	1.37	8.37	62.2	2610	0.0736	298.5
243	1.38	8.98	73.1	3060	0.0736	298.1
253	1.39	9.44	83.5	3510	0.0736	298.9
268	1.39	9.99	97.7	4730	0.0638	298.5
278	1.41	10.5	111	5370	0.0638	298.9
279	1.41	10.6	112	5890	0.0589	299.2

Table 15. Continued

E/N (Td)	Reduced Mobility ($\frac{cm^2}{V\text{-}sec}$)	Drift Velocity ($10^4 \frac{cm}{sec}$)	ND_L (10^{17}/cm-sec)	D_L (cm^2/sec)	Pressure (Torr)	Temp. (°K)
299	1.45	11.7	141	8890	0.0491	299.0
305	1.45	11.9	146	7690	0.0589	299.4
317	1.47	12.5	166	10400	0.0491	298.5
329	1.47	13.0	182	11500	0.0491	299.1
344	1.51	13.9	209	13200	0.0491	298.5
355	1.51	14.4	240	15100	0.0491	299.1
381	1.54	15.8	278	17500	0.0491	299.4
406	1.58	17.3	322	20300	0.0491	299.4
430	1.61	18.6	370	23300	0.0491	298.1
445	1.64	19.6	392	30800	0.0393	297.9
455	1.64	20.0	417	26200	0.0491	297.9
474	1.67	21.2	438	34400	0.0393	297.5
494	1.67	22.2	463	36700	0.0393	300.5
505	1.69	22.9	498	39300	0.0393	299.1
521	1.68	23.6	498	45000	0.0344	300.0
556	1.72	25.7	566	50900	0.0344	298.2
583	1.74	27.2	591	53200	0.0344	298.9
605	1.73	28.2	607	54500	0.0344	297.6
620	1.73	28.7	626	65900	0.0295	299.4
650	1.74	30.4	659	69300	0.0295	299.3
684	1.74	31.9	682	71600	0.0295	298.6
708	1.74	33.0	704	73800	0.0295	298.1

APPENDIX II

USEFUL FORMULAS

Collected in this appendix are some of the more useful formulas which appear in drift tube work. Many of the equations also occur in the text, in which case the appropriate equation number is given. The following units are used consistently throughout:

K_0 in $cm^2/V\text{-}sec$	ND, ND_L, ND_T in $cm^{-1}sec^{-1}$
v_d in 10^4 cm/sec	M, m in amu
E/N in Td (= 10^{-17} V-cm^2)	T, T_{eff} in degrees Kelvin
N in cm^{-3}	

(1) Einstein (or Nernst-Townsend) Relation

$$ND = 2.315 \times 10^{15} K_0 T \qquad (3\text{-}13b)$$

(2) E/P_0 Conversion to E/N

$$E/N = 2.829 \times \left(\frac{E}{P_0}\right),$$

where E/P_0 is in V/cm-Torr.

(3) Number Density of Neutral Gas Using Ideal Gas Law

$$N = 9.657 \times 10^{18} \frac{P}{T},$$

where P is the neutral gas pressure in Torr and T is the temperature.

(4) Mean Free Path Using the Viehland-Mason Omega Integral

$$\lambda = 2.082 \times 10^{-6} \frac{v_d \, (\mu \, T_{eff})^{\frac{1}{2}} \, T}{\left(\frac{E}{N}\right) P} ,$$

where the mean free path λ is in cm and the gas pressure P is in Torr.

(5) Average Ionic Energy from the Wannier Theory at 300° Kelvin

$$\text{Energy} = 0.039 + 3.742 \times 10^{-8} \, (M + m) \left(\frac{E}{N}\right)^2 K_0^{\,2} ,$$

where the energy is in eV.

(6) Drift Velocity

$$v_d = 0.02687 \, K_0 \left(\frac{E}{N}\right) \qquad (1\text{-}3)$$

(7) Langevin Polarization Limit for the Zero-Field Reduced Mobility

$$[K_0(0)]_P = 35.9/(\mu\alpha)^{\frac{1}{2}} , \qquad (3\text{-}6)$$

where $\mu = mM/(m + M)$ is the reduced mass in units of the proton mass; α is the polarizability in atomic units, a_0^3, with a_0 = 1 Bohr radius. Another useful form of this equation is

$$[K_0(0)]_P = 13.876/(\mu\alpha)^{\frac{1}{2}}$$

with α in Å^3 (1 Å = 10^{-8} cm) and μ is amu.

(8) Original, Unmodified, Wannier Diffusion Equations with Constant τ_s for the Pure Polarization Model

$$ND_L = 2.315 \times 10^{15} \, K_0(0) \, T + 6.701 \times 10^{11} \qquad (3\text{-}18)$$

$$\times \frac{M(M + 3.72m)}{(M + 1.908m)} \left(\frac{E}{N}\right)^2 [K_0(0)]^3$$

$$ND_T = 2.315 \times 10^{15} K_0(0)\ T + 6.701 \times 10^{11} \tag{3-19}$$

$$\times \frac{M(M + m)}{(M + 1.908m)} \left(\frac{E}{N}\right)^2 [K_0(0)]^3 ,$$

where m is the ion mass, M the gas mass, and $K_0(0)$ is the zero-field reduced mobility.

(9) Modified Wannier Longitudinal Diffusion Equation for Polarization Model

$$ND_L = 2.315 \times 10^{15} K_0(0)\ T + 0.3455 \times 10^{17} \tag{3-21}$$

$$\times \frac{M(M + 3.72m)}{(M + 1.908m)} \frac{v_d^3}{\left(\frac{E}{N}\right)}$$

In terms of the reduced mobility

$$ND_L = 2.315 \times 10^{15} K_0(0)\ T + 6.701 \times 10^{11} \tag{3-18}$$

$$\times \frac{M(M + 3.72m)}{(M + 1.908m)} \left(\frac{E}{N}\right)^2 [K_0(E/N)]^3 ,$$

where $K_0(E/N)$ is the reduced mobility at a particular E/N and is <u>not</u> the constant zero-field reduced mobility $K_0(0)$.

(10) Omega Integral from Viehland-Mason Theory

$$\bar{\Omega}^{(1,1)}(T_{eff}) = 497.4 \left(\frac{z}{v_d}\right) \left(\frac{1}{\mu\ T_{eff}}\right)^{\frac{1}{2}} \left(\frac{E}{N}\right) \tag{3-28}$$

$$T_{eff} = T + 0.4009\ Mv_d^2 \tag{3-29}$$

where $\bar{\Omega}^{(1,1)}(T_{eff})$ is in $Å^2$ and z = the number of elementary charges on the ion. v_d is the drift velocity at the value E/N and temperature T. In terms of the reduced mobility

$$\bar{\Omega}^{(1,1)}(T_{eff}) = 1.851 \times 10^4 \left(\frac{1}{\mu\ T_{eff}}\right)^{\frac{1}{2}} \frac{z}{K_0(E/N,T)} .$$

Here $K_0(E/N,T)$ is the reduced mobility measured at a specific E/N and gas temperature T corresponding to the drift velocity v_d used in the calculation of T_{eff}.

(11) Zero-Field Reduced Mobility at Gas Temperature T_{eff} Derived from Drift Velocity as a Function of E/N

$$K_0(0,\ T_{eff}) = 37.21 \frac{v_d}{\left(\frac{E}{N}\right)} \tag{3-32}$$

Here $K_0(0,\ T_{eff})$ is the zero-field reduced mobility for a neutral gas temperature of T_{eff} as calculated in (10) above.

BIBLIOGRAPHY

1. E. W. McDaniel, D. W. Martin, and W. S. Barnes, Rev. Sci. Inst. 33, 2 (1962).

2. D. L. Albritton, T. M. Miller, D. W. Martin, and E. W. McDaniel, Phys. Rev. 171, 94 (1968).

3. G. M. Thomson, J. H. Schummers, D. R. James, E. Graham, I. R. Gatland, M. R. Flannery, and E. W. McDaniel, Jour. Chem. Phys. 58 2402 (1973).

4. A. M. Tyndall, The Mobility of Positive Ions in Gases (Cambridge University Press, Cambridge, 1938), p. 92.

5. R. W. Crompton and M. T. Elford, Proc. Phys. Soc. (London) 74, 497 (1959).

6. N. E. Bradbury and R. A. Nielsen, Phys. Rev. 49, 388 (1936).

7. M. T. Elford, Aust. J. Phys. 20, 471 (1967).

8. M. T. Elford, Aust. J. Phys. 24, 705 (1971).

9. I. R. Gatland, Phys. Rev. Letters 29, 9 (1972).

10. M. T. Elford and H. B. Milloy, Aust. J. Phys. 27, 211 (1974).

11. I. A. Fleming, R. J. Tunnicliffe, and J. A. Rees, J. Phys. B2, 780 (1969).

12. T. M. Miller, J. T. Moseley, D. W. Martin, and E. W. McDaniel, Phys. Rev. 173, 115 (1968).

13. J. T. Moseley, I. R. Gatland, D. W. Martin, and E. W. McDaniel, Phys. Rev. 178, 234 (1969).

14. R. M. Snuggs, D. J. Volz, J. H. Schummers, D. W. Martin, and E. W. McDaniel, Phys. Rev. A3, 477 (1971).

15. D. J. Volz, J. H. Schummers, R. D. Laser, D. W. Martin, and E. W. McDaniel, Phys. Rev. A4, 1106 (1971).

16. H. R. Skullerud, J. Phys. B6, 918 (1973).

BIBLIOGRAPHY (Continued)

17. G. H. Wannier, Bell System Technical Journal 32, 170 (1953).

18. D. R. James, E. Graham IV, G. M. Thomson, I. R. Gatland, and E. W. McDaniel, Jour. Chem. Phys. 58, 3652 (1973).

19. G. E. Keller, R. A. Beyer, and L. M. Colonna-Romano, Phys. Rev. A8, 1446 (1973).

20. R. P. Creaser, J. Phys. B7, 529 (1974).

21. T. Kihara, Rev. Mod. Phys. 25, 844 (1953).

22. E. A. Mason and H. W. Schamp, Jr., Ann. Phys. (N.Y.) 4, 233 (1958).

23. L. A. Viehland and E. A. Mason (to be published in Annals of Physics).

24. E. W. McDaniel and E. A. Mason, The Mobility and Diffusion of Ions in Gases (Wiley, New York, 1973).

25. J. T. Moseley, D. W. Martin, E. W. McDaniel, R. M. Snuggs, and T. M. Miller, Technical Report, Georgia Institute of Technology, Atlanta, Georgia (1968), Chapter IV.

26. I. R. Gatland, Case Studies in Atomic Physics 4, 369 (1974).

27. E. Graham IV, D. R. James, W. C. Keever, I. R. Gatland, and E. W. McDaniel, Technical Report, Georgia Institute of Technology, Atlanta, Georgia (1974), Chapter III.

28. P. Langevin, Ann. Chim. Phys. 28, 289 (1903).

29. P. Langevin, Ann. Chim. Phys. 5, 245 (1905). A translation appears in Appendix II of reference 30.

30. E. W. McDaniel, Collision Phenomena in Ionized Gases (Wiley, New York, 1964), p. 28.

31. H. R. Hassé, Phil. Mag. 1, 139 (1926).

32. For a complete exposition of the Chapman-Enskog theory, see S. Chapman and T. G. Cowling, The Mathematical Theory of Non-Uniform Gases, Third Edition (Cambridge University Press, London, 1970).

33. E. W. McDaniel, op. cit., p. 78.

34. E. W. McDaniel and J. T. Moseley, Phys. Rev. A3, 1040 (1971).

BIBLIOGRAPHY (Concluded)

35. E. W. McDaniel, op. cit., p. 71.

36. J. H. Whealton and E. A. Mason, Annals of Physics 84, 8 (1974).

37. R. E. Robson, Aust. J. Phys. 25, 685 (1972).

38. J. H. Schummers, G. M. Thomson, D. R. James, E. Graham, I. R. Gatland, and E. W. McDaniel, Phys. Rev. A7, 689 (1973).

39. J. H. Schummers, G. M. Thomson, D. R. James, E. Graham IV, I. R. Gatland, D. W. Martin, and E. W. McDaniel, Technical Report, Georgia Institute of Technology, Atlanta, Georgia (1972), Appendix IV.

40. E. Graham IV, et al., op. cit., Chapter IV, p. 91.

41. H. S. W. Massey, Electronic and Ionic Impact Phenomena, Second Ed., Vol. 2 (Oxford Univ. Press, 1969), pp. 790-793.

42. N. Takata, Phys. Rev. A10, 2336 (1974).

43. J. H. Schummers, op. cit., Chapter III.

44. E. W. McDaniel and D. W. Martin, Rev. Sci. Inst. 42, 157 (1971).

45. I. Amdur, J. E. Jordan, K. Chien, L. Fung, R. L. Hance, E. Hulpke, and S. E. Johnson, Jour. Chem. Phys. 57, 2117 (1972). I. Amdur, J. E. Jordan, L. Fung, L. J. F. Hermans, S. E. Johnson, and R. L. Hance, Jour. Chem. Phys. 59, 5329 (1973). H. Inouye and S. Kita, Jour. Chem. Phys. 56, 4877 (1972); 57, 1301 (1972); 59, 6656 (1973); Jour. Physical Soc. Japan 34, 1588 (1973). H. Van Dop, A. J. H. Boerboom, and J. Los, Physica 61, 626 (1972).

46. J. H. Schummers, op. cit., Chapter V.

47. H. B. Milloy, Phys. Rev. A7, 1182 (1973).

48. R. P. Creaser, Ph.D. Thesis, Australian National University

49. H. B. Milloy and R. E. Robson, J. Phys. B6, 1139 (1973).

VITA

David Randolph James was born on June 13, 1948, in Atlanta, Georgia. He graduated from North Fulton High School in Atlanta in 1966 and entered the Georgia Institute of Technology in the fall of that year. He received the Bachelor of Science in Physics in 1970 and the Master of Science in Physics in 1971, both from Georgia Tech. During his graduate study, Mr. James was a research assistant in the School of Physics.

Mr. James is a member of the American Physical Society, Sigma Pi Sigma, and Phi Kappa Phi.